Chapter 5 Bed formation and external measurements

5.1 Description of settling and consolidating beds

Most sedimentation and consolidation column experiments performed at Oxford and elsewhere in the literature are started by placing a slurry of known concentration into the column. In this case the slurry surface drops in the column, leaving clear water above, while the bed builds up from the bottom. The majority of numerical methods for consolidation, first described by Kynch (1952), are based on this type of slurry experiment. Good descriptions of slurry settling experiments, specifically of the type performed in Oxford, are given in Been and Sills (1981) and Sills (1998). These experiments have provided excellent detail about the consolidation of slurries, and numerical methods are highly evolved for predicting these types of experiments. However, such conditions do not represent the flocculating and consolidating conditions found in natural environments.

Closeup photographs of the beds prepared from an initial slurry and by slow sedimentation show a significant difference between the two bed structures. Figure 5.1a is the bed surface of isis1 which was settled from a slurry with an initial density of 1.137 Mg/m^3, below the structural density. Figure 5.1b shows the bed of cos5 which was settled under conditions of steady sedimentation at around 4mm per day where flocculation could occur in the water column. The Tamar Estuary sediment used in each case is identical, and the scale on the left of each image is in millimetres. It is obvious from the photographs that the flocculated bed retains some of its floc structure, whereas the bed sedimented from a slurry has a totally different structure. Photographs taken later in the aggregated bed show that, as sedimentation progresses, and the flocs become buried, they begin to break down, and the beds begin to look more like those in Figure 5.1a, although periods of fast and slow sedimentation remain distinguishable.

The channels cutting through the bed in Figure 5.1a are worm burrows. The presence of worms had consequences on the strength of the bed surface, where the worms preferred to feed (Lintern et al., 2000), and possibly also on the consolidation properties of the beds. As a result, those experiments in which worms were observed are not considered

quantitatively in this chapter. However, this experience has highlighted the need to consider biological factors when considering the behaviour of the bed and its susceptibility to erosion, a topic discussed in Chapter 7.

During some of the slurry experiments, drainage channels were visible in the bed. Figure 5.1c shows the bed of a Weston-super-Mare mud in which drainage channels became clearly visible during the consolidation of a slurry with an initial concentration of 1.041 Mg/m^3. The channels become less visible towards the top of the image. Channels have been observed in other experiments and according to Holdich (1996), they are associated with slurries of medium concentrations. The channels provide a means by which pore water can escape efficiently, thus allowing the bed to settle more quickly. The channels are present in the consolidating portion of the bed only, and not in the overlying sedimentation portion. That is, the channels begin to disappear approximately three quarters of the way to the top of the image. These exist where the bed is at a density higher than the structural density, so that an effective stress exists and the solid particles are supported by one another. Above this the particles are supported by the overlying water and are in suspension. Figure 5.2 shows the falling sedimentation surface and the rising channel surface for the slurry experiment wsm2. These likely intersect where sedimentation is complete and consolidation takes over entirely, although the channels were not clearly visible beyond the points shown.

5.2 Bed Height and dimensionless bed height

Figure 5.3a shows the settlement curves for several experiments which used Tamar mud. The isis and rwm experiments, shown as solid squares and triangles respectively, are those which are settled from a slurry, all others are settled under slow sedimentation. The rwm data are taken from Murphy (2001). The isis (slurry) beds, which all had similar starting conditions (Table 3.3), settled similarly to one another under self weight to roughly 0.11 to 0.13m, in the middle of the range for all of the experiments shown.

Experiment cos16 was one in which the bed was built up rapidly under highly concentrated

sedimentation conditions at a rate of approximately 381 mm/day for 30 hours. The high concentration in the water column led to large and highly porous flocs, perhaps best described as 'fluffy', which were subjected to a large number of collisions (Figure 5.4). Figure 5.3a clearly shows that from about 30 hours onwards cos16 has an initial settlement stage, similar to that shown by the slurry experiments rwm1, rwm4 and rwm5. Other experiments which had high rates of sedimentation, cmw1 and wsm1, also showed a rapid initial sedimentation stage or fluid supported sedimentation phase above the consolidating bed (these are not shown here). In these high concentration experiments, the slow process of consolidation is not able to keep pace with the faster sedimentation rates so that the bed builds up, followed by sedimentation once input ceases. The beds deposited more slowly (eg. all other cos experiments) show no sign of this rapid sedimentation and in fact scarcely show any sign of consolidation after sedimentation is stopped.

Figure 5.3b contains the settlement curves for Dibden Bay experiments. The three sets of open circles represent data from dbd experiments which were settled using the sedimentation system, and the solid triangles represent slurry experiments carried out by Bartholomeeusen at Oxford. The dbd experiments had intermediate sedimentation rates, as compared to the Tamar experiments reported above. As a consequence, they show a small amount of rapid settlement, which quickly shallows out to resemble a consolidation behaviour.

It is not possible to compare the experiments to one another, in terms of bed height, since most of the beds contain different masses of solid sediment. It is possible to normalise the bed heights with respect to this mass. A dimensionless height, H, is calculated with

$$H = h / h_s$$

where h and h_s are the heights of the bed and of the solid mass in the bed. The solids dry mass and solids density are used to calculate h_s. This is directly comparable to the more commonly used soil mechanics measure of specific volume[10], which is the total volume of

[10]This is different to the definition used by chemists, where the specific volume is the number of cubic metres occupied by one kilogram of a substance.

a soil containing a unit volume of solid material. The following are presented in terms of H though, since that is the feature under examination here.

H is plotted throughout the elapsed experiment time for various Tamar mud experiments in Figure 5.5a. Again slurry experiments are shown with solid markers, whereas slowly deposited experiments are shown with open markers. The curves for the slowly deposited experiments start at the end of sedimentation, and the different starting heights and times indicate the sedimentation rates. The slowly sedimented experiments are normally conducted over a much longer time period than the slurry experiments. It is clear that the rwm1, 4 and 5 slurry experiments, with initial densities ranging from 1.156 to 1.24 Mg/m^3 achieve a self weight consolidation H below the other experiments at around 5 to 6, although the slowly deposited experiment cos3 achieves a similar height. The isis slurry experiments which have lower initial densities, all around 1.137 to 1.164, achieve a higher self weight H around 7.2. The steadily sedimented experiments, shown by open circles, achieve variable H values.

Data are shown in the same form in Figure 5.5b for various Dibden Bay experiments. Three of these experiments are sedimented from a slurry (solid triangles) and the remaining three are steadily deposited at different rates. Here, the flocculated beds achieve much higher values of H during self weight consolidation, that is they retain much greater heights given the same proportion of mud. The shape of the curves and the near complete dissipation of pore pressures indicate that the flocculated beds are unlikely to reach the H values achieved by the slurry beds under self weight.

The rate of sedimentation for this particular set of steady sedimented beds has little effect on the H value. Experiment dbd2, the most slowly deposited sediment shows very little sign of a fluid supported sedimentation stage, thus it is believed that for this experiment the sedimentation rate (in terms of change in bed height) is approaching the consolidation rate. A bed deposited slowly builds up to the same H value as a more quickly deposited bed which has simultaneously undergone consolidation. In fact, all three beds are undergoing

consolidation while being deposited, and at a given time after the start of sedimentation the H values seem to match for the different beds (Figure 5.5b, positions i and ii). The three slurry experiments end up with H values distinctly lower than the slowly deposited sediment.

It is now established that H is dependant on whether the sediment is deposited almost instantaneously, as in a slurry experiment, or over a longer period of time. To look more closely at this dependence of H on sedimentation rate, single values have been chosen from each experiment to represent its settlement. Figure 5.6 represents the approximate final H for the self weight consolidation of all of the Tamar slurry beds. These points are taken from the height of the bed at the end of each experiment (several hundred hours of settling time), where although the bed might still be consolidating slightly, the rate of surface settlement is very low. The data suggests that for slurry experiments the final bed height is related to the initial slurry density.

It is not possible to plot the slowly sedimented bed heights in terms of initial slurry density, therefore sedimentation rate is used instead. The bed heights and dimensionless heights are calculated by interpolation between measurements approximately 50, 100, 200, and 300 hours (where available) after sedimentation has stopped. This method of choosing times and interpolating the heights provides a much clearer view of the data over a relatively short time period, than plotting the measured values of H, since in some experiments few bed height data exist at these short intervals after sedimentation is complete. The accuracy of the interpolations is of the order ±2%. The overall sedimentation rate is calculated from total mass over the sedimentation time, where the sedimentation time includes both the time that the sedimentation system is running, plus the time occupied by the steep part of the surface settlement plot, if it exists.

The values of H at each of these times are given in Table 5-1, and are shown in Figure 5.7 plotted against time. The curves for the cos experiments (Figure 5.7a) are distinct from one another, whereas those for experiments dbd2 and dbd3 are almost identical (Figure 5.7b).

Experiment dbd1, the most quickly deposited of the Dibden Bay experiments has higher H values. The self-weight consolidation for this later experiment took place over 200 hours and the shallowing of the curve for dbd1 indicates that it may not achieve the H of the other experiments for many hundreds of hours, if at all.

Figure 5.8 shows H at each of the specified times for each of the experiments plotted against the sedimentation rate. These are beds which have been deposited slowly using the sedimentation system. The Tamar experiments cos1, 2, 3 and 4 show a clear trend in that more quickly deposited beds, up to approximately 21 g/day, have higher dimensionless bed heights at the given times. By 200 hours after sedimentation the settlement taking place in these beds is small (see figure 5.7a) indicating that this trend will remain to much longer timescales. Experiment cos16, however is still undergoing considerable consolidation by t=200 h (after which a hydraulic gradient was applied), and it entirely possible that under self-weight consolidation it will achieve the H of the other slowly deposited experiments given time. Nevertheless the data suggests that there is a positive relationship between the sedimentation rate and the bed height achieved, given the same mass of sediment.

Table 5-1 Dimensionless bed heights at specified hours after end of sedimentation.

Expt.	Initial Density (Mg/m^3)	Dry mass (kg)	Sedn. rate (g/day)	H after sedn.	H 50 hours	H 100 hours	H 200 hours	H 300 hours
Tamar								
cos1	na	0.31	20	8.40	8.25	8.11	8.05	7.98
cos2	na	0.16	16	7.12	7.12	7.12	7.12	7.12
cos3	na	0.17	11	6.31	6.13	6.06	6.00	5.94
cos4	na	0.46	21	8.37	8.20	8.32	8.29	8.27
cos16	na	0.51	348	10.96	10.42	9.65	9.10	na
isis1	1.137	0.39	772	9.03	7.74	7.61	7.48	na
isis2	1.164	0.36	2230	9.36	8.40	6.99	6.83	6.72
isis3	1.164	0.38	2347	9.46	8.46	6.89	6.67	6.73
isis4	1.164	0.36	2230	9.26	8.31	6.98	6.92	6.87
isis7	1.11	0.35	467	10.70	8.86	7.67	7.43	7.25
tam3	1.131	0.35	347	9.06	8.88	8.34	na	na
rwm1	1.197	1.73	17300	8.59	6.48	6.29	na	na
rwm4	1.24	1.73	17300	7.03	5.46	5.38	na	na
rwm5	1.156	1.73	2076	7.60	6.39	6.26	na	na
Didben								
dbd1	na	0.41	31	10.54	9.54	9.06	8.39	na
dbd2	na	0.55	16	7.37	7.12	6.88	6.70	6.52
dbd3	na	0.47	25	7.37	7.10	6.93	6.69	6.60
dib2	1.22	2.05	20517	6.76	6.33	6.05	5.60	5.20
dib6	1.209	2.75	27513	7.12	6.99	6.92	6.84	6.74
dib7	1.186	0.65	6534	8.02	6.74	5.70	4.87	4.78

For the Dibden Bay experiments, there are fewer data which can be presented in this way. However, in Figure 5.8b the higher overall sedimentation rate of dbd1 for the slowly deposited experiments does lead to significantly higher dimensionless bed heights than either of the other sedimentation experiments dbd2 and dbd3 after 200 hours. Since a hydraulic gradient was applied at this stage, it is not possible to say whether the bed of dbd1 would reach the same H as the other beds given more time.

A combination of all of the experiments for which long term data is available is presented in Figure 5.9. This figure contains experiments using Tamar, Dibden Bay, Weston-super-Mare and Combwich mud. It reinforces the notion that at the lower sedimentation rates there is a positive relationship between sedimentation rate and dimensionless bed height, whereas in slurry deposits there is an overall inverse relationship between sedimentation rate and dimensionless bed height.

5.3 Effect of hydraulic gradient on flocculated beds

Earlier in this chapter it is shown that different flocculation concentrations lead to differences in the dimensionless bed height H achieved. Low to medium concentrations generally lead to increasing H, whereas high concentrations such as those in slurries lead to low H. Since H is normalised by mass this difference in H must be due only to a different bed structure. Many authors have qualitatively introduced the concept of a flocculated bed. For instance Partheniades (1965) suggested decades ago that the structure of flocs could have an influence on the strength of the beds. More recently Sills (1995) discusses a concept, where the breakdown of flocs in the bed is partly responsible for secondary compression, or creep. Large H values might suggest a fragile structure that would break down under a suitable increase in vertical load. To apply this load a hydraulic gradient was used since it produces are more suitable effective stress gradient than that due to a step load surcharge. It is possible that by increasing the stress would cause complete collapse of the flocs, so that all beds, no matter how formed, would settle to the same H.

After a lengthy settling and consolidation time, a hydraulic gradient has been applied to one of each of the Tamar (cos16), Combwich and Weston-super-Mare experiments, and to all of the Dibden Bay experiments. The effect of the hydraulic gradient on the bed height is obvious in Figure 5.10, where H suddenly drops a substantial amount. On experiment dbd1 a hydraulic gradient was first driven by a peristaltic pump at the base of the column. Pore water was pumped from the bottom of the column and returned to the top of the column. This method turned out to be inadequate as the pinch between the rollers and the housing of the peristaltic pump (Figure 5.11) was not tight enough to stop the backflow of pore water under a considerable suction. Therefore, at approximately 1542 hours the pump was replaced by a Mariotte bottle, which has been described in detail in Chapter 2. This caused the bed to reduce further.

The figure shows that all of the slowly sedimented Dibden Bay experiments dbd1, 2 and 3 were brought to a lower H under a hydraulic gradient. However, even with these additional stresses much higher effective stresses, the beds still did not consolidate to the level of the

slurry experiments dib2 and dib7. Similarly, the Tamar and Combwich slurry experiments did not consolidate to the levels of more quickly deposited sediment. In the next chapter the internal structure of the beds is examined in terms of density, effective stress and void ratio, by means of x-ray and pore pressure measurements, to explain how well the flocculated bed structures stand up to increased loading.

5.4 Bed deposition

It is worth noting observations from the high magnification television images at the bed near the column wall. These images were not of sufficient quality to warrant recording, since their quantification would not be possible. Large flocs approaching the bed behave as shown in Figure 8.1. It was shown in Chapter 4 that the larger flocs are normally vertically elongated. Upon landing on the bed, a vertically elongated floc does not always fall in the direction that would be expect due to gravity alone. Rather it remains oscillating in an upright position for a short period of time (a fraction of a second) before repositioning (often with a sudden jump in position) and reshaping itself to spread out over the bed. Sometimes the spreading of the floc is so complete that the floc essentially disappears into the rough bed surface. Most of the time the floc remains intact, although it spreads horizontally on the bed surface. From the rapid spreading it appears as though the floc is either extremely weak, and cannot even maintain its own shape.

The reason for jumping, or tumbling, to a new position on the bed is unknown, although it may be due to water being ejected upward from the bed, or to electrostatic forces between the floc and the bed, or to a combination of these. It does not seem to be due to turbulence above the bed as the flocs normally approach in a vertical direction. Evidence of well developed streams of water emitting from the beds are found in at least one experiment. Figure 5.12a shows an image from experiment cos17. The image has been enhanced in Figure 5.12b, by equalising the histogram of grayscale intensities, which has a similar effect to enhancing the contrast. Above the bed, streams of darker colour can clearly be seen emanating from the bed surface, amidst the turbid (lighter) column water. These are not visible with the naked eye, and just barely visible in the unenhanced images. A time-

lapsed movie was created from a sequence of images of this bed as it settled. These streams remain in the same spot on the bed during the several hours that the bed surface passes from the top to the bottom of the image. Just after this image was taken, an aggregate with approximate dimensions 0.5 mm by 0.4 mm appeared to be lifted in one of the streams, although the upward forces acting on this aggregate may have also been helped by wall friction.

5.5 Tracking the bed surface

It has been suggested in a previous study (eg. Sills and Elder 1984), that the density at the bed surface changes in time. The exact cause is not known, but since the effective stress at the surface is, by definition, zero this change in density is probably occurring due to a rearrangement of particles or due to the growth of cementing material between particles. This change in bed properties, without the existence of effective stress, is an example of creep. In the following section imaging techniques are used to describe what is happening visibly at the surface.

Images of flocculated beds have been shown earlier in this chapter. A computer program has been written to search iteratively for the surface of the bed based on brightness levels of both the bed and overlying water. Figure 5.13 shows a selection of images taken over a 3 day sequence for one of the sedimentation stages in experiment cos17. Overlayed on the image is a rectangular area that has been positioned at the bed surface by the iterative program. The height of the rectangle represents 0.5mm at the very surface. The image in Figure 5.13a was captured while sedimentation was taking place. After this image was taken the surface continued to rise quickly above the field of view. Sedimentation was stopped and approximately 10 hours of settling allowed the surface to reappear at the top of the image and to continue settling (Figure 5.13b). Settling continued for nearly three days (Figure 5.13c). During this time the camera was lowered to keep the bed surface in view, thus the height of the beds in the figure frames cannot be related to one another. In these figures the brighter pixels are solids, whereas the darker pixels are shadows cast across pore spaces. There are aggregates above the bed, adhered to the column wall, particularly

in the second and third images where the settling bed leaves these behind.

Figure 5.14a shows the relative height of the bed surface during this sedimentation stage, determined by the tracking algorithm. The experiment was already underway at the start of this analysis. Thus the bed was being built up and settling simultaneously. The relative bed height is the height relative to the lowest point (measured at the end of this analysis), not relative to the base of the entire bed. The smoothness of the curve gives confidence that the surface tracking algorithm was working well. This figure has been adjusted in two places so that the bed heights match up after the camera was lowered.

The mean brightness of the area within the surface rectangle indicates the ratio of the solids area to the pore space area. This mean brightness throughout the experiment has been plotted in Figure 5.14b. Here it can be seen that while the bed was settling, its top 0.5 mm of surface was becoming more bright. That is, the ratio of solids area to pore space area is increasing. Loosely packed flocs at the surface are being destroyed and the fragments are becoming more tightly packed. This is sometimes obvious from the original images, however by using the mean brightness a quantitative approach can be developed. Quantitative methods have not been developed further in this research, but it is important to emphasize the evidence that flocs at the surface are breaking down, despite the fact that effective stress levels there are extremely low.

5.6 Internal collapse

It has been proposed in Chapter 1 that the flocs in the bed have some strength, which will allow them to carry a finite load. This would account for the higher bed heights found where flocculation was enhanced. This has been confirmed in observations of the bed during deposition. In experiment dbd6, the bed was photographed throughout the beginning of the experiment. In this particular batch of Dibden Bay mud there existed particles of darker material, thought to be composed mainly of organic matter (Figure 5.15a). These particles provided useful points with which the settlement of the bed could be tracked over time. The result of the analysis is shown in Figure 5.15b, for a twenty hour period. It is

apparent that the particles settle a relatively small amount from 55 to 65 hours. However, after this the slope of the settlement curve abruptly becomes steeper. This change in settling speed occurs at between 68 and 69 hours for all heights in the bed, and is more pronounced at the bed surface where the settlement is due to movements lower in the bed as well as local movement.

This buildup, and then collapse of the beds has been photographed for several experiments. On high magnification time-lapsed movies the collapse is clearly visible, and resembles a landslide or avalanche in appearance. The process is described here, since it is difficult to reproduce the movie frames in hard copy, starting with the experiment just shown. Figure 5.16 initially follows the datapoints from experiment dbd6. Once momentum is established, the increased settling continues for many hours until the addition of sediment to the top of the bed is stopped. The self weight height at each level in the bed is then achieved through time, starting near the bottom. The application of a hydraulic gradient mainly affects the bottom, causing it to collapse further, and subsequently the entire bed settles by the amount of collapse at the bottom.

The important point here is that the flocs in the bed are able to retain some strength until a certain threshold of applied load is reached. This is clearly shown by the data. After this point the bed consolidates throughout. The initial structure, and its collapse, can only be measured on a scale of millimeters (in both displacement and depth of overburden). This likely has important consequences on the development of strength in beds deposited in estuaries, since the natural deposition and erosion rates over a tidal cycle are often acting at the same small-scale on the bed surface.

5.7 Conclusions

- Photographs reveal that slowly sedimented beds have a much more aggregated structure than those deposited from a slurry
- The normalised bed height of a consolidated bed appears to be dependant on the

rate of sedimentation. Beds deposited at a medium rate of sedimentation are the least dense. Those deposited at low rates and from slurries have higher densities.

- The aggregates at the surface of a freshly deposited bed break down over time, without any application of load.
- There is evidence that the bed builds up with flocs, and eventually an overburden pressure is reached at which the bed avalanches in on itself.

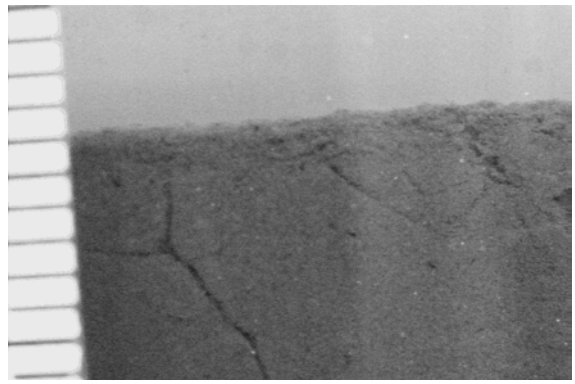

a) isis1 experiment. Image 06

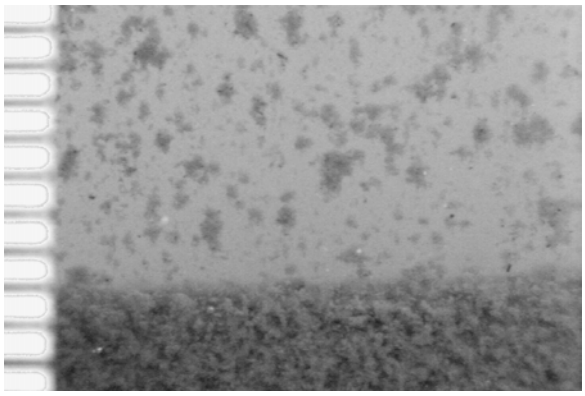

b) cos5. Image 09

c) wsm2. Channel 01

Figure 5.1 Examples of different types of experiments. a. Slurry experiment, b. slowly deposited experiment and c. slurry experiment in which channels allow water to escape.

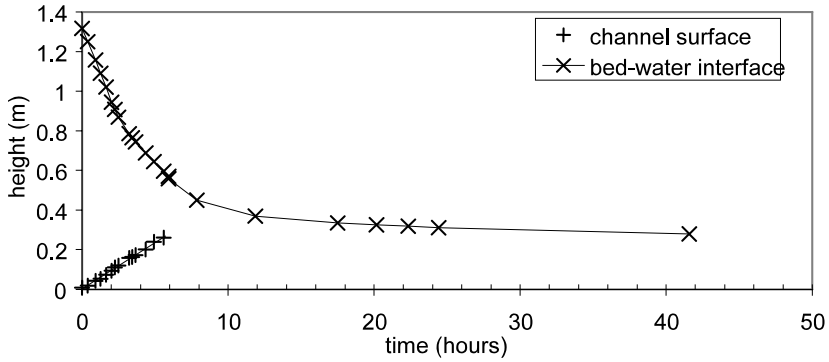

Figure 5.2 wsm2 settling curve. The top curve is the sediment water interface. The bottom curve is the top of the visible channels, probably representing the interface between bed and suspension.

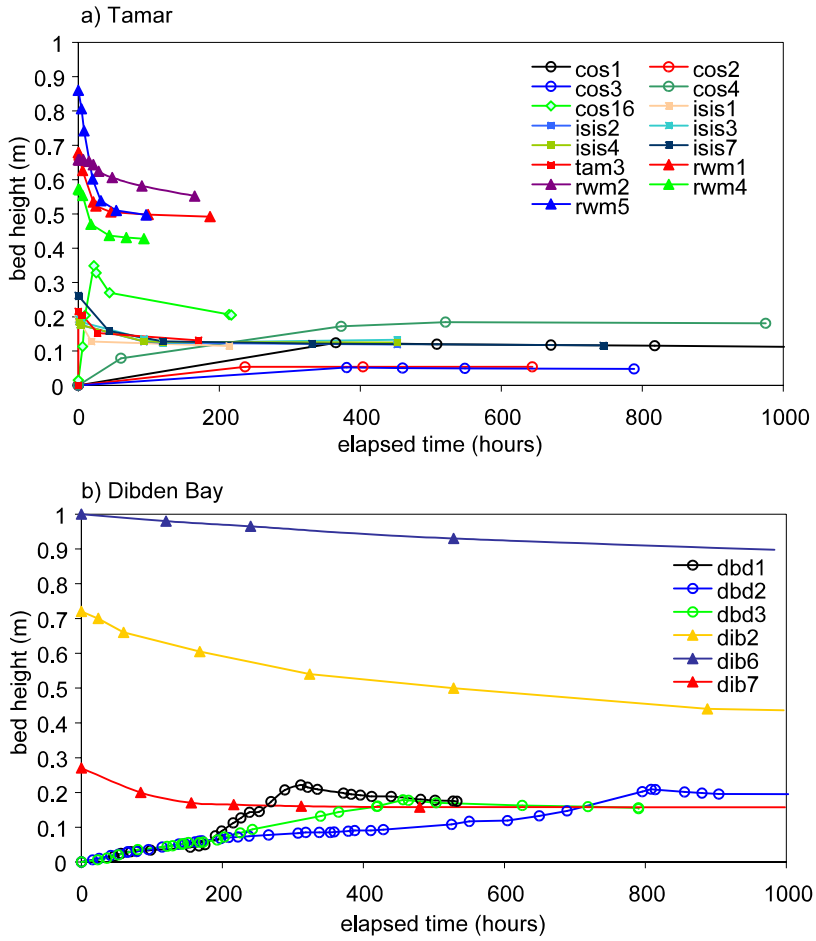

Figure 5.3 Development of bed heights with time for Tamar and Dibden Bay experiments.

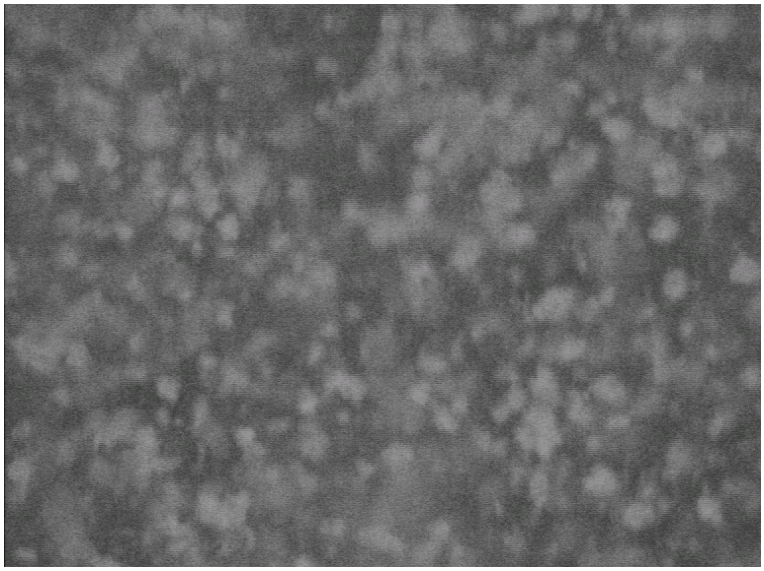

Figure 5.4 A frame from a movie taken at the column wall in experiment cos16.

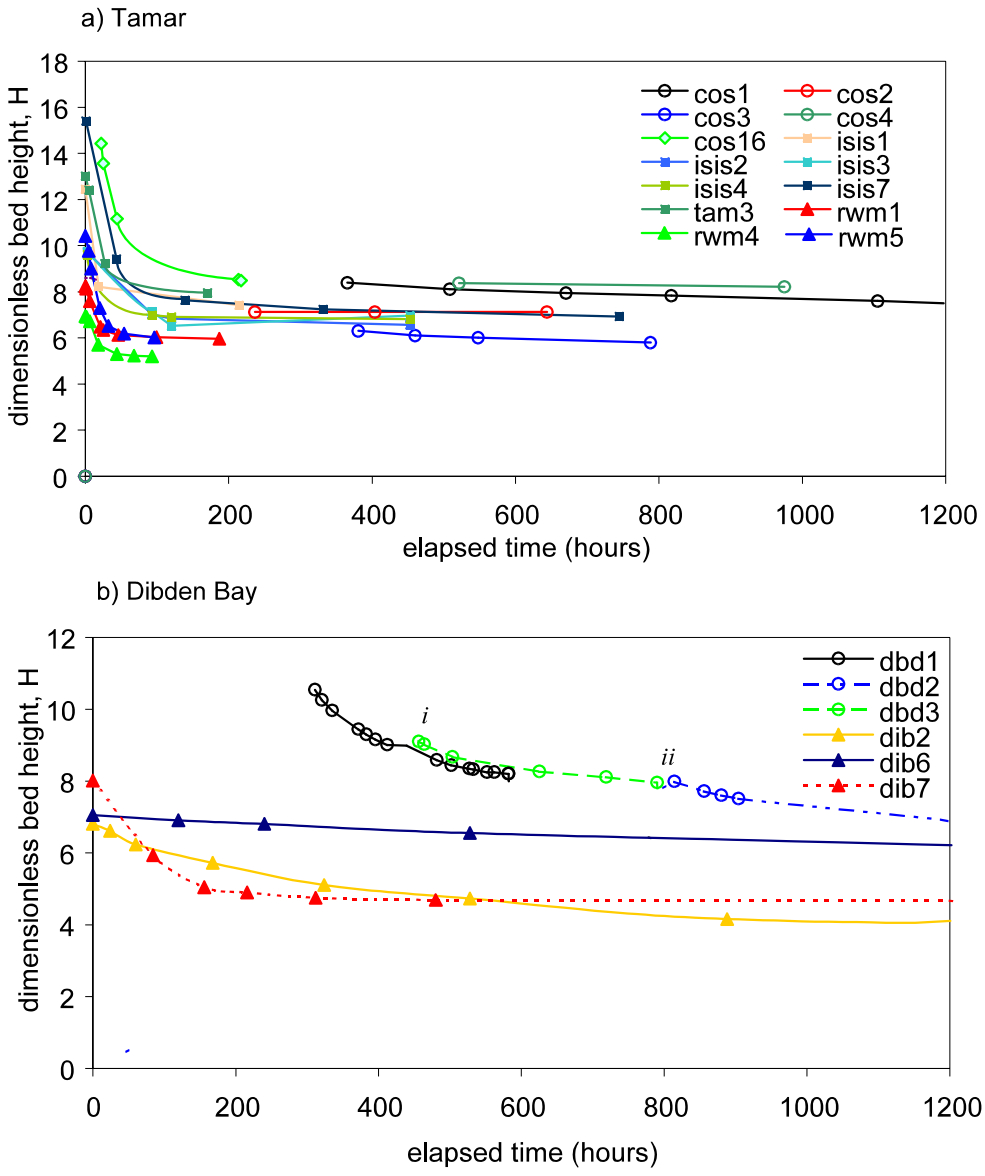

Figure 5.5. Dimensionless bed height, H, for experiments using a. Tamar Estuary mud, and b. Dibden Bay mud.

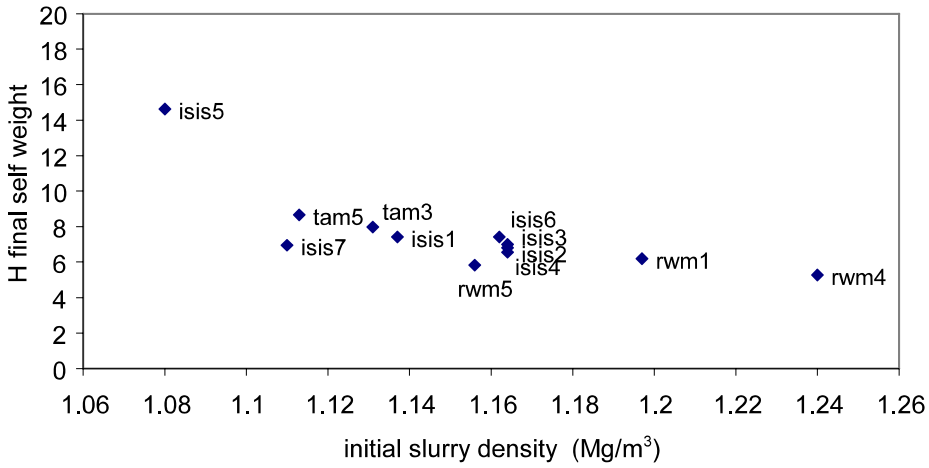

Figure 5.6 Self-weight bed heights of all Tamar slurry experiments.

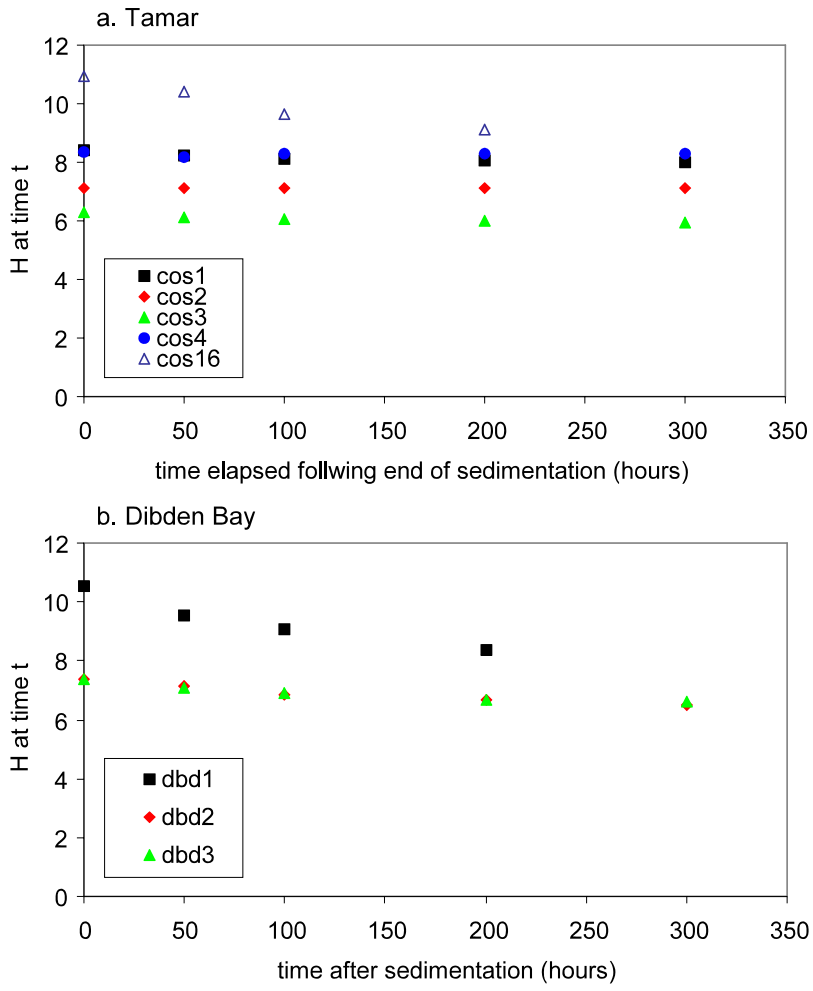

Figure 5.7 H at specified times after end of sedimentation for a. Tamar and b. Dibden Bay mud.

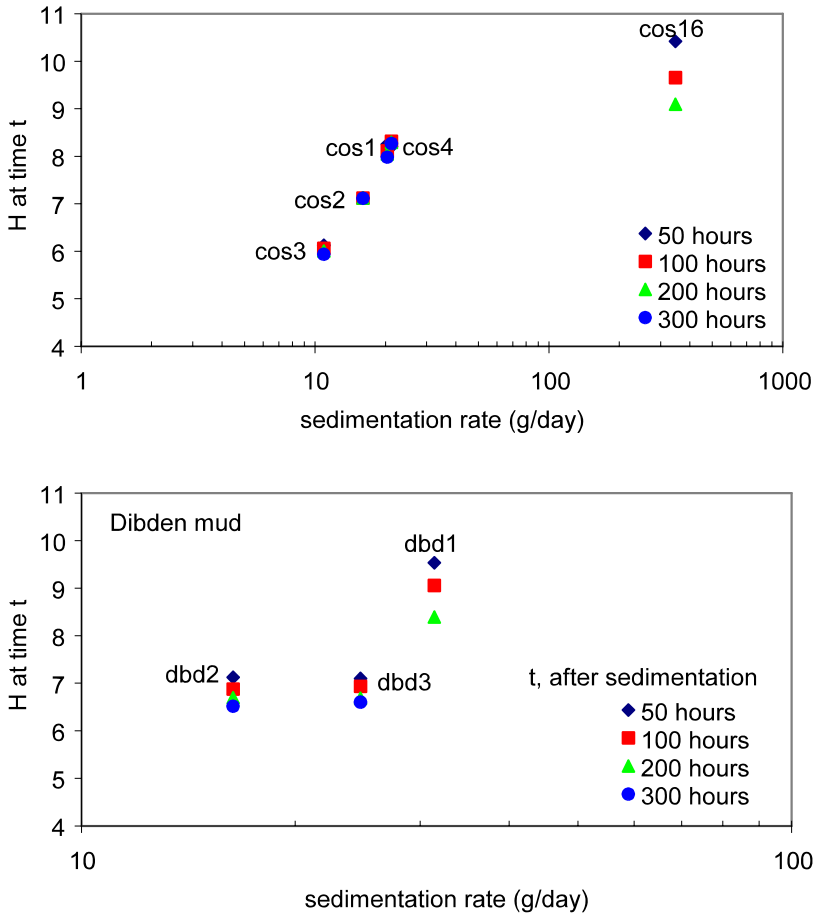

Figure 5.8. Dimensionless bed height H at time t after sedimentation is completed for a. Tamar, and b. Dibden Bay muds.

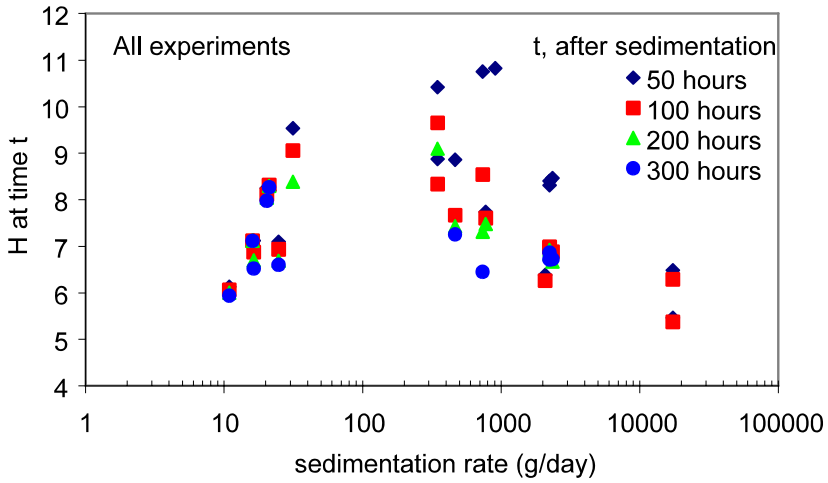

Figure 5.9 Dimensionless bed height at time t after sedimentation is completed for all experiments.

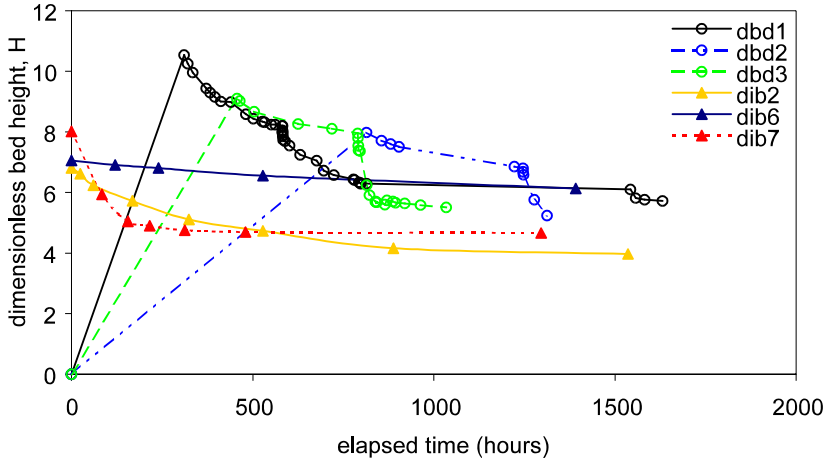

Figure 5.10 Dimensionless bed heights of Dibden Bay mud subjected to a hydraulic gradient (circles), and those formed from a slurry (triangles).

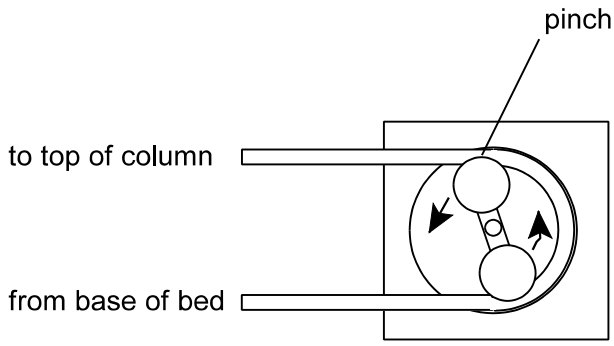

Figure 5.11 Schematic of a peristaltic pump used to apply a hydraulic gradient.

a. isis7bed2_118.bmp original image

b.enhanced by equalising the histogram of gray scale intensities

Figure 5.12 Experiment cos17 a) Image of settling bed surface, b) with grayscale histogram equalisation making the outflowing water channels clearly visible.

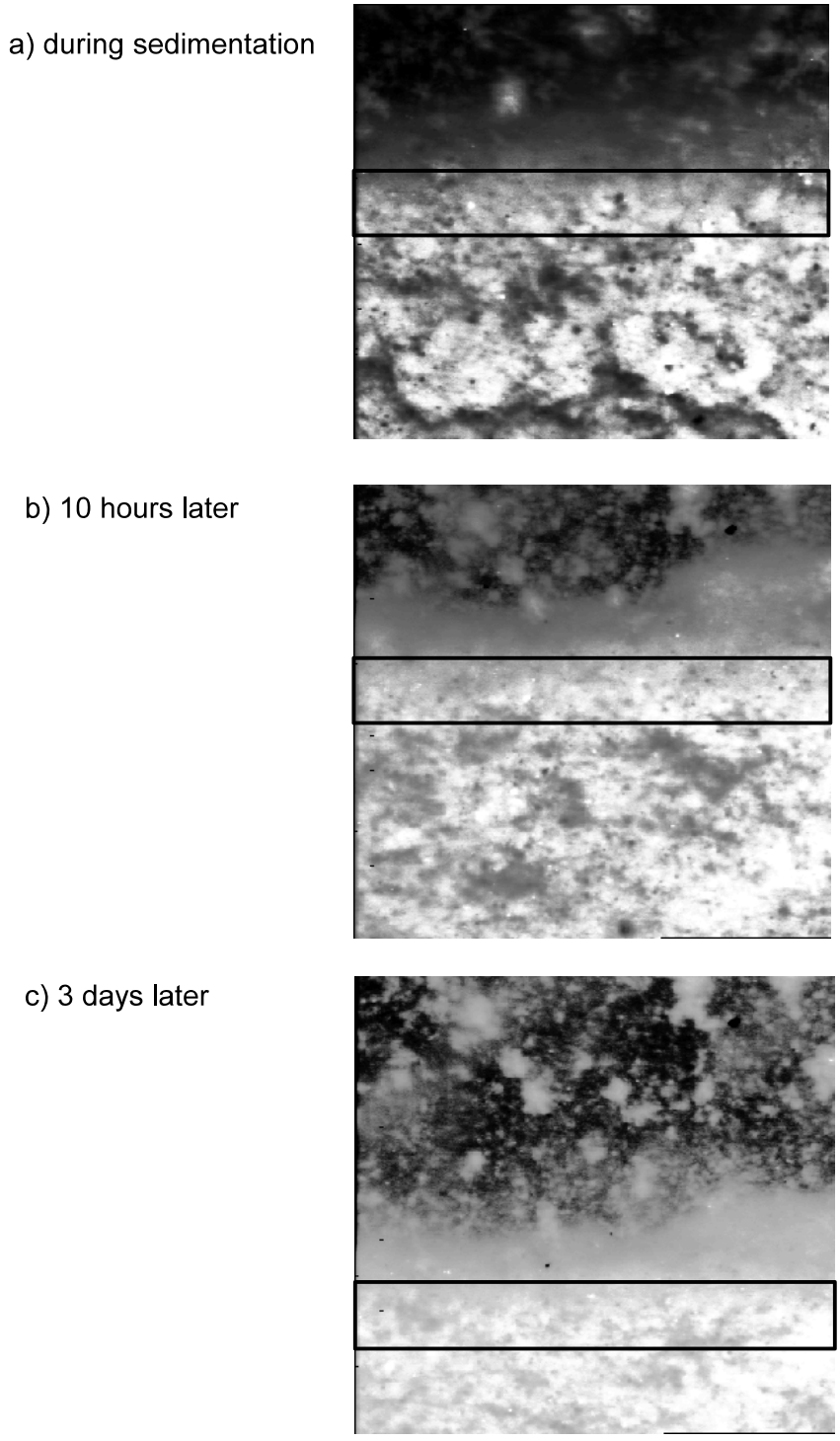

Figure 5.13 Automated tracking of the bed surface, experiment cos17.

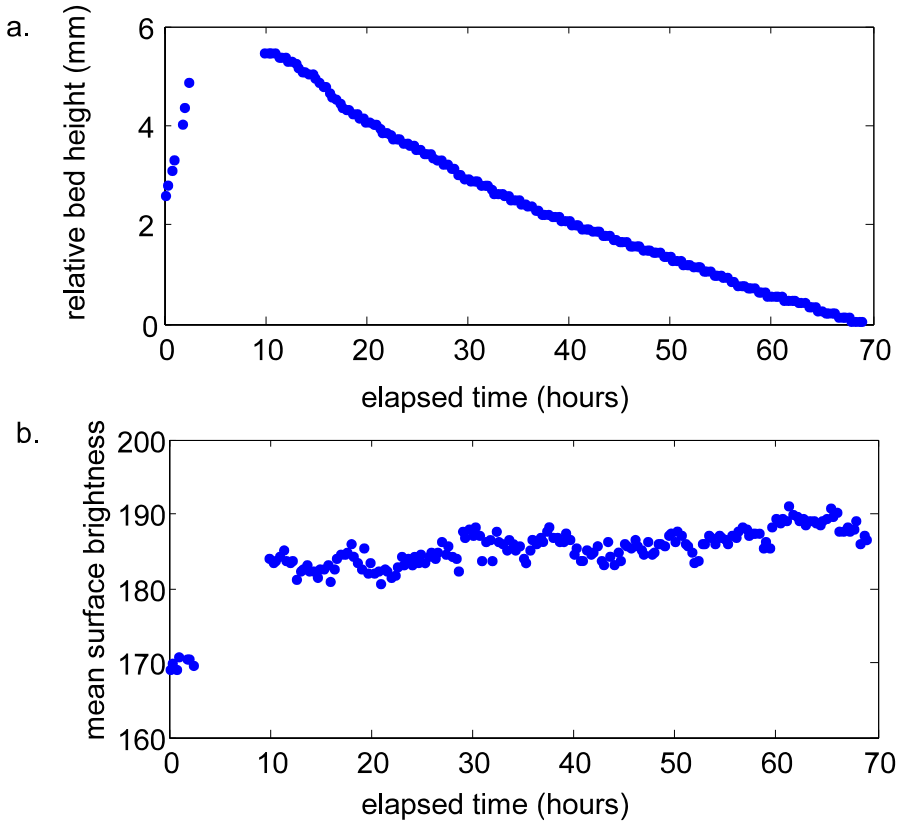

Figure 5.14 Surface brightness and relative surface height (see text) over a period of sedimentation and settling for experiment cos17.

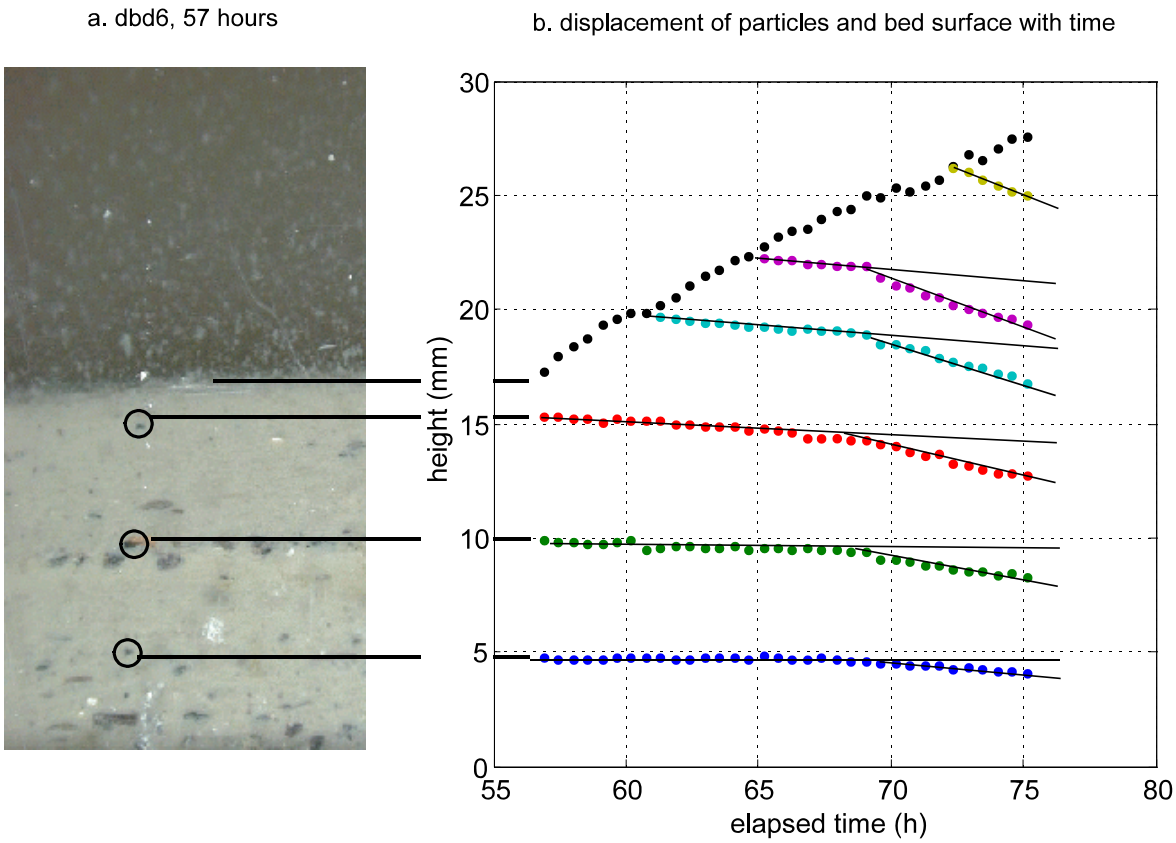

Figure 5.15 a. Particles of organic matter in the bed of dbd6. b. The circled particles have been followed in time.

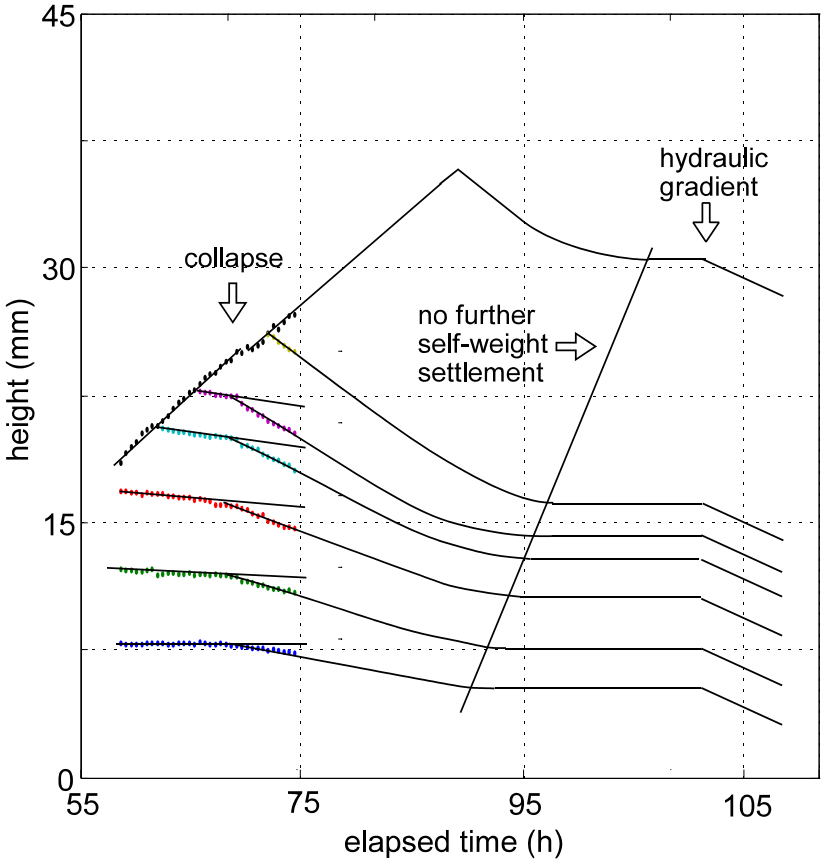

Figure 5.16 Proposal of bed settlement based on observations from time-lapsed movies, and starting with data from experiment dbd6.

Chapter 6 Bed formation - internal measurements

It has been shown in the previous chapter that a bed formed by slow sedimentation differs markedly in appearance from one formed out of a settling a slurry. The two also settle and consolidate different amounts, with the slurry often forming a more compact bed than a more slowly deposited sediment. It has also been shown that differences in the rate of the slow sedimentation can influence the pore space, measured as a ratio of bed height to mass of solids.

Few studies have been made with slowly or steadily sedimented cohesive sediments. And of these, only a handful have examined the bed processes in detail (Sills and Thomas 1984; Torfs *et al.* 1996; Gonzales and Sills 1997). This chapter describes the characteristics of a settling bed. It includes beds which have been formed both by the slurry method and by the slow sedimentation method. It goes on to describe the soil properties in terms of void ratio, effective stress, material coordinates, and bed shear stiffness and strength. Specifically, this chapter aims to find a relationship between void ratio and effective stress, and to follow the development of this relationship in terms of time dependent behaviour.

6.1 Density profiles

The use of xrays to measure bed densities has been introduced in Chapters 1 and 2. The methodology involves a xray source and xray photomultiplier (receiver) on opposite sides of the column. These are raised and lowered to provide a vertical profile of the xray intensities that pass through the column. With calibration techniques these xray intensities can be converted to density.

Different methods of sediment input produce characteristic differences in the density profiles (Figure 6.1). The experimental details are given in Table 3.3. Figure 6.1a shows a series of density profiles over time as a bed consolidates from a Tamar slurry. The first profile (0 hours) shows the density of the input slurry to be just above 1.15 Mg/m^3. As time passes (5 hours), the sediment water interface (top surface) of the suspension settles, while a region lower in the column becomes more dense. As no mass is added or lost, the area

under the curves must remain the same so that the amount of settlement is counterbalanced by the increased density, or vice versa. After some time (or more correctly, some density) is reached the consolidation abruptly slows down, thus in the figure the settlement between 27 and 170 hours is only twice the settlement that took place in the first 5 hours.

Figures 6.1 b and c show the development of densities following a period of much slower, and controlled sedimentation of Tamar sediment. The experiment cos1 provides an excellent example of the structural changes due to varied sedimentation rates (Figure 6.1b). In this experiment the sedimentation rate was varied between extremes of very low input followed by very high input rates, with a mean sedimentation rate of around 10mm per day, for 10 days. The bed has consolidated while being deposited. Therefore there is very little settlement occurring at the mud water interface and there is comparatively little change in density with increasing time in this experiment.

As a result of the variable sediment input rates, peaks of high density can be seen to be separated by less dense regions, at intervals of approximately 10 to 20 mm. The mud was subsequently extruded from the column, and it sheared spontaneously into distinct segments as shown in Figure 6.2, with the shearing surfaces corresponding to the 10 to 20 mm intervals that were apparent in the density profile. Grainsize analysis found no difference associated with the layers, suggesting that these surfaces of weakness were not a consequence of grain sorting during each burst of sedimentation. They must, therefore, have been due entirely to the different sedimentation rates. Thus not only have the sedimentation conditions (and therefore flocculation conditions) affected the bed density but they have had a profound effect on bed strength. As cos1 was the first experiment to be conducted using a controlled rather than a slurry sedimentation this was an encouraging result towards the remainder of the research. In fact, the bed structure proved to be so sensitive to deposition rate that variations occur in all of the subsequent steadily deposited beds, even with very slight differences in sedimentation rate.

In experiment wsm1 (Figure 6.1c) mud from Weston Supermare was sedimented at a controlled constant rate of around 400mm per day for nearly one day. Since the sedimentation rate was rapid the sediment water interface continues to settle and the beds

continue to become considerably more dense after sedimentation is stopped. That is they continue to consolidate since the excess pore pressures have not fully dissipated. Sedimentation was more steady in this experiment, so variations in the bed density are not as marked as in experiment cos1.

Hydraulic Gradient

For the wsm1 experiment just described a hydraulic gradient was applied immediately before wsm1g, 764 hours after the start of the experiment. This has the effect of increasing the consolidation, leading to higher densities, as shown in Figure 6.3a. At first this hydraulic gradient affected only the lower part of the bed (wsm1g), and within 2 days it worked its way up to above the middle of the bed. As mentioned in Chapter 2, the strength of the hydraulic gradient is limited by the distance between the bottom of the bed and the drainage outlet. In wsm1 the effective stress at the base of the soil bed was increased from around 0.2 to slightly over 4 kPa.

A bed with more variation in density is plotted in Figure 6.3b. This experiment shows density profiles from experiments dbd2, an experiment on Dibden Bay silt for which considerable floc information has been presented in Chapter 4. The sedimentation rate for dbd2 was approximately 6.2 mm/day, although this varied leading to quite considerable fluctuations in the density profiles. Profiles dbd2a and dbd2d show the self-weight consolidation process, with the latter taken immediately after sedimentation had finished. The last two profiles, dbd2e and dbd2f, show the effect of a hydraulic gradient, which has increased the effective stresses at the base of the beds from approximately 0.4 kPa to 9 kPa. It can be seen that, once established, density variations continue to be clearly visible, even after significant further loading. This important result is verified in all experiments in which the input rate varied, even following an order of magnitude increase in loading.

Figure 6.4 shows the bed of cos4 (Tamar mud) 60 hours after the start of sedimentation, and again at 372 hours when sedimentation was complete. For this experiment, the bulk density of the bed has been calculated using samples of known density to calibrate the xray counts. The excess pore pressures remained near zero for the entire length of this experiment since consolidation was occurring at a rate faster than deposition. The dotted

line indicates that sedimentation is still underway. The profile for the earlier bed shows that the bed can develop a structure below 1.15 Mg/m^3. The density of the earlier bed is increased as more sediment is placed on top of it up to nearly 1.2 Mg/m^3.

Similar data is shown for experiments cos13 in figure 6.4b. The profiles again (dotted lines) show that the bed density increases during deposition. The last profile, at cos13h occurs after sedimentation is complete and the surface is settling. The density throughout the bed continues to increase despite no further loading of sediment through consolidation behaviour.

6.2 Void ratio, effective stress and time correlations

Terzaghi (1936) suggested that the structure and behaviour of a soil is uniquely associated with the effective stress conditions. As a measure of structure, soil mechanics often uses the void ratio, e, or the porosity, n. Following the analysis made by Sills (1995) and Sills (1998) the forthcoming section interprets the data in terms of void ratio, effective stress and time relationships.

Figure 6.5 shows an example of pore pressure measurements taken during experiment dbd1. These are shown as excess pore pressures, that is the pressure minus the hydrostatic gradient. Immediately after deposition (dbd1a) the excess pore pressures are at their highest values as the beds consolidate. These gradually dissipate to 0 kPa (or near 0 kPa) by dbd1d. After this, a hydraulic gradient is applied and the pore pressures become negative, particularly near the bottom of the bed. The vertical effective stress, F', at a height in the column can be calculated by subtracting the measured pore water pressure from the total vertical stress, which is obtained by integrating beneath the density profile. The void ratio can be calculated from the bulk density at a specific height and the specific gravity of the soil. This provides points to create a void ratio - effective stress correlation.

Figure 6.6 shows a series of these void ratio - effective stress correlations for experiment cos3, on Tamar mud. The average sedimentation rate for this experiment was 3.2 mm/day over 380 hours (approximately 16 days). The time elapsed since the start of the experiment

is marked in the legend. Profile cos3a, at 380 hours, was taken at the end of the sediment input stage. The results show, as expected, a decrease in void ratio with an increase in effective stress. However the correlations also show a significant downward movement with time. Thus, the data contrasts with that of a traditional soil mechanics approach, normally studied at much higher stress levels, in which a particular soil has a unique relationship between void ratio and effective stress, independent of time.

The same type of correlation is shown for cos16, an experiment which also used Tamar mud, but with a much higher deposition rate at an average of 181 mm/day (Figure 6.7). In this case, the decrease in void ratio at constant effective stress is enhanced for the self weight correlations cos16a to d (note the larger vertical axis scale and the smaller time interval on this figure as compared to the previous one). The last correlations displayed, cos16g, illustrates the effect of a hydraulic gradient applied to increase the effective stress range from 0.4 kPa to around 3.2 kPa.

The void ratio effective stress correlations are shown for experiment dbd2 in Figure 6.8. In this experiment Dibden Bay mud was deposited at an intermediate rate of 6.2 mm/day. The correlations under self weight consolidation (dbd2a to dbd2d) reach a minimum void ratio of approximately 4. However under a hydraulic gradient (dbd2e and dbd2f) the void ratios are decreased further to less than 3 at the base of the column. Again, under self-weight consolidation (regardless of effective stress) there is strong evidence of a time dependancy. However, for the Dibden Bay mud at intermediate sedimentation rates this is not as prevalent as it was for the Tamar experiments just shown. This figure shows clearly that variations in void ratio, caused by variations in sedimentation conditions, continue to be visible under an order of magnitude increase in effective stress, as was also apparent in the density profiles.

A final void ratio - effective stress plot of this type is shown for experiment cmw1, which used Combwich mud (Figure 6.9). The sedimentation period stopped after 22 hours, when the first bed measurements were made. The initial void ratios were very high, over 17. Elder (1985) confirms these high values (up to 20) for experiments using Combwich mud. The correlations following the initial curve show that time dependancy is very marked. In

this experiment a hydraulic gradient was applied at 264 hours, first by using a peristaltic pump to remove the water from the bottom of the bed and then by the Mariotte bottle method, which increased the effective stress from around 0.4 kPa to over 10 kPa.

The examples above show clearly that the void ratio behaves in a time dependant manner for each of the soils studied. This occurred in all of the slowly deposited beds. This behaviour has been observed previously (Sills 1995), and suggests the occurrence of creep. The experiments reported and referenced in that paper are slurry experiments, and the decrease in void ratio over time was normally not as large as the decrease seen in the slowly deposited beds above. In fact, most slurry experiments show comparatively little signs of creep. The increased creep shown in the slowly deposited beds is probably due to the collapse of the aggregates that was described in the last chapter.

The data in the previous figures can be utilised more appropriately by plotting the changes in void ratio at a specific soil horizon throughout the experiment. The Eulerian coordinates of the settling bed are transformed into material coordinates. Since no mass is added after sedimentation has stopped, the material coordinate is taken as the proportion of sediment mass above a specific soil horizon to the total bed mass. This is calculated by normalising the excess total stress above the soil horizon with the overall excess total stress, and therefore may be referred to as the normalised excess total stress, or 0. This allows a specific soil horizon to be observed throughout the length of the experiment. A result of this conversion is shown in Figure 6.10 for experiment dbd2. The void ratios at any given time are decreasing overall from the top to the bottom of the column (with increasing 0). And since the bed is consolidating with the pore pressures and effective stresses changing for constant values of 0, the void ratios are decreasing from one time to the next. The triangles shown in the figure are used in a later section. A hydraulic gradient was applied to this experiment at times dbd2e and dbd2f, which had the effect of decreasing the void ratios, particularly at the bottom of the bed where the increase in effective stress was greatest. The figure again shows that the variations caused by deposition conditions remain through consolidation, and through the application of a hydraulic gradient.

The data points for specific material coordinate may be followed through time, as shown

for several experiments in Figure 6.11. The void ratio at each of the material coordinates decreases over time, showing the combined effects of consolidation and creep, at all material levels in the bed.

In slurry experiments, or in experiments where there is no variation in structure with depth, the void ratio - time curves for higher values of 0 would lie below those for lower values of 0, and these curves would not intersect one another. This is because the void ratios at the material coordinates towards the top of the bed are normally expected to be less than the void ratios lower in the bed. This is the case in Figure 6.11b and c, except for very few points. However, experiment dbd2 had considerable variation in the bed, and so some of the curves in figure 6.11a lie 'out of sequence' revealing that it is possible to get higher void ratios deeper in the bed. More importantly, however, these curves sometimes intersect one another, which indicates that different rates of deformation are associated with different bed structures.

Analysis of peaks and troughs

Analysis of slurry or very steadily deposited beds, where the bed structure does not vary, allows the time and effective stress components of consolidation to be separated. In that case, it is expected that the void ratio of the material coordinates from near the top of the bed will always lie above those from the further down the bed. However, in the case where there is variation in the bed the void ratio will also be a function of this difference in initial structure. As seen in figure 6.11 a higher value of 0 can lie above the lower values of 0 due to this initial variation in void ratio. Normally the higher values of 0 in these lower beds are brought lower under a hydraulic gradient since it is the lower bed which is more immediately and more prominently affected. For the highly variable beds a different technique is needed. It is possible to select values of 0 that correspond to peaks and troughs in the void ratio-material coordinate plot, and then follow these through effective stress and time to get boundaries within which a soil behaves. Experiment dbd2, with few but large variations in void ratio throughout the bed, provides an excellent set of data to determine how well these structures are maintained throughout the experiment.

The triangles in Figure 6.10 represent the peaks and troughs. Since these are material

coordinates, the peaks and troughs should lie directly below one another at each increment in time. However it is seen in the figure that some adjustment is made manually (ie. the triangles are not vertically aligned) in order to locate the maximum and minimum of the peaks and troughs. This is due to the accuracy of the measurements . This accuracy of the x-axis is much more important for experiments which are highly variable on the y-axis, than for experiments that have much gentler variation, such as slurry experiments. Aligning the curves by using the normalised excess total stress simply provides an easy method to match positions of the peaks and troughs at various times in the experiment. The effective stress, rather than the normalised excess total stress, and the void ratio may then be read from the data at these positions. It is beneficial to use 0 to find the void ratio and effective stress values at certain bed structures, since it is often difficult to define exactly where these structures are located on a void ratio effective stress plot, and is even more difficult to trace the position of the structures through time as the curves become deformed. For example it is difficult to track a single peak over time directly from Figure 6.8, particularly after a hydraulic gradient is applied. It is much more clear in Figure 6.10.

The material coordinates in Figure 6.12 have been defined by the location of the troughs only. The curves from the troughs only are less likely to intersect one another, and those with higher material coordinates (lower in the columns) are more likely to lie below those from more shallow curves. There is no way of knowing from the data where the possible physical lower boundary of these curves lies. However, using the troughs is perhaps more sensible than using arbitrary values, since at the very least it can be said that these data are approaching the lower boundary of the possible void ratios.

In the manner described above the bottom of the troughs have been selected from the void ratio - material coordinates plots for experiments dbd2, cos16 and cmw1. The void ratio and effective stress data from these troughs are shown in Figure 6.13, in which the same scale of void ratio is used for each of the three soils. Again, Dibden mud (Figure 6.13a) undergoes less time dependent strain than either the Tamar mud (Figure 6.13b) or the Combwich mud (Figure 6.13c). The latter is most affected by time, confirming similar onservations for Combwich slurry experiments reported in Sills (1995).

It is interesting to show the lower boundary of the void ratio - effective stress plot for each of the muds. (Figure 6.14). There is no reason to suspect that different soils should behave along a unique path, so a more sensible comparison between soils can be made by normalising the soils in terms of a volumetric parameter of some sort. Liquidity index is one possibility, while another is void index, described by Burland (1992). This is the topic of a section in Chapter 8.

6.3 Development of stiffness and strength

Bender element stiffness

The most complete bender element tests were made on the Dibden Bay experiments. Figure 6.15a and 6.15b show the received shear wave signals at the times of xray profiles dbd1a through dbd1l, and dbd2a through dbd2f. The waveforms start out very weak. There appears to be some trace of an arrival wave in experiment dbd1d at approximately 0.020 seconds and in experiment dbd2a at approximately 0.019 s. As the bed stiffens, the signal generally becomes stronger and arrives more quickly. However in some instances, such as dbd1L, the amplitude weakens although the arrival time still quickens. In other cases, such as dbd2E, the shear wave nearly disappears altogether.

Figure 6.16 shows the shear wave velocities for experiments dbd1 to dbd3 throughout the lengths of the experiments. The bed heights have been overlaid on the figure. As only one set of bender element test equipment was developed, all three experiments could not be measured intensively during the settling stages. However, it was found that the shear waves did not appear to pass through the sediment until bed heights of at least 10 cm were achieved, approximately 6.5 cm above the bender element transducers. The velocities range from around 2 m/s at the start of the experiments to above 22 m/s after some consolidation has taken place. This is consistent with the data reported elsewhere for very soft sediment (see Chapter 1). Increases in effective stress created by the application of a hydraulic gradient (see arrows) had a very pronounced effect on shear wave velocity.

Shear stiffness G_{max} has been calculated for the developing beds in number of experiments using a rearrangement of equation 2.2:

$$G_{\max} = \rho V_s^2 \quad (6.1)$$

where D is the soil bulk density and V_s is the shear wave velocity.

The density of the bed surrounding the bender element has been used in Equation 6.1 to calculate the stiffness, G_{max}. Rather than selecting a density at a specific height (approximately 3.5 cm at the centre of the bender elements), an average density over the width of the bender element has been used (ie 3.25 to 3.75 cm). This is because it is unknown whether small variations in density at this scale of mm in height are true or due to accuracy of the x-ray. Figure 6.17 shows that the stiffness is considerably higher at lower void ratios.

Figure 6.18 is a plot of effective stress vs. G_{max} for all three Dibden experiments. The pattern of results appear to show that shear wave transmission begins to be possible as effective stresses develop. That is, the very low stiffnesses are associated with the very low effective stresses. This is not a straight forward relationship, due to the variations of density that occur in the beds independent of effective stress. It appears that the shear modulus plays a similar role to that of effective stress in monitoring the development of structure in the soil bed, and may provide a useful tool in this respect for future research.

Shear vane strength

Cohesive beds are non-Newtonian in behaviour. That is, a shear stress exerted on a mud bed is not proportional to the induced shear rate. This property has been examined on natural muds in a number of cases (eg. Merckelbach 2000 and references therein). It is also extensively studied in industrial fields by rheological techniques where management of sludges is important (eg. Yen et al., 2002 and references therein). Mud beds are also thixotropic - their internal structure collapses with time and shear rate. If a constant shear stress is applied using a vane the mud has an initial strength able to withstand the shearing forces. As this ‘peak’ strength is surpassed the vane then turns more easily and is opposed only by the ‘residual’ strength of the mud.

Vane strengths have been measured near the top and near the bottom of the bed for the

three Dibden Bay experiments. The results are shown in Figure 6.19. The soil shows clear differences between peak and residual strengths, at least some of which may be attributable to the unloading caused by removing the hydraulic gradient. The higher strengths are clearly associated with the beds consolidated to higher stress levels, at the bottom of the columns.

6.4 Conclusions

This chapter has described the general behaviour of both slurry beds and flocculated beds. A number of interesting features have been observed in beds developed from flocs.

- Variations in sedimentation rate, even if slight, lead to large variations in the structure of the beds as revealed by density profiles and void ratio values
- Variations in bed structures lead to variations in the strength of the bed
- The structure of the beds is not determined solely by the effective stress. Time dependent behaviour is apparent in all slowly deposited beds, particularly in the initial stages of consolidation
- Stiffness measured with bender elements may provide a means, other than effective stress, to monitor the development of bed structure

a. Slurry experiment

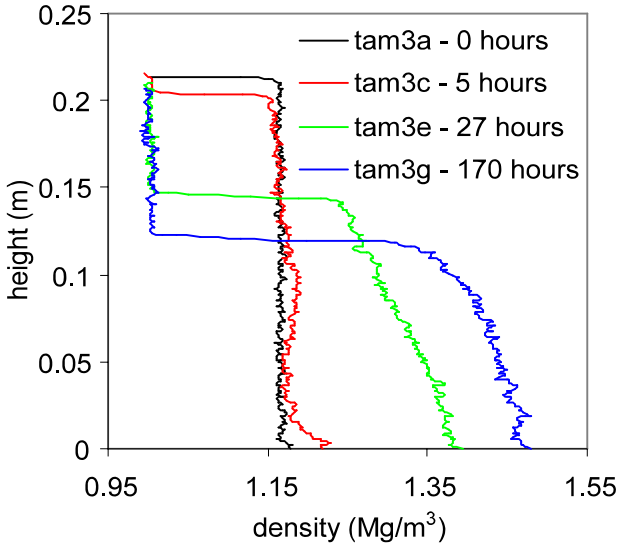

b. Slowly deposited experiment with variations in rate

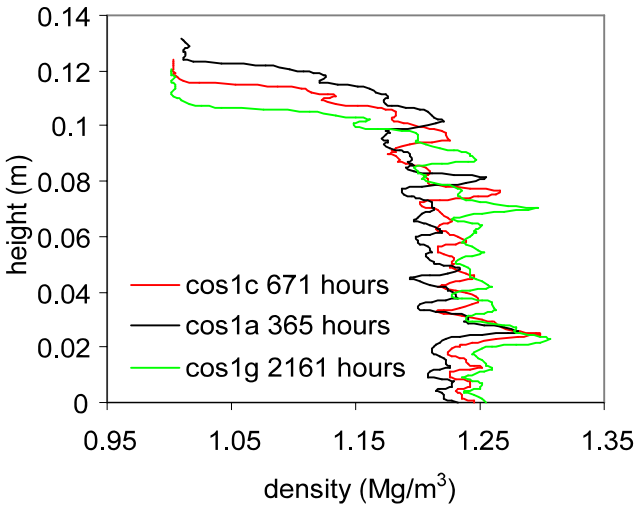

c. Intermediate deposited experiment

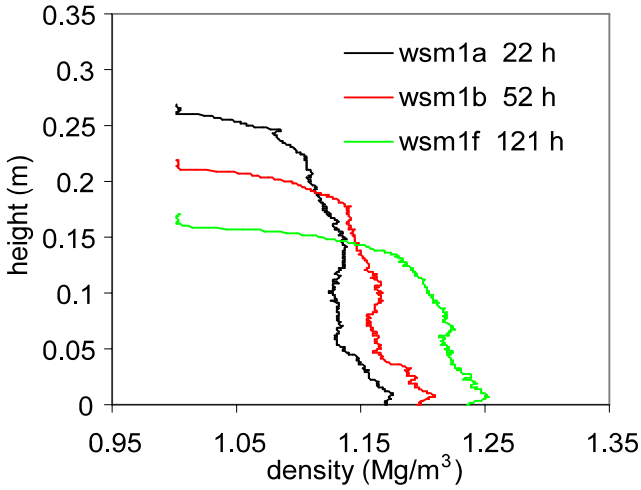

Figure 6.1 Density profiles for various types of experiments.

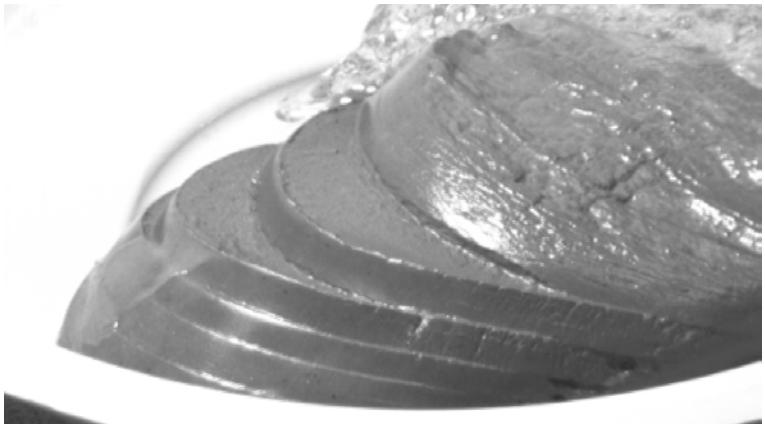

Figure 6.2 Plains of weakness (shear plains) developed by varying the sedimentation rate.

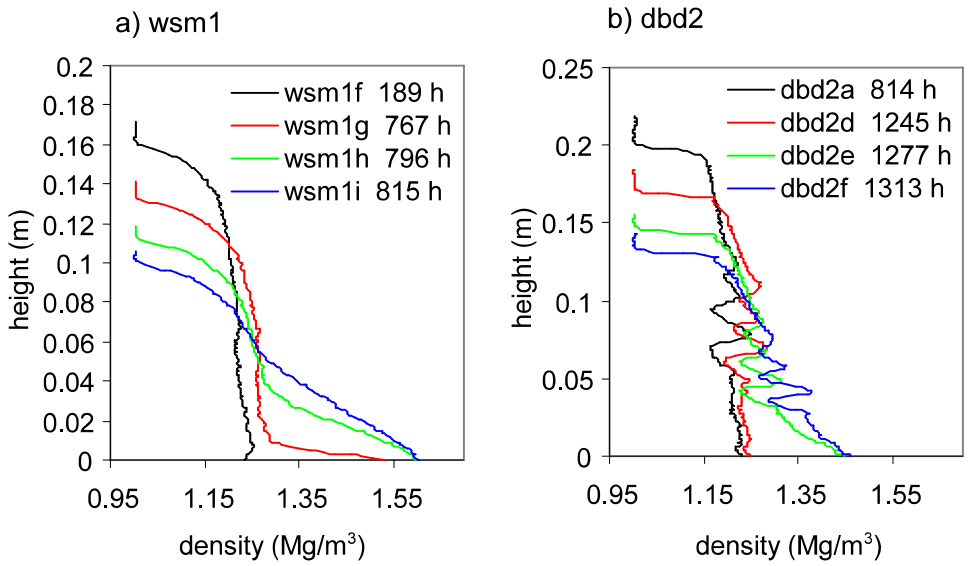

Figure 6.3 X-ray density profiles for experiments wsm1 and dbd2 showing the effect of a hydraulic gradient.

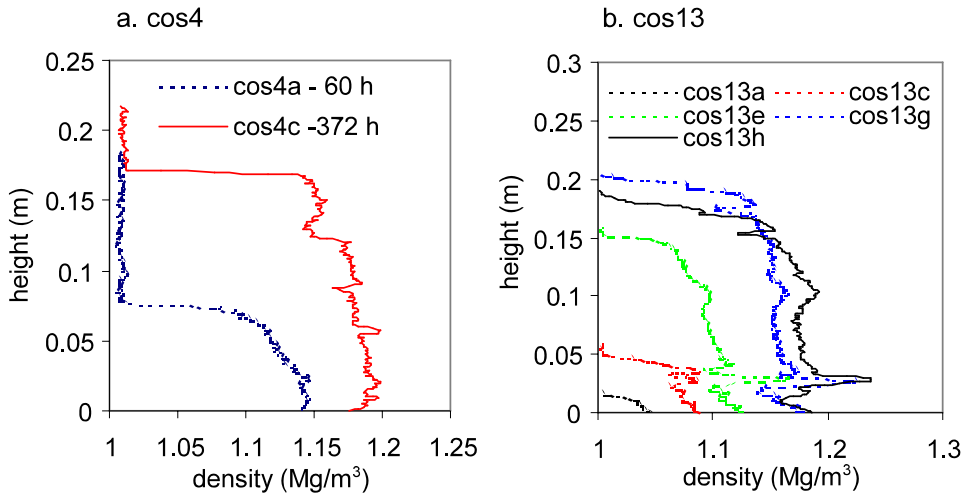

Figure 6.4 Density development during sedimentation for experiments a. cos4 and b. cos13.

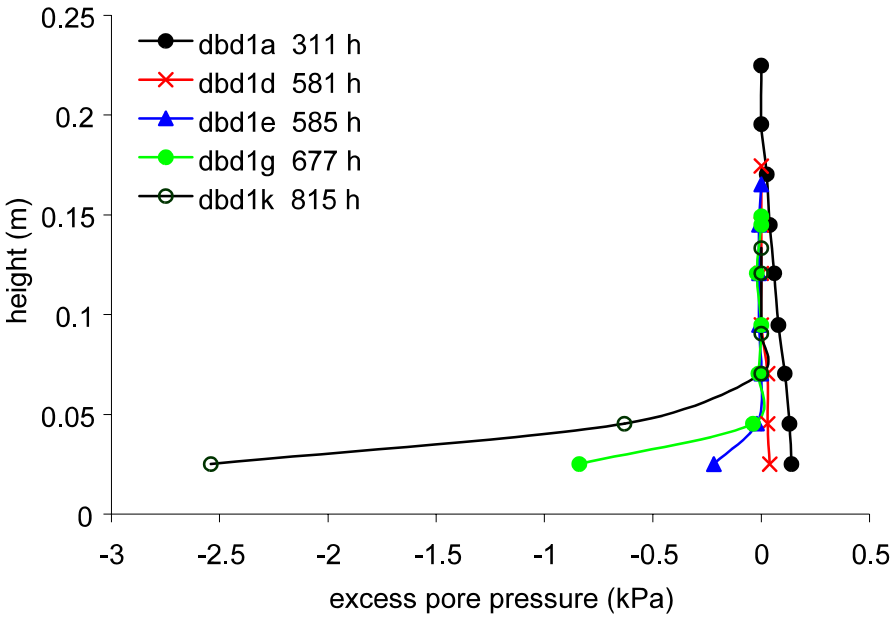

Figure 6.5 Pore pressure measurements from experiment dbd1.

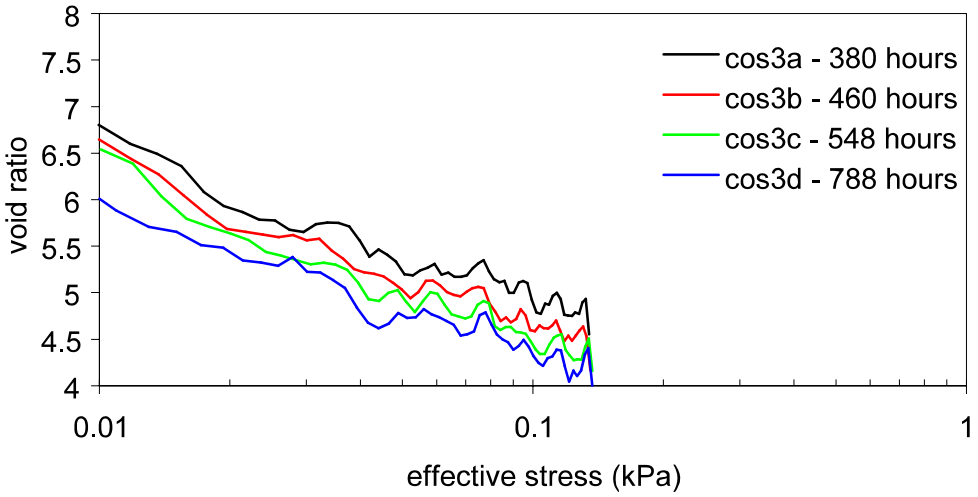

Figure 6.6 Void ratio effective stress relationship throughout experiment dbd3.

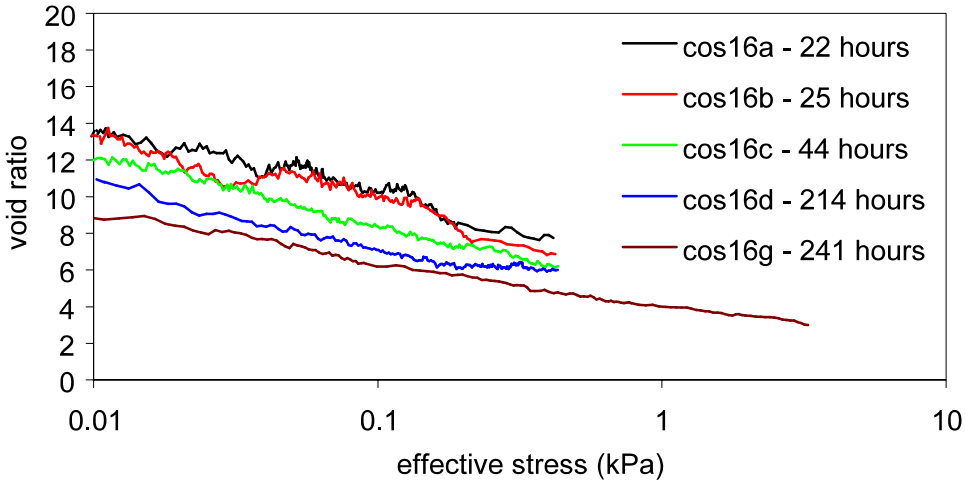

Figure 6.7 Void ratio - effective stress relationship throughout experiment cos16.

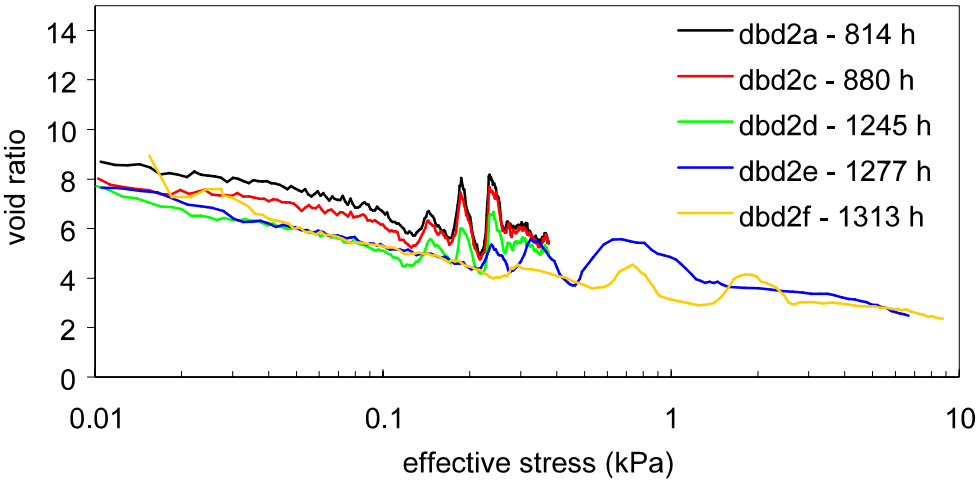

Figure 6.8 Void ratio - effective stress relationship throughout experiment dbd2.

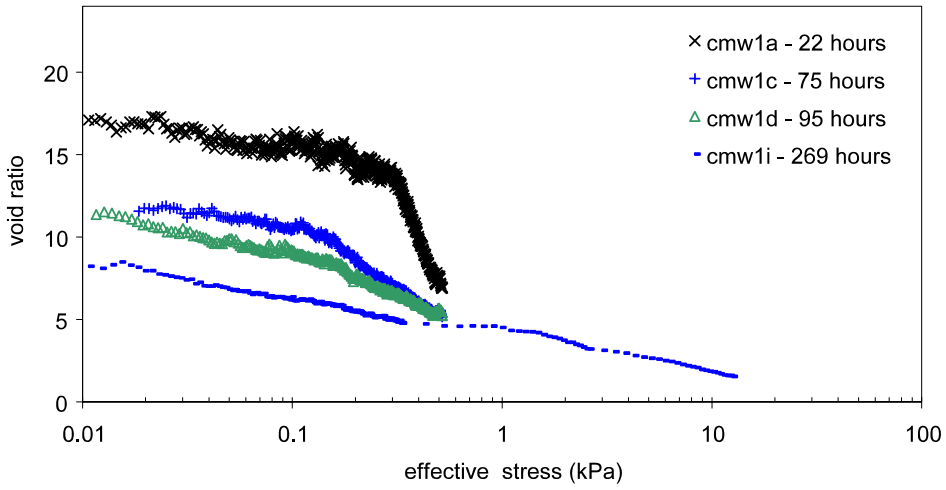

Figure 6.9 Void ratio effective stress relationship throughout experiment cmw1.

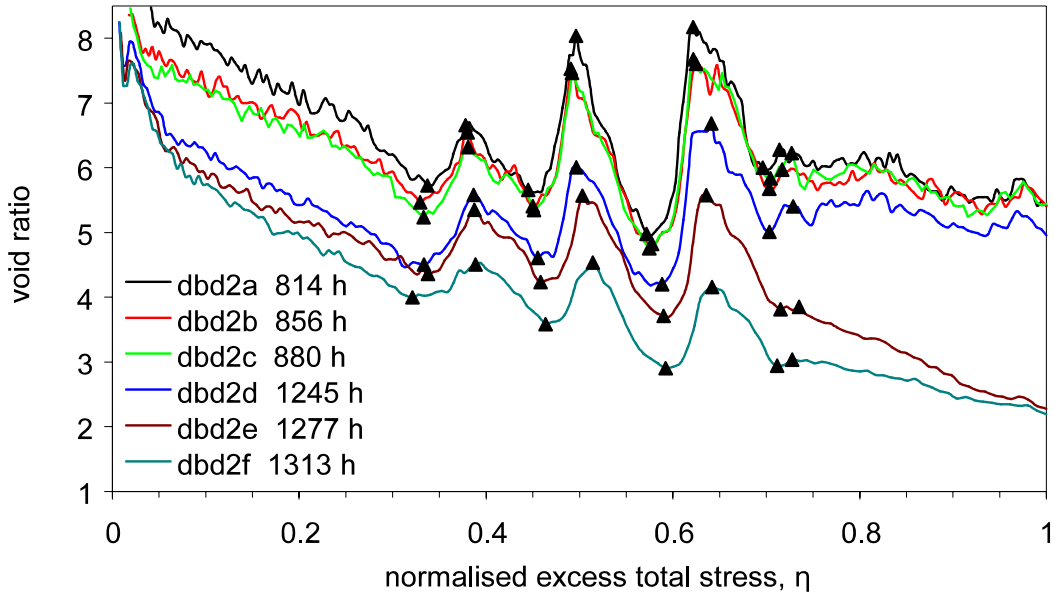

Figure 6.10 Void ratios at material coordinates for experiment dbd2.

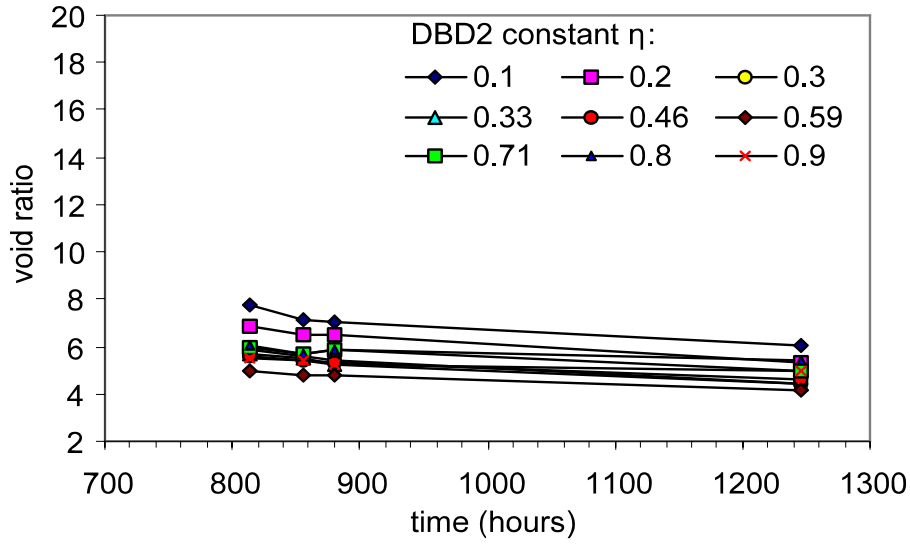

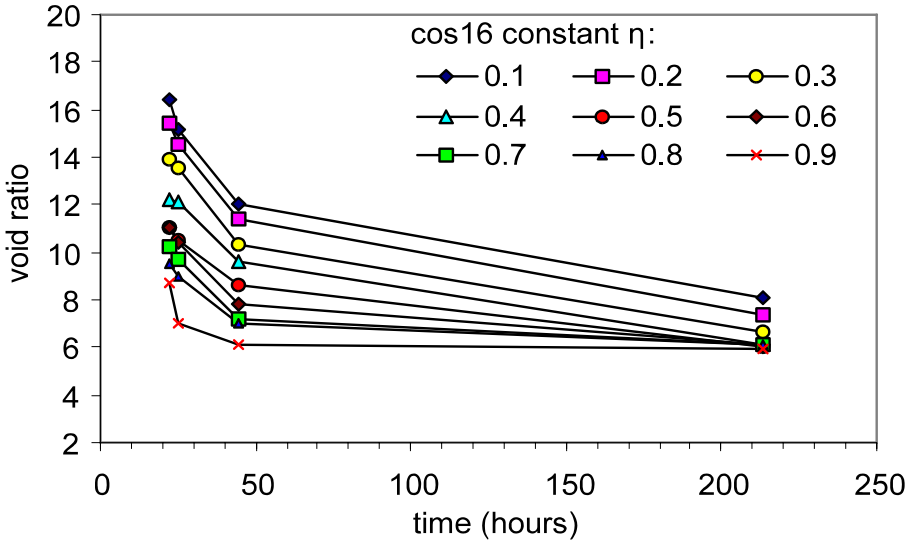

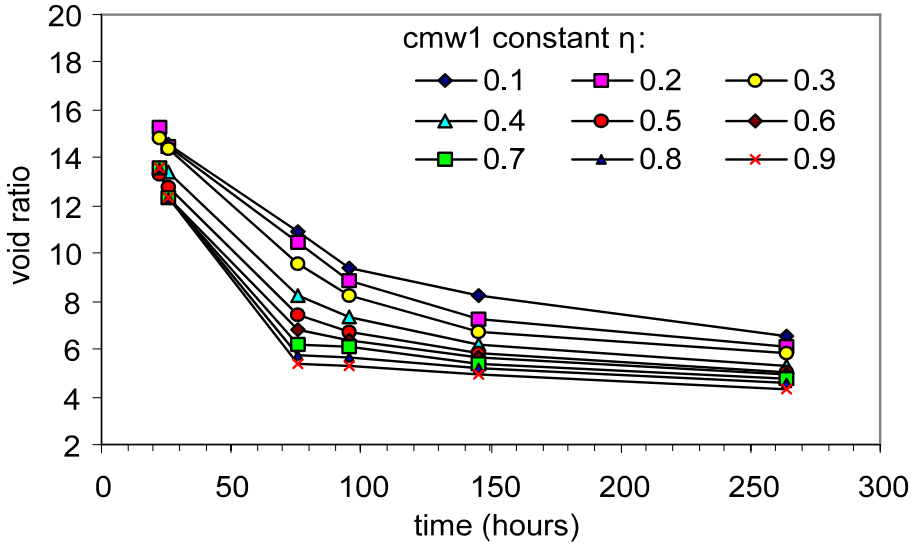

Figure 6.11 Void ratio versus time using material coordinates for experiments dbd2, cos16, cmw1.

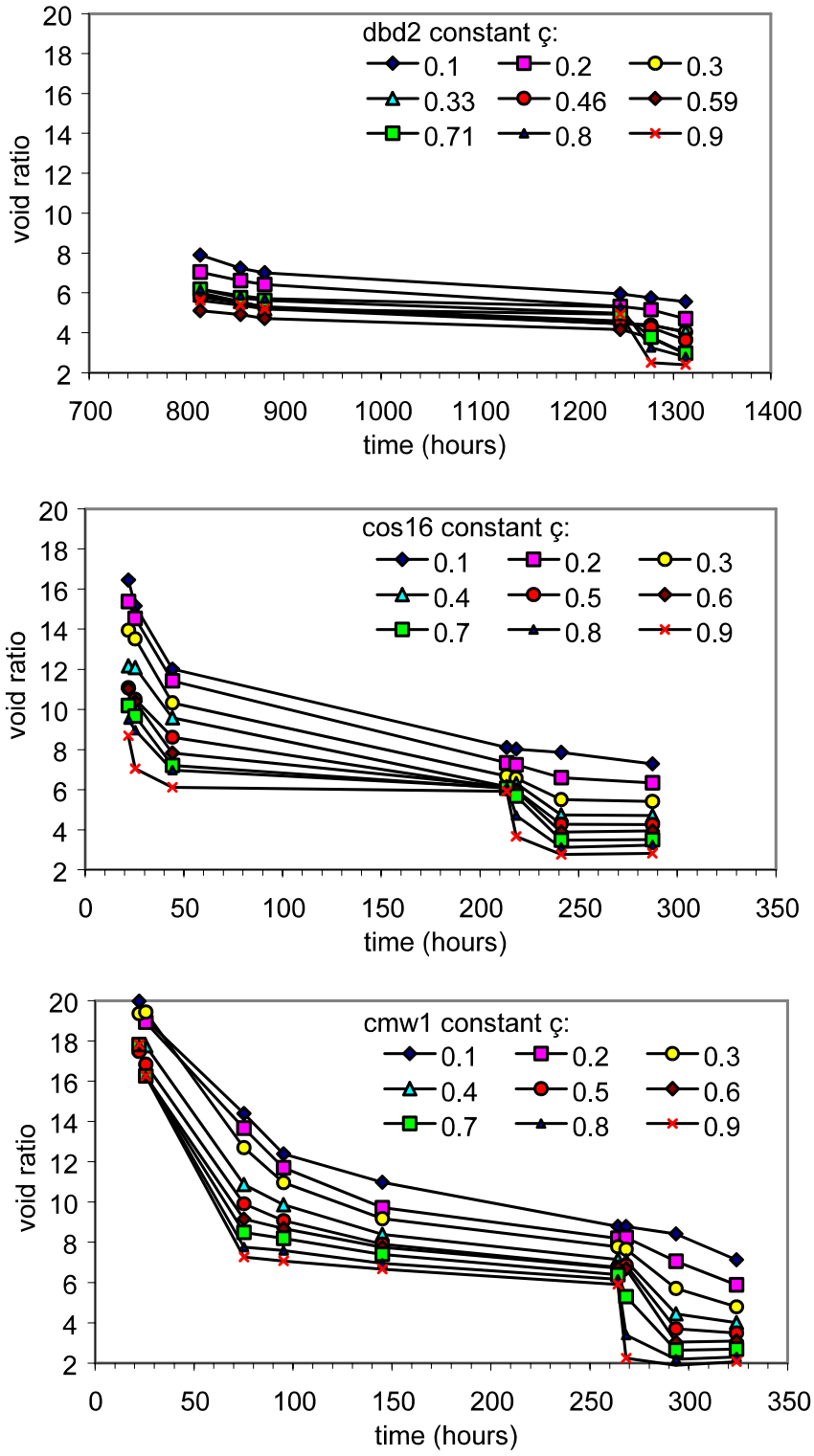

Figure 6.12 Void ratio versus time for the lowermost datapoints (troughs) in experiments dbd2, cos16 and cmw1.

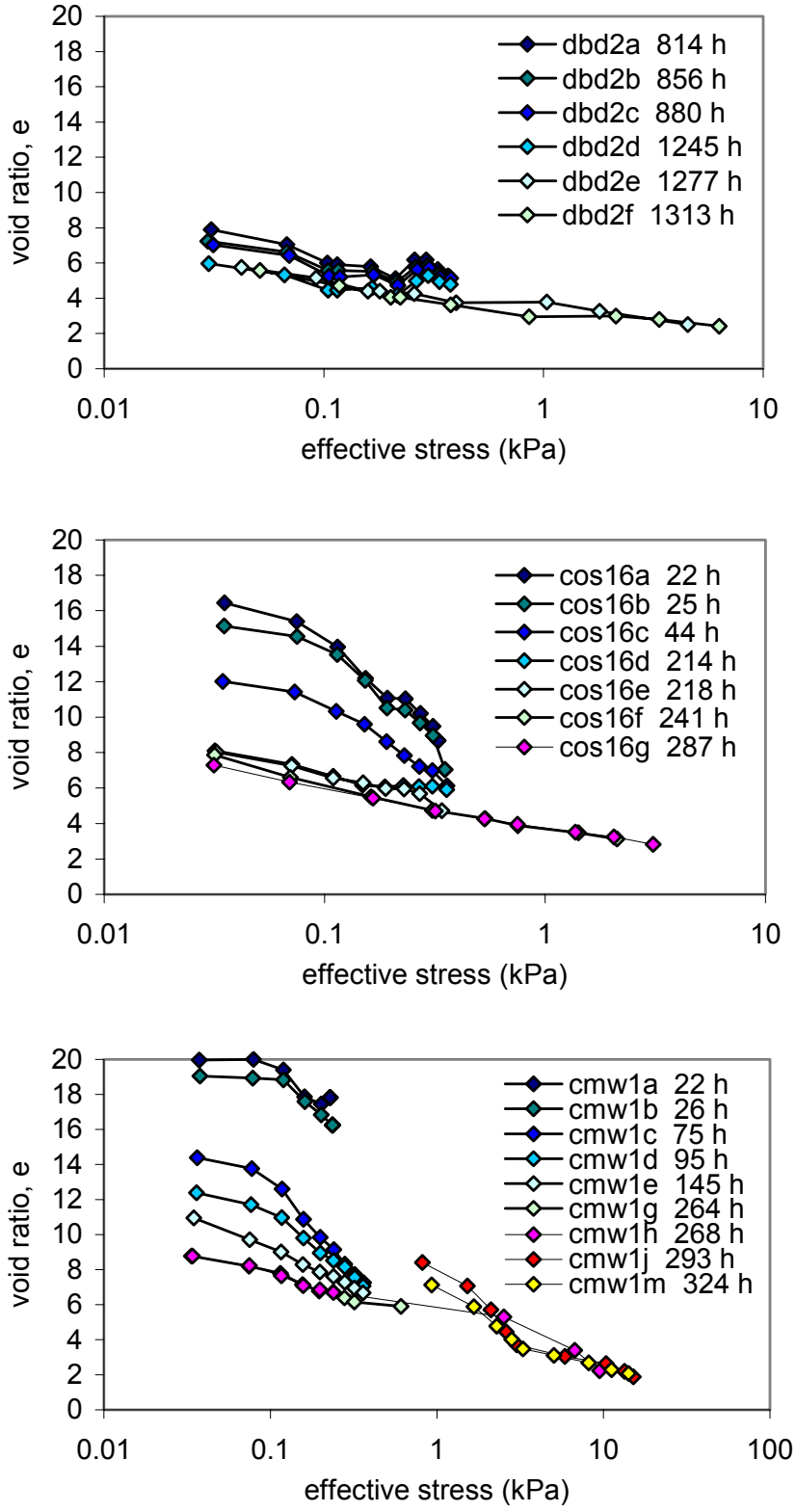

Figure 6.13 Void ratio versus effective stress for the lowermost datapoints (troughs) for experiments dbd2, cos16 and cmw1.

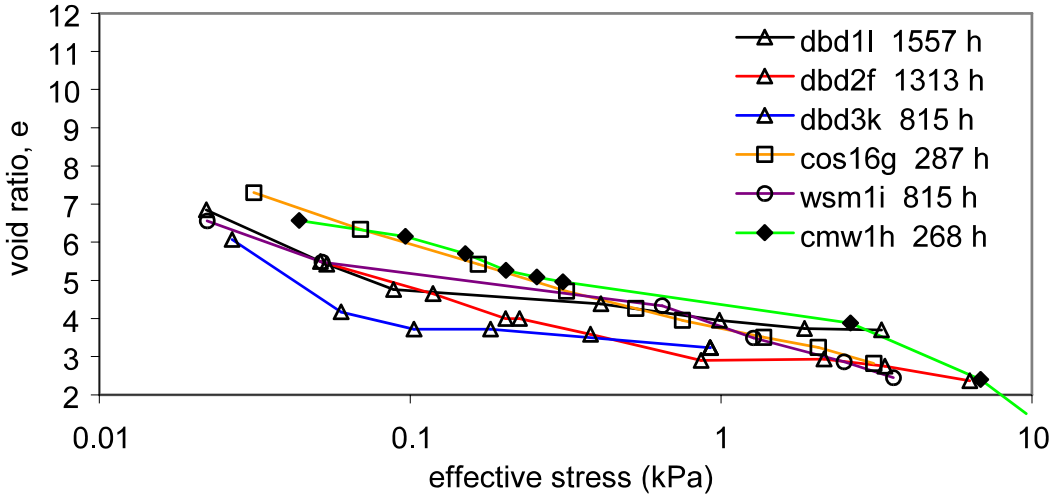

Figure 6.14 Lowermost position of the void ratio versus effective stress curves, taken from the last measurement in each experiment.

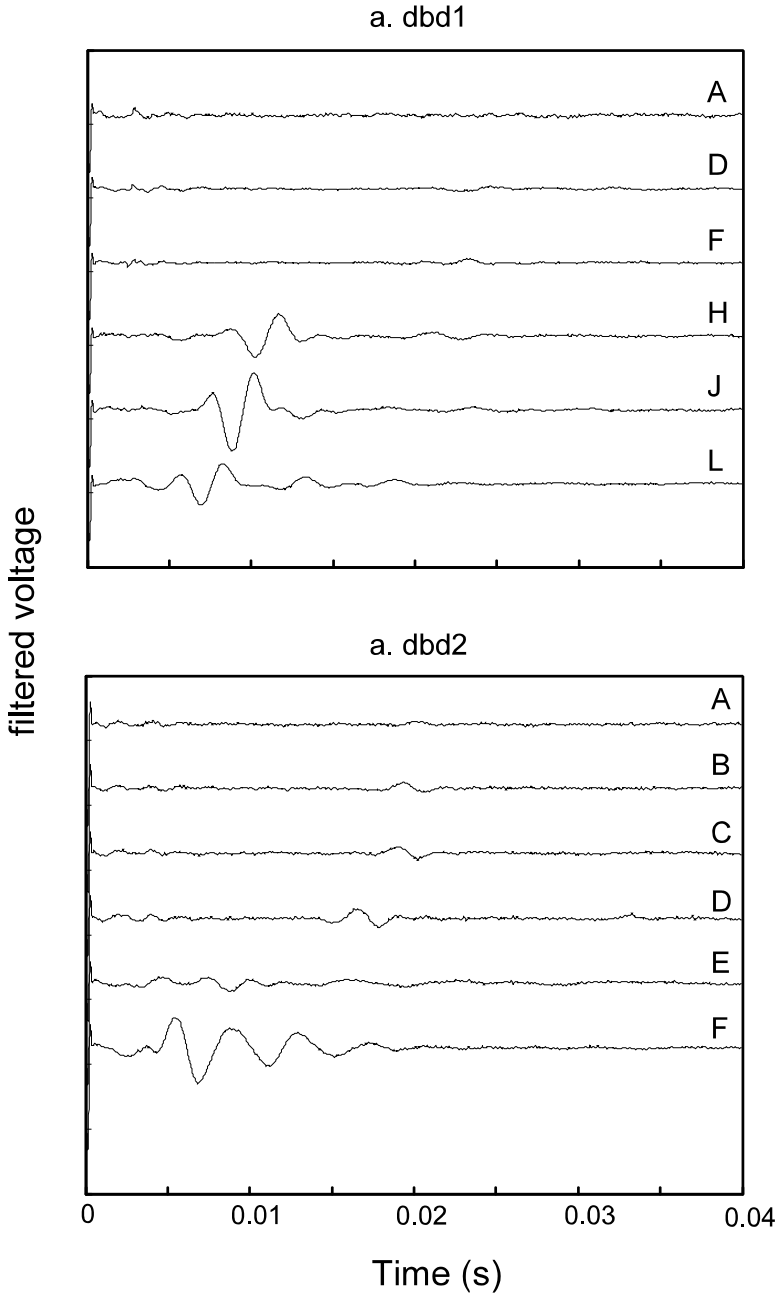

Figure 6.15 Shear wave arrival times at x-ray profiles for experiments dbd1 and dbd2.

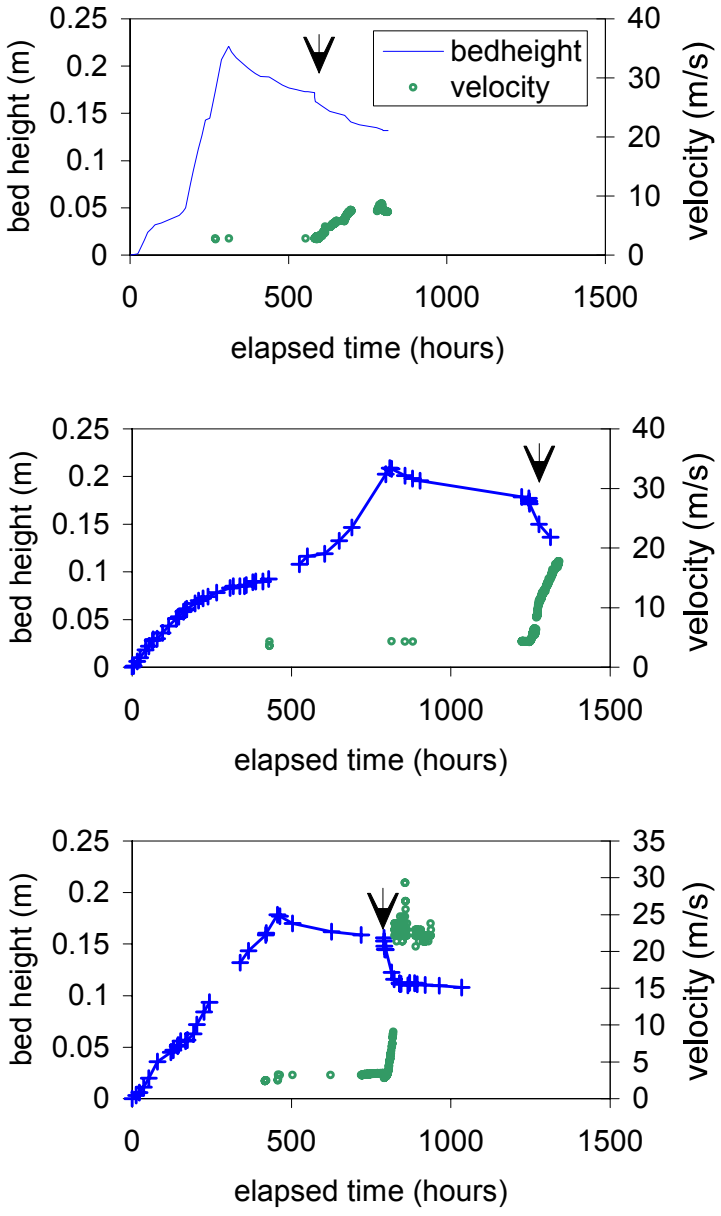

Figure 6.16 Bed height and shearwave velocity throughout experiments dbd1, dbd2 and dbd3.

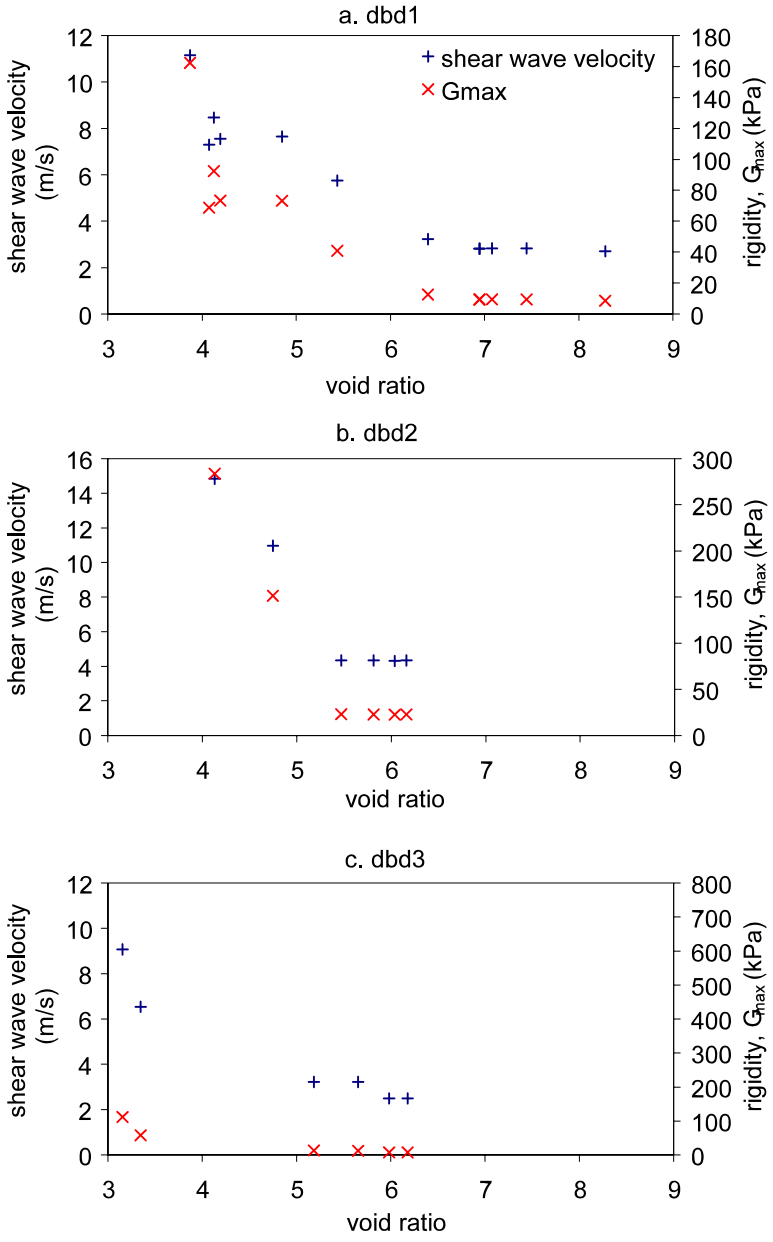

Figure 6.17 Shear wave velocity and rigidity versus void ratio.

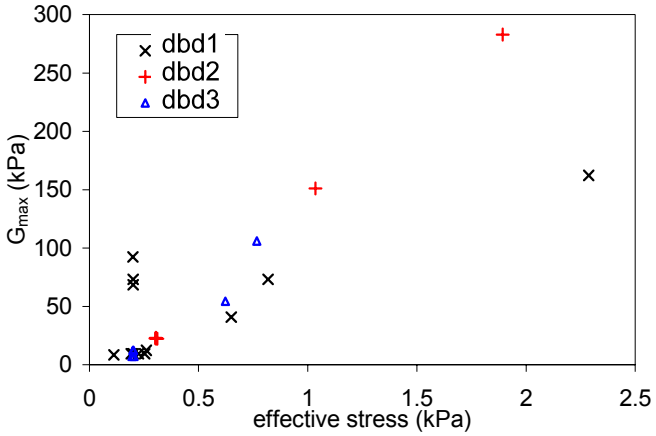

Figure 6.18 Rigidity versus effective stress for experiments dbd1, dbd2, and dbd3.

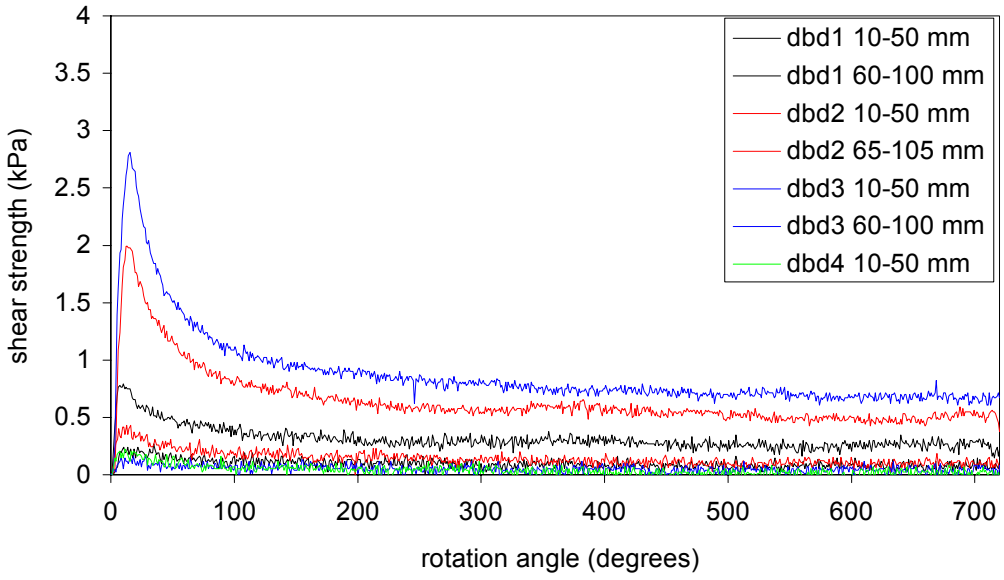

Figure 6.19 Results of shearvane tests near the bottoms and tops of experiments dbd1, dbd2 and dbd3.

Chapter 7 Erosion of Natural mud beds

7.1 Introduction

The x-ray facility makes it possible to examine the relationship between the bed characteristics and its resistance to erosion. It was expected that a longer consolidation time would lead to increased resistance to erosion, due to structural collapse of the electrically charged clay aggregates and due to bed cementation, or gelling. Krone (1999), for instance, reviews papers by Roberts *et al.* (1998) and Zreik *et al.* (1998). Both of these papers show that resistance to erosion is directly related to bed density, where the changes in density occur through time with structural alteration of aggregates.

However, it was noted early in this research, and by other investigators (G.C. Sills, personal communication), that natural muds in settling columns may be altered, sometimes significantly, by biological activity, particularly at the bed-water interface. Thus, it was biology, and not mechanics, that was influencing the erosion properties of the bed. This became a major discussion point in the COSINUS project, and was featured in many papers during the culmination of that project at the INTERCOH conference at Delft, The Netherlands (Winterwerp and Kranenburg 2000). As a result of the obvious need for research and the implications biological influences on the bed, the focus was shifted from a geotechnical to a biological perspective, but still with the use of geotechnical investigation tools.

Biological activity is generally thought to lead to increased resistance of the beds to erosion. Stabilisation by biofilm (mainly diatom) exudates has been suggested for many years, but was first experimentally examined by Holland (1974). Burrows of benthic organisms were traditionally thought to increase bed strength (Luckenbach 1986; Meadows and Tait 1989); however this is still a topic of debate, since evidence to the contrary has been found. This evidence, and an excellent review of biological effects on sediment stability is given by Paterson and Black (1999), in which the authors propose evolutionary theories to explain why these organisms would require that they decrease the stability of the beds.

The ideal environment to study erosion is one in which large scale turbulence can be set up over a deposited bed. However, it is very difficult in practice to monitor the condition of water flow and bed level over a large area, and many erosion devices deployed in the field focus on the erosion of a comparatively small section of the bed. This therefore makes it possible to introduce into a settling column an erosion device similar to one used in the field. This was achieved in these experiments using ISIS, an instrument developed at HR Wallingford, UK, and described in Chapter 2.

7.2 Erosion Experiments

Mud beds have been formed by filling columns with a well mixed initial slurry. The test names and conditions are given in the first three columns of Table 7.1. The stress history of the soil is similar to that of dredged slurry prior to disposal, where the subsequent consolidation and erosion conditions are often of major interest. These beds have been left to consolidate for a number of weeks, and in some cases primary consolidation was nearly complete by the time the erosion measurements were made. Density measurements were made throughout the consolidation stage and after erosion by the x-ray method described in earlier chapters.

7.3 Results

High resolution video observation gives an indication of how the erosion takes place. In the initial stages of the experiment aggregates are rather gently lifted off the bed, but often these are too heavy to be circulated up the ISIS. Continually increasing the flow rate causes larger aggregates (sometimes up to several millimeters) to be eroded, until a shear rate is reached where thin layers of the bed are eroded. Increasing the flow rate even further causes the upper bed to liquify. Layers continue to erode from the bed until, at a very high bed shear stress, a massive failure of the top several centimetres occurs. This has been called the failure threshold, J_f. Figure 7.1 shows the bed surface immediately before, during and after a massive failure of the bed surface. The white flakes are a combination of biochemically altered mud and algal material consisting mainly of diatoms, which are commonly found on top of the beds in column tests. During liquification these migrated down the column wall.

Figure 7.2a shows data from the first erosion experiment, isis1, which was allowed to consolidate for one week before the erosion test was made. The figure shows the experiment duration time on the horizontal axis. Continuously increasing the pump speed at set time intervals is represented in the stepped nature of the shear stress profile.

There is a distinct shear stress at which the mass of eroded sediment circulating throughout the ISIS is increased, representing the first significant piece of bed to be eroded. This can be seen to occur on Figure 7.2a at a time of approximately 19 minutes. At this time the corresponding shear stress is 0.177 N/m^2, as shown by following the dotted line to the the right hand axis of the Figure. After this, mass is eroded at a greater rate than before, given increasing shear stress. The critical shear stress, J_c, is defined as the shear stress at which this greater erosion rate first occurs.

The critical shear stress may also be represented by other methods of analysis. Figure 7.2b shows the erosion rate, or mass of sediment eroded per unit bed area per unit time, and Figure 7.2a shows the accumulated mass of sediment eroded per unit bed area. Both methods show the variation in relation to applied shear stress. Figure 7.2a clearly indicates a significant increase in eroded mass at a shear stress of 0.177 N/m^2, followed by an

Table 7.1 Experimental conditions and results.

Name	Consolidation interval (days)	Initial density (Mg/m^3)	J_c (N/m^2)	J_f (N/m^2)	M $J_{0.1}$ (mg/m^2)	M $J_{0.2}$ (mg/m^2)	M $J_{0.5}$ (mg/m^2)
isis1	7	1.137	0.177	na	0.045	0.201	0.615
isis2	13	1.164	1.3	3.6	0.067	0.071	0.178
isis3	19	1.164	0.01	3	0.107	0.178	0.517
isis5	5	1.08	0.1	1.225	0.062	0.071	0.196
isis6	58	1.162	0.073	na	0.196	0.272	complete
isis7	30	1.11	0.075	0.425	0.076	0.187	complete
TAM3	15	1.11	0.65	2.05	0.036	0.058	0.134
tam5	43	1.113	0.065	0.5	0.107	0.357	complete

increased slope in the graph. In Figure 7.2b all values above zero indicate that sediment mass is actively being eroded. The data plots rather chaotically since both erosion rate and shear stress may increase or decrease during the sampling interval of one second. However it is again clear on Figure 7.2b that the first significant and sustained erosion for isis1 occurs at a shear stress of 0.177 N/m^2.

Although a calculation of erosion rate is possible with the ISIS instrumentation, the testing procedure used in these experiments does not allow an analysis to be made in terms of erosion rate. A rather short interval of two minutes was used for increasing the shear stress, which differs from more commonly reported laboratory techniques of fewer shear stress levels over much longer time periods. The latter technique allows the bed state to reach a steady state before the shear stress is increased. There are several reasons why the former technique was chosen in this case. First, there may be time dependant changes taking place on the scale of hours which may alter the properties of the bed during the experiment. Most important of these were thought to be the further consolidation and cementation in the young beds. As described later, the pore pressures in the bed were also affected by erosion. Shorter time intervals were also suggested by the developers of ISIS as it is the interval used for both the ISIS and the related instrument, SedErode, in their field sampling projects. To allow appropriate statements to be made about the 'erosion rate', the bed must have sufficient time to respond fully at each stress interval. In the present experiments the increasing erosion is driven by the history of the stress application. This stress history is standardised as far as possible for the tests, with an interval of two minutes, allowing the data from the various experiments to be compared to one another. There are a few (infrequent) exceptions to the two minute rule where x-ray measurements or pore pressure measurements were made.

The large majority of mass is eroded at the instant the shear stresses are increased. That is, the erosion is driven by the increase in shear stress, and the data may be appropriately presented in terms of shear stress and mass eroded. This method is consistent with the methods used commonly in the field for the SedErode (Feates *et al.* 1999), and the ISIS (Williamson and Ockenden 1996), and is also similar to methods used with other in situ devices such as the University of St. Andrew's Microcosm (up to ten minute intervals) and

their cohesive strength meter (intervals of a few seconds). It may be argued that beds in natural tidal environments rarely actually reach a state of equilibrium, so increasing the shear stress before the bed has time to come to such an equilibrium is acceptable, so long as the measuring technique is consistent throughout compared experiments (Trevor Black, Gatty Marine Laboratory, University of St. Andrews, personal communication).

The tests following isis1 went further to investigate the effect of consolidation time. Five columns were prepared using Tamar mud. Three of these, isis2, isis3, and isis4, were sedimented from an initial slurry density of 1.164 Mg/m^3 and height 190 mm, and allowed to mature for 13, 19, and 32 days. The remaining experiments isis5, isis7 and tam5 all had slightly lower initial slurry densities and consolidated for 5, 15, and 43 days. Density profiles showed that all columns settled at similar rates with consistent density changes throughout the beds during consolidation.

Plotting cumulative mass eroded against applied shear stress gives an indication of the erosion reactions of each of the beds given increasing shear forces (Figure 7.3). While not being a direct measure of erosion rate, it does allow a comparison of the different behaviours of the beds of different initial conditions, which are subjected to very similar stress/time histories during the erosion tests. It can be seen in Figure 7.3 that these reactions are different for the different beds. In addition to having different slopes the curves have different shapes, and in most experiments the slopes at lower shear stresses are different from those at higher shear stresses.

In Figures 7.2b and 7.3a-h the horizontal axes are adjusted to show the shear stresses up to 0.30 N/m^2 only, since at shear rates higher than this the beds in a few experiments start to erode massively . In some experiments there is a peak at very low shear stresses, showing that these beds are very fragile at the outset of the experiment. This is particularly noticeable in isis6, the most mature of the beds. In fact, the more mature experiments generally have slightly larger initial peaks in their mass erosion than the younger experiments (Figures 7.3e,f and h).

Figure 7.3 shows that the mass eroded at any given shear stress varies between

experiments. One way of analysing these data further is to compare the mass eroded at a set of arbitrarily chosen shear stresses: 0.1, 0.2 and 0.5 N/m^2. The mass of the sediment circulating in the isis at these specified shear stresses are given in Table 1 ($MJ_{0.1}$, $MJ_{0.2}$, $MJ_{0.5}$). These have been plotted in Figure 7.4, against the length of consolidation time for each experiment. At the lower shear stress levels of 0.10 and 0.20 N/m^2 the mass eroded increases with consolidation time. That is, the older beds are less resistant to erosion than the young beds. This relationship continues into the higher shear stresses. The more mature beds undergo massive failure much sooner than the immature beds, thus a a shear stress of 0.50 N/m^2 is never even achieved. These results are, at first sight, surprising, given the normal expectation already described, ie. that increased consolidation time leads to stronger beds due to bed restructuring and cementation.

X-ray measurements have been made before, during and after most of the erosion tests. Figure 7.6a shows the final density after consolidation in experiment isis2, along with the density immediately after erosion. The erosion has led to lower densities throughout the upper bed. This may be due, in some small part, to the decreased bed height (apparent in the figure) which would decrease the total stress loading the upper bed. However, this unloading would cause only a small swelling, given the irreversible behaviour of soil consolidation. It is therefore most likely that this density reduction is a consequence of liquefaction or dilation, which has affected all of the bed except the bottom 4 cm. This reduced density due to entrainment and maintenance of water during and after erosion has important consequences in erosional processes. For example Mehta (1991) refers to a type of erosion where the bed is first fluidised, and then destabilises causing the fluid mud to be entrained and mixed.

Results to determine how pore water pressures respond to the erosion are also available for one experiment. When the water level in the column is kept constant the pore pressures rise overall during the testing. This might indicate that the force of the water pressure coming down the column walls is having an effect deeper in the bed, and is the likely cause of the liquefaction of the upper bed.

7.4 Biological features of the beds

An overall increase in eroded mass, given increasing bed shear stress, has been shown to be distinctive for each of the experiments (Figure 7.3). The density profiles for the experiments may help reveal some aspects of the bed surface which may account for these differences. During the consolidation process, it has frequently been observed that there is not a sharp density change between water and bed. Rather the top surface on the density profiles becomes more well-rounded as a biological layer forms. Figure 7.5 illustrates this; the density in the earlier profiles changes abruptly between the bed surface and immediately below the bed surface, whereas at a time of 170.5 hours this change is much less abrupt. This has been observed repeatedly throughout the years in column experiments at Oxford. There are several mechanisms which may account for this. One is the breakdown of the flocs at the surface, which has been shown to occur in Chapter 5. Microscopic analysis of material from the top layer of experiment tam3, the experiment shown in Figure 7.5 has revealed an abundance of dormant diatoms and other organisms (Dr. John Hamer, University of Wales, Bangor, personal communication.). The weakening of the mature beds may be attributed to the lower resistance to erosion of this biochemical 'fluff' layer. Similar features have been described in nature. For example, Amos *et al.* (1997) describe an easily eroded fluff layer on beds of the Fraser River Delta in Southwestern British Columbia. Erosion of this fluff layer is also the likely cause of the large peak in mass eroded at the outset of the more mature experiments (Figure 7.3). The small peak seen in the younger beds at the onset of erosion may be due to a surface layer of finer particles that settle out of the overlying water after the main body of the soil. Curiously, this prominent biological layer does not seem to form in beds which are formed by slow sedimentation using the sedimentation system.

X-ray profiles have also revealed another interesting feature about the bed surfaces. The profiles shown in Figure 7.7 are taken from experiments of different length using the same mud, at a similar initial slurry, though with slightly different initial heights. The two more mature profiles, isis3D and isis4E, show a density minimum at around 7 mm below the surface, whereas the third profile for tam1A is more typical and does not show this density minimum. This minimum has been seen on occasions in various experiments at Oxford,

and for consolidation or soil mechanics research it is rather insignificant. However it becomes considerably more important when the research is focusing on the properties of the bed surface. Close visual observation of the surface reveals that there is a gaseous sublayer corresponding to the low density layer in the more mature experiments. Figure 7.8 shows a photograph of this gaseous layer forming just below the surface. It should be emphasized that this photograph is of a bed in which there was visibly more gas, and a greater reduction of density than occurred in the erosion experiments. It therefore represents an extreme example, but nevertheless a relevant one. It is likely that this gaseous sub-layer, which shows up so distinctly on the density profiles of the more mature beds, is also weakening the bed at this level, and contributes to the larger (bulk) erosion processes.

In Figure 7.1b there is a rather large piece of bed missing, marked 'mass failure'. In the initial experiments it was believed that these pockets of higher erosion were caused by turbulent vortices at higher flow rates. However on much closer observation using the video cameras it has since been found that these pockets often occur where a feeding benthic worm is present. The photograph in Figure 7.9 is a single frame taken from a movie of the surface of experiment isis1. This experiment was unique in the number of worms that appeared, as in most experiments none or few worms were observed. The image quality is poor, especially of the fast moving worm and faecal pellet, since the movie has been captured using the interlaced camera (see the section on Video System in Chapter 2). Nevertheless, by watching the movie it is clear what is occurring. The worms' feeding behaviour may weaken the surrounding bed. This worm feeds at the surface, with its head anchored in the sediment, and its body an oscillating cantilever in the water column. As it feeds it ejects pellets which settle to the bed surface. Thus after several days the entire bed surface surrounding the worm is composed of these pellets mounds. The constant oscillation, combined with the sediment surrounding a worm being deficient in living organic matter and being composed of faecal pellets rather than fine-grained cohesive material, may hinder the processes of bed strengthening through consolidation and creep processes. There is supporting evidence in the literature for this conclusion. Paterson and Black (1999) report on a study by Widdows (1998) in which benthic invertebrates destabilise the sediment leading to increased erosion. They postulate that this erosion leads

to the periodic renewal of food surrounding the organisms.

7.5 Conclusions

Biological factors have been linked to geotechnical measurements at the bed surfaces of slurry experiments.

- Over time, diatoms migrate to coat the bed surface
- A gaseous layer may form immediately beneath the surface biolayer.
- Worms feeding at the surface deposit faecal mounds
- The ISIS has been modified to allow measurements of erosion resistance in laboratory columns
- Biological factors lead to an overall weakening of the bed surface despite increased consolidation time.

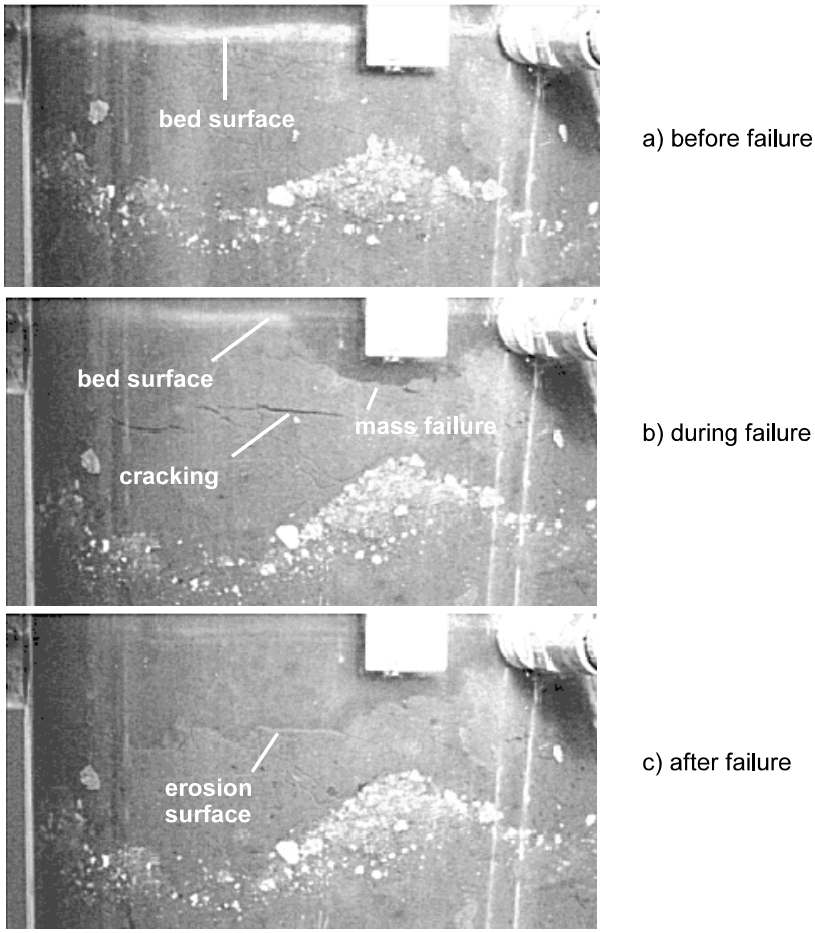

Figure 7.1 Photographs of the bed before, during and after massive failure.

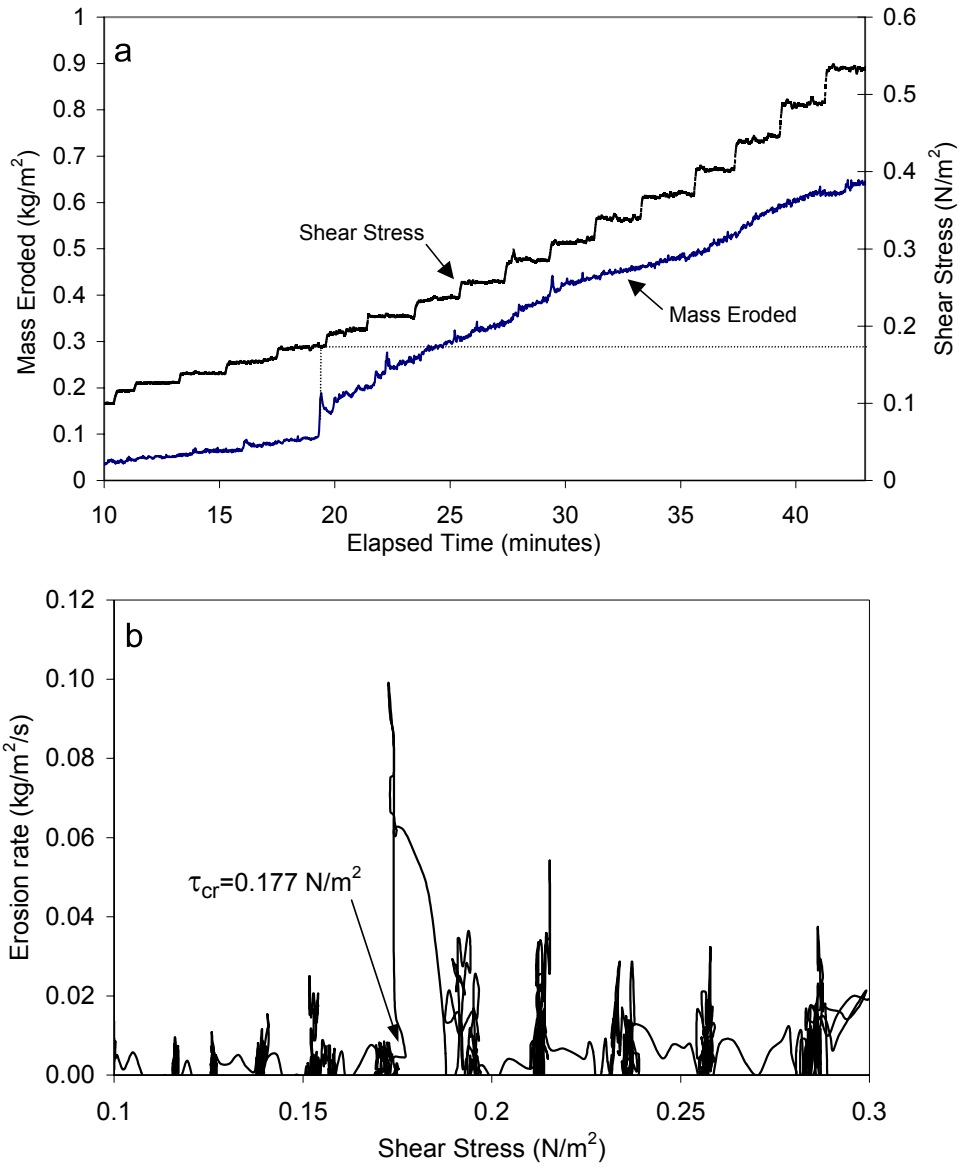

Figure 7.2 Methods to represent the critical erosion threshold, J_c, for experiment isis1.

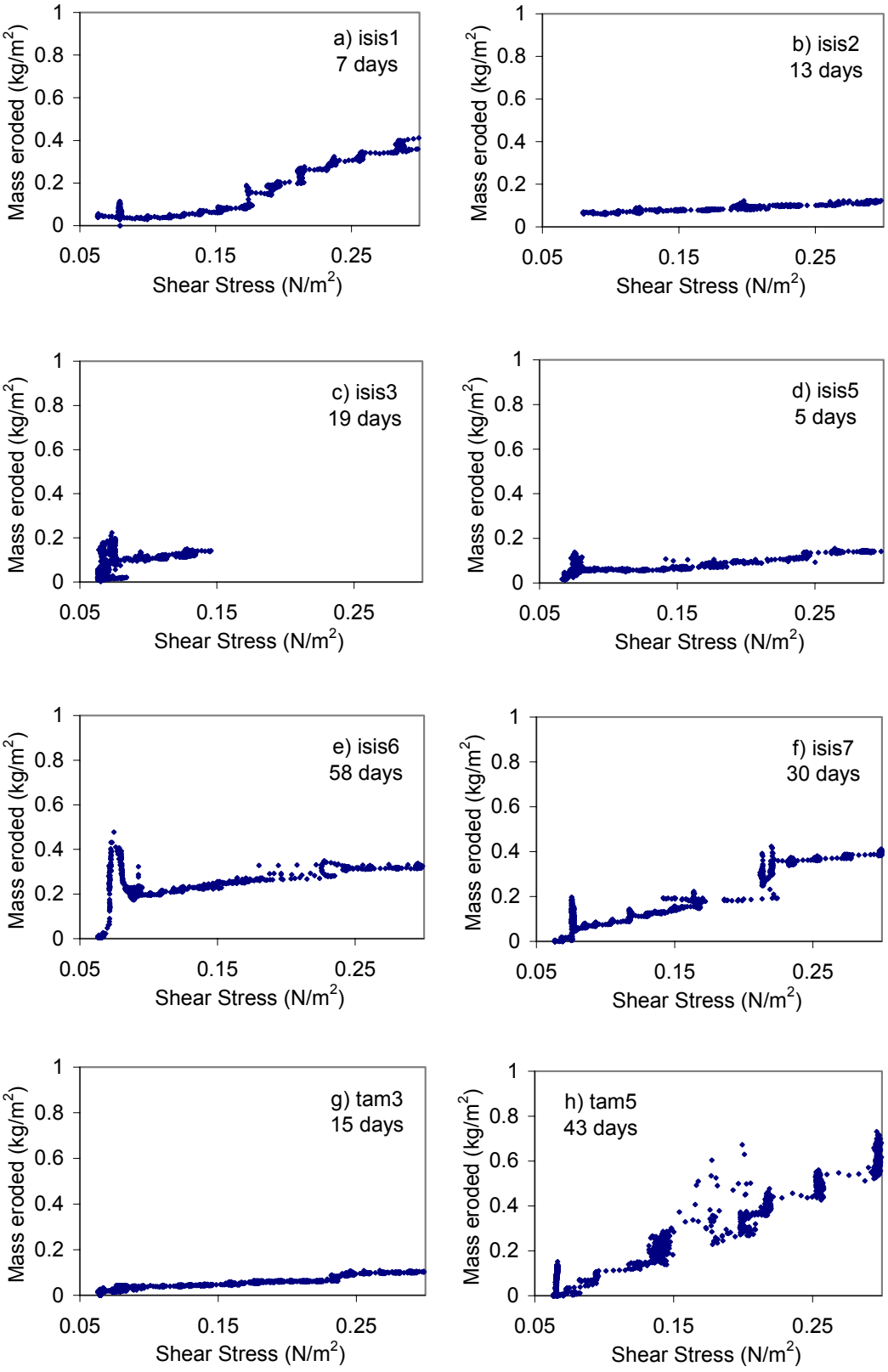

Figure 7.3 Cumulative mass eroded given increasing shear stress for each of the beds.

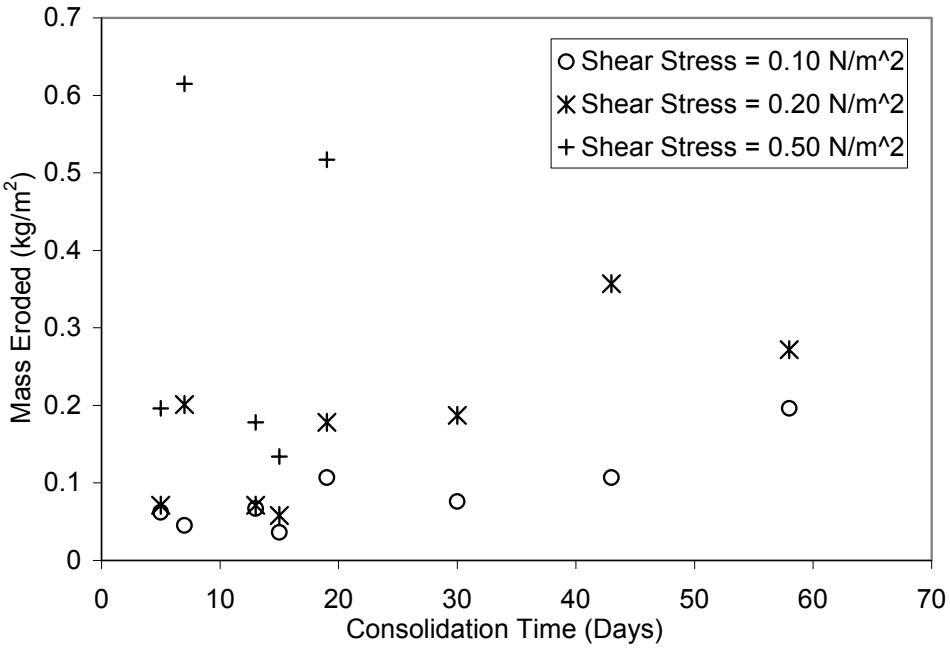

Figure 7.4 Cumulative mass eroded at specified shear levels during the experiments.

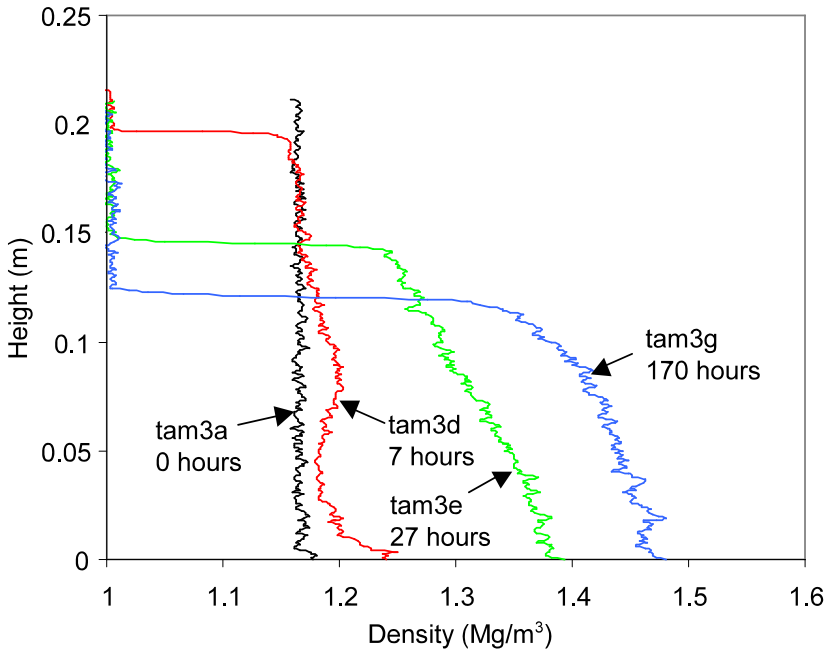

Figure 7.5 Density profiles showing the settling and consolidation of experiment tam3.

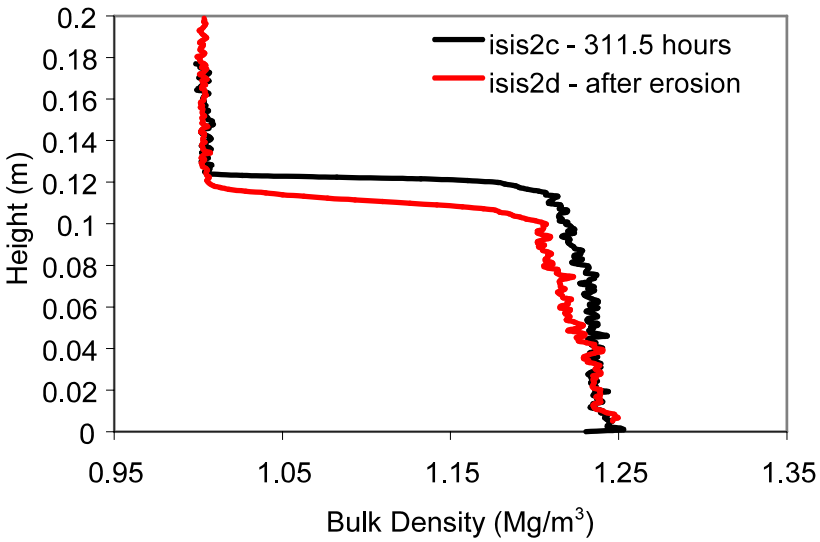

Figure 7.6 Reduced bed density in upper bed due to erosion of experiment isis2.

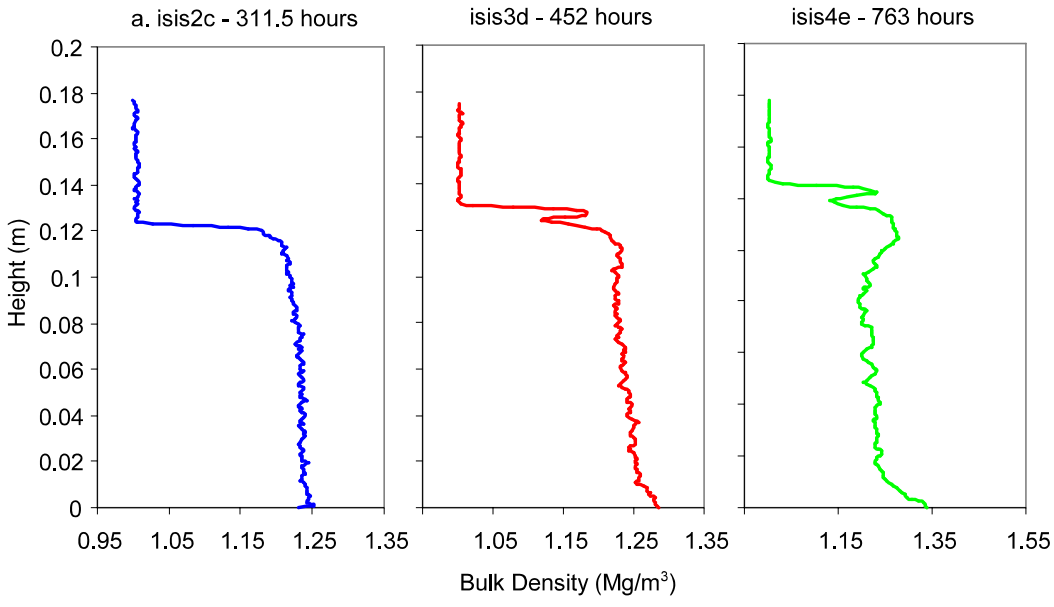

Figure 7.7 Development of a layer of reduced density thought to be gas in mature beds.

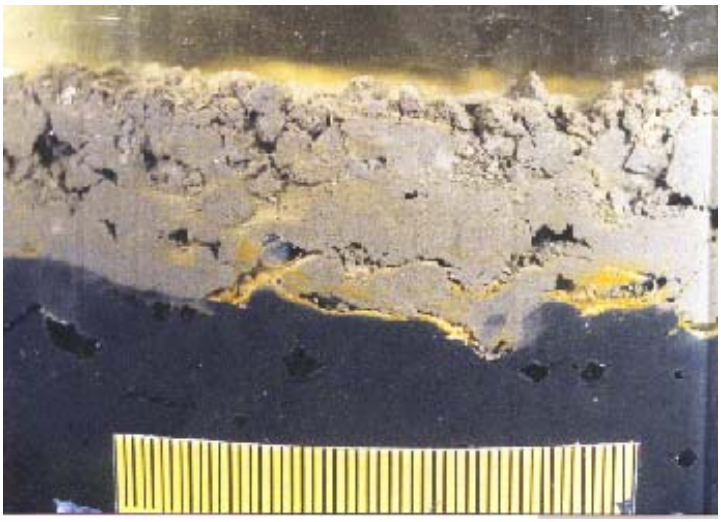

Figure 7.8 Low density layer at the top of a slurry deposited bed is characterised by a different colouration, and often gas bubbles, as seen in this extreme case. Photo courtesy of Ramon Gonzales, Department of Engineering Science, Oxford.

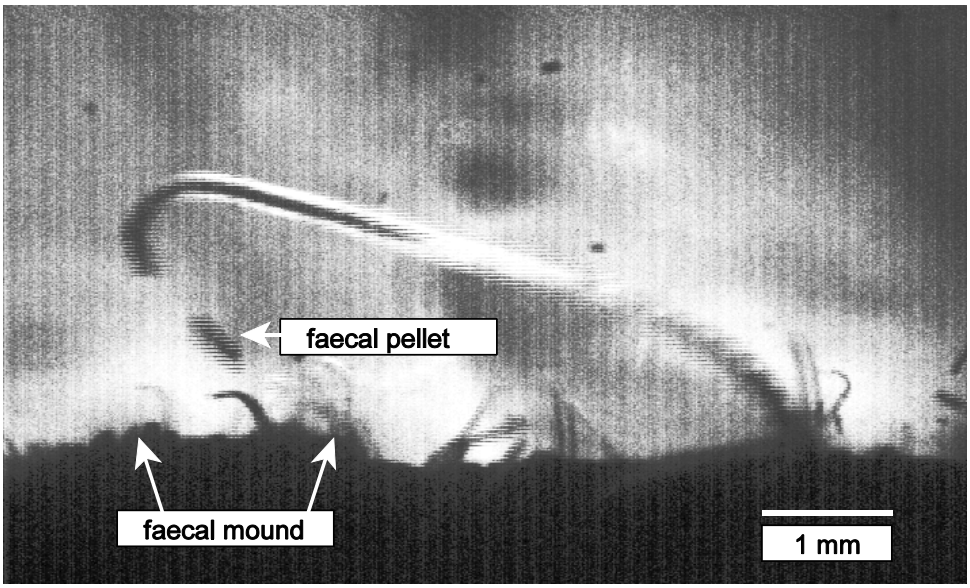

Figure 7.9 A feeding worm drops faecal pellets on the bed of experiment isis1.

Chapter 8 Influences of flocs on the bed

Chapter 4 describes the development of flocs in the water column. Chapters 5 and 6 look specifically at the bed structure, and make remarks about the influence of flocculation on this structure. In this work, evidence has been collected to support the idea that flocculation conditions have significant effects on bed structure. This chapter brings together the data to interpret what is happening throughout the flocculation, sedimentation and consolidation processes. It presents a discussion of the various links that have been found between the processes. It introduces features that can be measured both in the water column and in the bed, namely solids volume fraction and fractal dimension. It then makes use of the idea of intrinsic properties of soil to determine whether the sedimentation conditions have an effect on the compression behaviours of the beds.

8.1 Floc formation, construction and deconstruction

Sediment is introduced to the water column where it forms flocs. These flocs collide with (or, rather move into the range of influence of) other flocs. This causes flocs to break apart or to aggregate further. Numerous experiments reported in Chapter 4 showed that as sedimentation rate increased, the equivalent spherical diameters of the flocs became larger (eg. Figures 4.10 and 4.11). It was also shown that larger flocs had slightly faster settling velocities. However, as concentration increased further (Figures 4.19 to 4.20) or as turbulence was increased (Figure 4.9) the flocs began to break apart. In Chapter 4 hindered settling was captured by video analysis at a mean floc size of 75 ∶m and a mean minimum centroid to centroid distance of 250 ∶m. This would give a mean minimum distance of [250 ∶m - 0.5(75 ∶m)]/75 ∶m = 2.8 floc diameters between floc surfaces. The smallest minimum distance between one floc and another would be less. There is evidence given in Chapter 4 that, even at a low concentration, the number of collisions is sufficient for floc breakage to begin to occur.

Despite evidence of floc breakage at lower concentrations, increasing the concentration further, to a few g/l (cf. cos16, wsm1, cmw1), causes flocculation to be enhanced, so that large ‘fluffy’ flocs are formed. These settle in a haphazard fashion, with many flocs

moving upward as well as downward. This bidirectional flow at intermediate concentrations leads to a very high number of collisions, and is the most likely reason for the larger flocs. Calculations of effective density quite clearly showed that the large flocs were less dense than smaller flocs. The breaking apart causes a larger number of smaller denser flocs. The forces acting on the flocs are the downward force of gravity and the upward drag forces from the water flow, the latter acting all round the floc.

8.2 Consolidation of the aggregates

As the flocs approach the bed the forces acting on them have now changed, since there's an upward localised reaction from the bed and a much reduced drag from the fluid. This must lead to a rearrangement of the floc structure as they pitch and strain. For sediment to move downwards, water has to flow out of the bed so there are various different time scales operating here - that of water flow and of the rate of sediment arriving at the surface. The freedom to move laterally must depend on the sediment flux. Once the sediment is part of the bed, it moves as water flows out round it and as the supporting sediment immediately beneath moves. This could be seen as giving rise to two different mechanisms, one of consolidation (associated with pore pressure dissipation) and one of collapsing support, or consolidation at greater depth.

It is difficult, given the inherent variability in the floc data, to relate bed density directly to floc size. In the experiments reported throughout this thesis, there does not appear to be any straight forward relationship between the two. It is therefore suggested that the bed density is not greatly affected by the floc size, but rather by the rate at which the flocs arrive at the bed. Chapter 5 describes the action of a floc as it arrives at the bed. It was found that upon arriving at the bed the flocs often maintain their vertically elongated shape for a short time, before jumping or tumbling laterally and then flattening out on the bed. Given the descriptions of that chapter, it can be surmised that floc deposited in small concentrations are able to fall into cavities in the bed, and to spread out fully, thus over a number of seconds they become vertically compacted. Flocs being deposited at higher concentrations, do not have the space nor the time to spread out as completely. For instance, at

concentrations high enough for hindered settling to occur, the mean interfloc distances were only several times larger than the mean floc sizes (see Figure 4.20), and any particular area on the bed may be bombarded several times by arriving flocs in the time that it takes a floc to settle into the bed. It is possible that lateral support is provided by flocs deposited side by side, and thereby inhibiting the flocs from spreading to their full horizontal extent. In this case, under high deposition rates of individual aggregates, the soil framework remains open. Under conditions of very high deposition (slurry experiments), the floc video measurements are no longer available. However images of the beds indicate that, at least below the surface, there is very little evidence of clusters of aggregates. This could be due to the flocs being destroyed by one another in the water column due to the high number of collisions. Alternatively, perhaps very large but weak flocs are formed in the water column which are destroyed either when they strike the bed, or are destroyed easily by the further bombardment of flocs. A third alternative is that the particles in a slurry bed can be considered to settle and consolidate as one large aggregate.

Image analysis presented in Chapter 5 has shown that the aggregates at the surface of a slowly deposited bed break down slightly over time. Images taken further down the bed indicate that an aggregated structure is still present at least to several centimetres into the bed. Void ratios confirm this, and in fact show that the aggregated structure continue to be present even to effective stress levels that represent depths of several metres.

Evidence is provided in the preceding chapters to indicate that beds formed from a slurry deposited at an intermediate rate (around 100g/day) are quite different to those formed by a slurry. The former beds are less densely packed than the latter. For slowly deposited sediment, from 10 to around 100 g/day, the density of the beds decreases. Images of the beds also show that the steadily sedimented beds are visibly different from the slurry deposited beds, and are composed of clumps or aggregates. Variations in the sedimentation rates lead to large variations in the bed structure, which continue to be present even when subjected to loading. These are significant findings since the vast majority of laboratory experiments on the settling behaviour of sediment, from which sedimentation and

consolidation theories are derived, are conducted using the slurry method.

8.3 Comparitive Measurements

Different measurement apparatus and techniques have been applied to the aggregates in the water column and to the aggregates in the bed. Each of the techniques is better suited for one or other of the sedimentation zones, with image analysis perhaps being the best suited for both. There are no properties which can be simultaneously measured and directly compared in both zones. However, there are some parameters which can be calculated for both, which will allow the zones to be compared with the same units of measurement. Two of these parameters are solids volume fraction (or its reciprocal, porosity) and fractal dimension. These are calculated below to determine whether they may be a way forward as a method for comparing flocs with beds.

Volume fraction and porosity

Chapter 6 discusses the structure of a bed in terms of its void ratio and bulk density, two commonly used measures in soil mechanics. In this chapter a different unit of concentration is used, namely volume fraction. There are two reason for this. First measures such as porosity and volume fraction are always between 0 and 1, giving convenient boundaries. Second, porosity and volume fraction (particularly the latter) are commonly used in the chemical engineering fields to which much of the available literature refers.

Huang (1993) uses mass balance, under the assumption that a floc consists of only solid particles and water, to relate the density of a floc, ρ_f, to its porosity, θ_f. From Huang (1993), the solids volume fraction can be defined as:

$$\phi_f = \frac{V_s}{V_f} = \frac{\rho_f - \rho_w}{\rho_p - \rho_w}$$

The numerator in the fraction is the floc effective density, so this calculation relies on the same assumptions about Stokes' Law as that for ρ_e derived in Chapter 4. The solids volume fraction of a floc, or the ratio of the volume of solid particles to the total floc volume, is simply the porosity subtracted from one

The floc volume is calculated using the ESD from the image analysis results, and the values for O_f are found using the equations above. Thus, the volume of solids, V_s, in a floc can also be calculated. A summation of these V_s (for all flocs), divided by the image volume, V_I, will give the overall (bulk) solids volume fraction N in an image:

$$\phi = \frac{\sum V_s}{V_I}$$

The calculation for solids volume fraction, N, relies on knowledge of both the volume and the settling velocity of each floc in an image. The first of these is relatively simple to calculate from the image analysis results, however the particle tracking software was unable to track every particle in an image. A correction has been applied that multiplies the above equation for N by a ratio of the number of flocs in the image, n_f, to the number of flocs that were successfully tracked, n_{tf}, thus:

$$\phi = \frac{\sum V_s}{V_I} \cdot \frac{n_f}{n_{tf}}$$

The results of the floc solids volume fraction analysis are shown in Figure 8.2, where the solids volume fraction of each floc is plotted against its equivalent spherical diameter for several images in experiment dbd3. The above equations rely on accurate calculations of floc density, D_f, and also on measurements of the bulk density of the solid material, D_s. In exceptional cases where the calculation of D_f yields a higher value than D_s, such as for mineral 'slivers', the porosities are calculated as negative and the solids volume fraction are calculated as greater than one. These data are not shown. The data shows that the smallest flocs are very nearly solid particles (N=1), whereas the largest flocs have much lower solids volume concentrations.

Figure 8.3 shows the solids volume fraction for the bed of experiment dbd3. The solids volume fraction is plotted against the burial depth. The first profile, dbd3e, was measured at the end of sedimentation, and dbd3l was measured after the application of a hydraulic gradient. This, along with other profiles from the experiment (not shown) indicate that the

bed surface has a solids volume fraction always below 0.1. Under increasing load in this experiment, N increases to a maximum of 0.7. The solids volume fraction profiles show high variability throughout the bed. Floc data is available for the entire experiment. Two heights have been chosen from the profile dbd3e, to determine how the floc properties might have affected the bed. The deposition times of these positions are estimated as between 190 and 200 hours, and between 200 and 210 hours. The solids volume fraction is significantly higher at the second time than it is at the first time. If this is related to the sedimentation conditions then it must be apparent in either the size of the flocs or the density (solids volume concentration) of the flocs. As mentioned earlier no correlation could be found with floc size. The floc volume fractions during sedimentation at these times are presented in Figure 8.4. The data is remarkably similar for both times. In fact, a plot such as this does not seem to shift noticeably during the experiment. Further analysis of the data has produced probability density contours (Figures 8.4b and c). The floc size distributions are roughly the same at each time, between 20 : m (the lowest calculable size) and 300 : m. It seems from the 75th percentile that the flocs at the second time (Figure 8.4c) have lower values of N ($N=10^{-0.35}$) than the 75th percentile for the flocs at the first time interval ($N=10^{-0.25}$). This does not correlate to the higher values found in the bed for the second time interval. However, the highest concentration of data (the 25th percentile), lies slightly higher for the second time interval, which could be a reason for the increase in bed density.

The solids volume fraction data are shown for the flocs of experiment cos17 in Figure 8.5. Again, two sets of data are shown, those immediately 246 hours of elapsed time under a low concentrated sedimentation, and those immediately before 296 hours under a much higher sedimentation rate. In the first instance the concentration was measured at below 1 mg/l, and in the second case the sediment input at the top of the column was permitted to flow freely to get a concentration approaching that of slurry experiments. The floc volume fractions under higher sedimentation overlap the higher side of the low sedimentation rate data, and extend slightly higher overall than those at lower sedimentation rates. The mean solids volume fraction at the lower concentration is 0.089, and at the higher concentration

it is 0.116. Thus, since large flocs should have a lower volume fraction, it may be concluded that under the high concentration there are probably fewer large flocs.

The solids volume fraction at the bed surface are shown for these two times in Figure 8.6. The bed at 246 hours was 0.059m high, and at 296 hours it was 0.089m high, although only the depth from the surface is shown in the figure. It is seen that the volume fraction of the bed surface is substantially higher at 296 hours ($N = 0.08$), under high concentration, than it is at 246 hours ($N < 0.07$). It is not possible to relate this directly to the values obtained for the flocs, and it is unknown whether it is mainly a consequence of more dense flocs forming it, or if it is also a consequence of the different behaviour of a bed being deposited more quickly.

Fractal Interpretation

Theories of fractal geometry have been successfully used to describe flocs (Meaken 1988; Li and Ganczarczyk 1989; Huang 1993; Huang 1994; Gregory and Chung 1995; Bache *et al.* 1997). According to these authors fractal geometry is suitable for describing flocs as they are porous structures in which the effective density decreases as the size increases.

Kranenburg (1994) and Huang (1994) present equations to show that the differential or effective density $)D_s$ can be related to a fractal dimension n_f of the aggregates. The fractal dimension is a measurement of the effectiveness of the flocs to fill space as a function of the floc size. The larger the fractal dimension, the more uniform the floc structure. The maximum fractal dimension for regular three-dimensional objects is 3, which is the Euclidean dimension for a three dimensional object and corresponds to a porous structure whose porosity or effective density is not a function of size (Huang 1994). For mud flocs the fractal dimension may be considerably lower, generally varying between 1.7 for large fragile flocs and 2.8 for strong estuarine flocs.

The form of the equation given by Kranenburg relates the effective density, $)D_e$, with the density of the solid material, D_s, primary particle diameter, D_p, and floc diameter, D, using

a fractal dimension, n_f:

$$\Delta\rho_e = (\rho_s - \rho_w)\left[\frac{D_p}{D}\right]^{3-n_f} \tag{8.3}$$

Figure 8.7 shows the results of the fractal dimension calculations for experiment dbd2. These are within the range found in other investigations (1.8 to 2.2). Fractal dimensions in this range imply that floc density rapidly decreases with increasing size, a feature of the data that has already been shown in Chapter 4.

Merckelbach (2000) extends this type of self-similar analysis into the sediment bed. The bed can be regarded as a cluster of many fractal aggregates, and may be assumed to have some fractal properties itself. Merckelbach derives an equation to relate the slope, S, of the relationship between log solids volume fraction N and log effective stress F' for the bed to the fractal dimension, D, of the bed:

$$\Omega = \frac{2}{3 - D}$$

An example of the use of this equation is given in Figure 8.8. In this figure N and F' are shown for the bed of experiment dbd2f. The power relationship is fitted by excel. The equation yields D = 2.7. This is a much higher value of D than was found for the flocs, but in keeping with the values reported in Merckelbach (2000).

It is interesting to note how the fractal dimension changes with consolidation. Figure 8.9a shows data from cos16a, immediately after sediment input is stopped, through cos16f at the end of self weight consolidation, to cos16g after a hydraulic gradient is applied. This experiment is one in which the sedimentation was very rapid, at 514 mm/day. The rapid sedimentation led to large, fluffy flocs, an example of which was shown in Figure 5.4. These large flocs, in turn led to a loose and open bed with one of the highest dimensionless bed heights of all the experiments (see Chapter 5) and highest void ratios (Chapter 6). Immediately after sediment input is stopped (cos16a) the sediment water interface drops

rapidly as sedimentation on to the bed is still taking place. The density profiles show that the bed surface is at first rounded, and then flattens out as the sedimentation gives way to consolidation. This provides evidence, further to that provided in Chapter 5, that the structure of the flocculated bed at the surface is different to that deeper in the bed. This shift can also be seen on the F' versus N plot in Figure 8.9a. The curve for cos16a starts out nearly vertical at the lowest effective stress, and then bends to a less steep curve as the effective stress increases. This indicates that the fractal dimension at the surface is higher than that deeper in the bed. As time progresses through self weight consolidation the curve is shifted to the right (cos16c then cos16f), however the slope remains roughly the same giving a fractal dimension around D = 2.65. The slope of the curve remains remarkably constant even after the effective stress is increased in cos16g (D= 2.67).

Other experiments for which steadily sedimented beds allow fractal interpretations include cmw1 and wsm1. These are shown in Figures 8.9b and c respectively. Experiment cmw1 again shows that early in the experiment, and at low effective stresses (at the bed surface) throughout the experiment, the fractal dimension is higher than at greater effective stresses. Experiment wsm1, on the other hand, does not show much variation in fractal dimension with time or with effective stress.

It might be expected that the bed surface should show an intermediate value of D between that for the flocs and that deeper in the bed. The higher value of D at the surface could be a feature of the large strains found there, as compared to in the settled and consolidated bed, although no explanation is known. This feature of the data could also be due, in part, to the accuracy of the measurements. Experience has shown that it is unlikely that the xray and pore pressure measurements are able to yield reliable values for effective stresses below 0.01 kPa. This means that the values shown at the very low effective stresses for experiment cos16 (Figure 8.9a) are unlikely to be accurate, and must be reported with caution. Nevertheless, they are not highly scattered either, a feature one would expect if the limits of measurement have been reached.

8.4 Creep and time dependent effects

Two types of creep have been shown to occur in these experiments. First, it was shown that the aggregates break down somewhat at the surface, where the effective stress is essentially zero. Second it was observed that the aggregates that remain build up the bed to a certain height, and then the whole structure collapses under its own weight. These events are both reported in Chapter 5. Creep which occurs at constant effective stress has been documented in Chapter 6.

The ongoing creep and consolidation seen in these experiments means that the beds are not expected to reach the same condition as they would in the field, where time scales are usually much larger, burial depths are greater and strain rate effects are different. Burland (1990) and references therein, make use of the concept of intrinsic properties of the clay. One method of comparing the properties of beds created in a lab to those existing in the field is to extrapolate the concept of intrinsic properties back to much lower effective stresses than had originally been intended. Figure 8.10a shows a typical void ratio effective stress plot for a clay that has been reconstituted[11] in the lab and has had a high load applied to it (at least 1000 kPa). The void ratios are designated with an asterisk to indicate that they are reconstituted. The term intrinsic is used in this case to refer to the basic, or inherent, properties of a given soil prepared in a specific manner, which are independent of its natural state. This curve is normalised by assigning fixed values, 0 and -1, to e_{100} and e_{1000} (Figure 8.10b). It has been found that the normalised curve is a unique line describing most muds, and this curve is called the intrinsic compression line, or ICL. The vertical axis now shows the void index, I_v.

As described above, a calculation of the intrinsic compression line would require knowledge of the compression behaviour of the reconstituted soil at pressures of 100 and 1000 kPa. This data is not available. However Burland provides an empirical method to calculate the ICL by the cubic:

[11]Mixed with water at a water content between the liquid limit and 1.5 times the liquid limit.

$$I_v = 2.45 - 1.285\sigma' + 0.015\log\sigma'^3$$

A calculation of I_v for several naturally deposited soils has allowed Burland to derive coordinates for the sedimentation compression line, or SCL. The sedimentation compression curves from the experiments may be normalised by empirical methods with knowledge of the void ratio of the liquid limit, e_L:

$$I_v = (e - e^*_{100})/(e^*_{100} - e^*_{1000})$$

where

$$e^*_{100} = 0.109 + 0.679e_L + 0.089e_L^2 + 0.016e_L^3$$

and

$$e^*_{1000} = e^*_{100} - 0.256e_L + 0.04$$

These compression curves may be then be compared to the ICL and to the SCL (average natural clay conditions) to determine whether the deposition conditions have had an effect on soil fabric.

According to Burland (1990) the deposition conditions profoundly affect the position of the sediment compression curves with respect to the ICL, indicating an effect on the fabric of the sediment (Burland, 1990; Sills, 1998). Thus it seems appropriate to use in this study. The application of a load reduces the void index and shifts the compression curve downward towards the ICL. Burland (1990) contains data from deeply buried sediment or reconstituted sediment which is highly stressed in triaxial chambers, oedometers or other high pressure apparatus. The concept of the ICL has been published for softer surface sediments by Sills (1998), who suggests that the ICL and the SCL might apply also over much lower stresses than the range of 100 - 1000 kPa than Burland had proposed.

Figure 8.11 shows the void ratio effective stress plots for experiments on Dibden Bay, Tamar (cos) and Combwich mud. The curves are from the beginning and end of the column experiments. Also shown on this figure are the curves for various reconstituted clays, at much higher stresses, reported by Burland. It is clear that there is a large amount

of variation between different clay types at all stresses. Also, there is a considerable change in void ratios during the consolidation of the clays at the lower effective stresses. Typically the column test clays start at low effective stresses with a steeper slope, which gradually shallows into a similar slope as the oedometer test clays.

In Figure 8.12 only the void ratios from the lowest points (the troughs) at the end of the experiments are shown. Several additional experiments are represented in this figure.

The void ratios have been normalised by the void index equation (equation 8.2) and the resulting sedimentation compression curves are shown in Figure 8.13. Whereas the high stress curves (>10kPa) form a unique line, the intrinsic compression line, the low stress curves do not. Moreover, the low stress experiments all lie above the ICL and closer to the SCL (except for a single point). It is clear that the experiments do not follow the behaviour of reconstituted clays, and is closer to the behaviour of average natural clays. It is also clear, however, that the beds produced in the lab also lie above the unique SCL curve that is derived from beds in the field.

A number of factors might explain why the column experiments lie above Burland's SCL. The SCL is designed to be a baseline to which sediment compression properties could be compared, thus revealing information about the deposition conditions. According to Burland (1990) slow deposition in still water leads to an open random fabric (high void index). Rapid deposition from a dense suspension or sediment deposited in a current gives rise to a more oriented fabric with a lower void index, thus for quickly deposited sediment the compression curve is shifted downward towards the ICL.

It has been proven earlier in this thesis that the column experiments are undergoing significant creep during the initial stages of consolidation. It is certain that the sediment from which the ICL and SCL were originally derived had already undergone creep during its significant geological compaction time. Since all points for the experimental beds lie above the SCL, it is likely with time, given the evidence of creep, that these points would

converge on the SCL. For instance it was revealed in Chapter 6 that experiment cmw1 underwent considerably more creep than the other experiments. It also has one of the highest and one of the steepest compression curves in Figure 8.13. The cos experiments in the figure are grouped towards the lower I_v values and the dbd experiments lie in the middle. Thus it seems that the void index effective stress plot relies on sediment type, just as the void ratio effective stress plots do. Finally, it must be said that Burland is unsure about the use of the empirical line described by the equations for sediment whose Atterberg limits lie well below the A-line, as is the case for Tamar (cos) mud.

8.5 Conclusions

- Solid volume fractions of the flocs are in the same range as those for the beds. However, given the variation in the floc solid volume fraction data it is difficult to quantify the relationships between the two.
- Although fractal dimensions of the flocs and of the beds are in agreement with those reported in other studies, it remains unclear as to how the high fractal dimensions in the bed related to the lower fractal dimensions that are calculated for flocs.
- The fractal dimension appears to change with burial depth and consolidation time
- Compression curves for very soft sediment are consistent with those measured for deeply buried or highly stressed sediment
- The slowly sedimented beds are more closely associated with the average natural compression curves (the SCL) reported by Burland (1990) than they are with the compression curves of a reconstituted soil. However, these relationships may change over time.

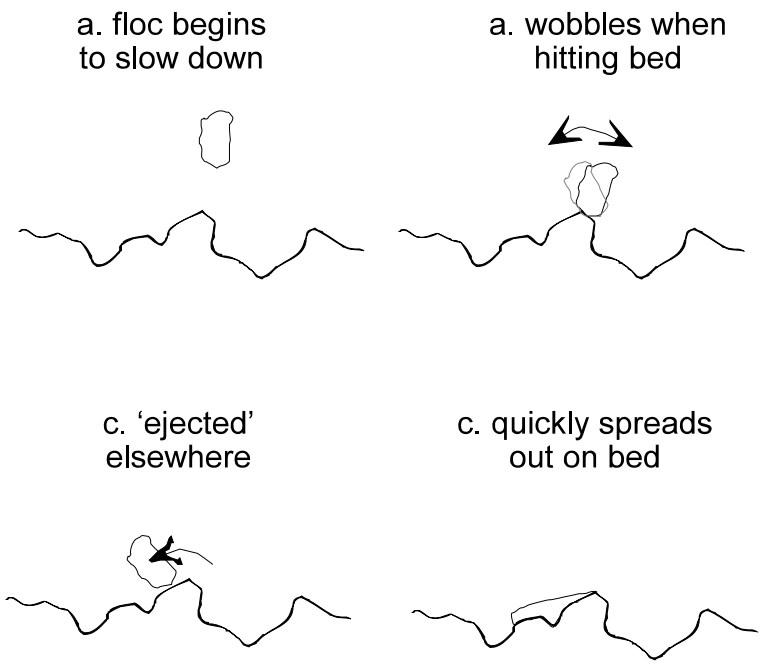

Figure 8.1 Schematic showing what often happens when a floc hits the bed surface.

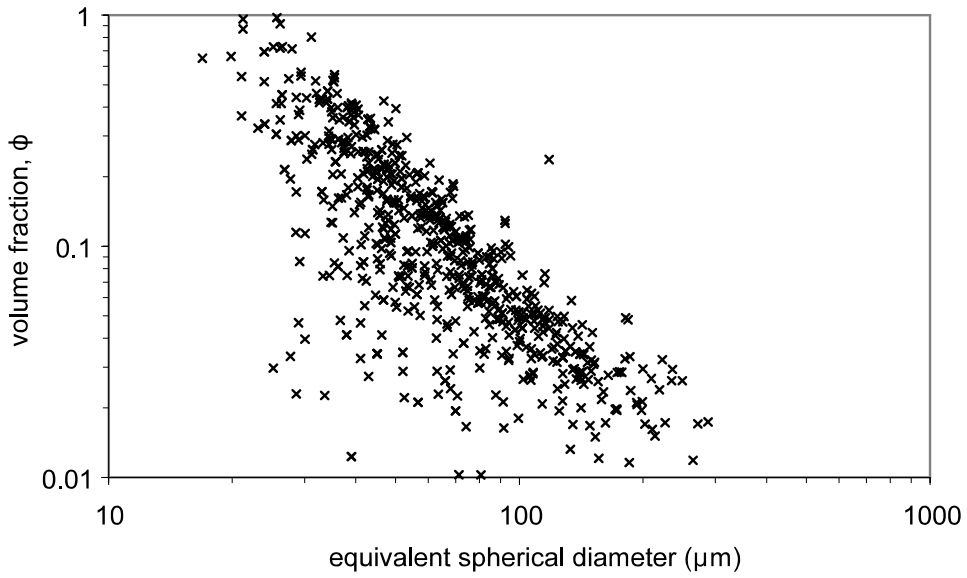

Figure 8.2 Volume fraction versus ESD for selected dbd3 flocs.

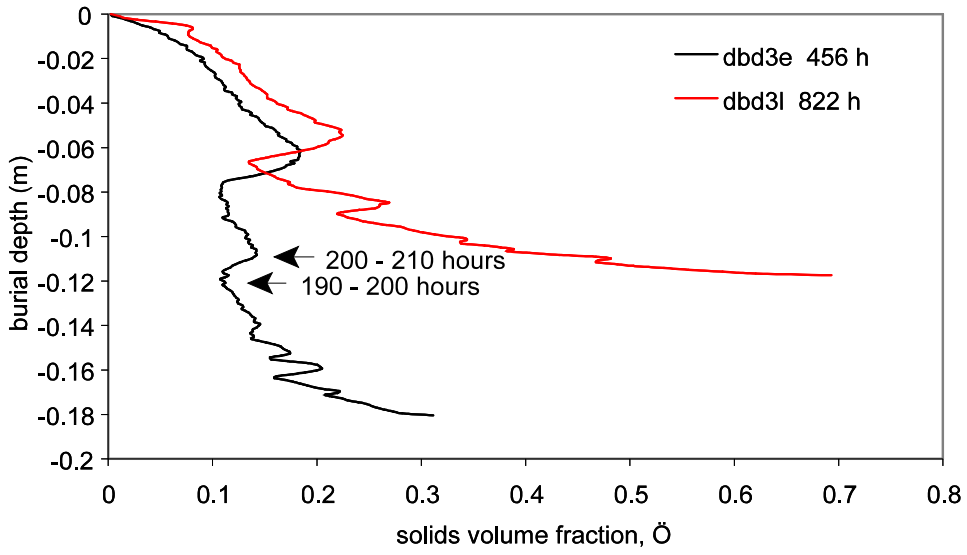

Figure 8.3 Volume fraction in the beds, at the end of sedimentation (dbd3e) and after the application of a hydraulic gradient (dbd3l).

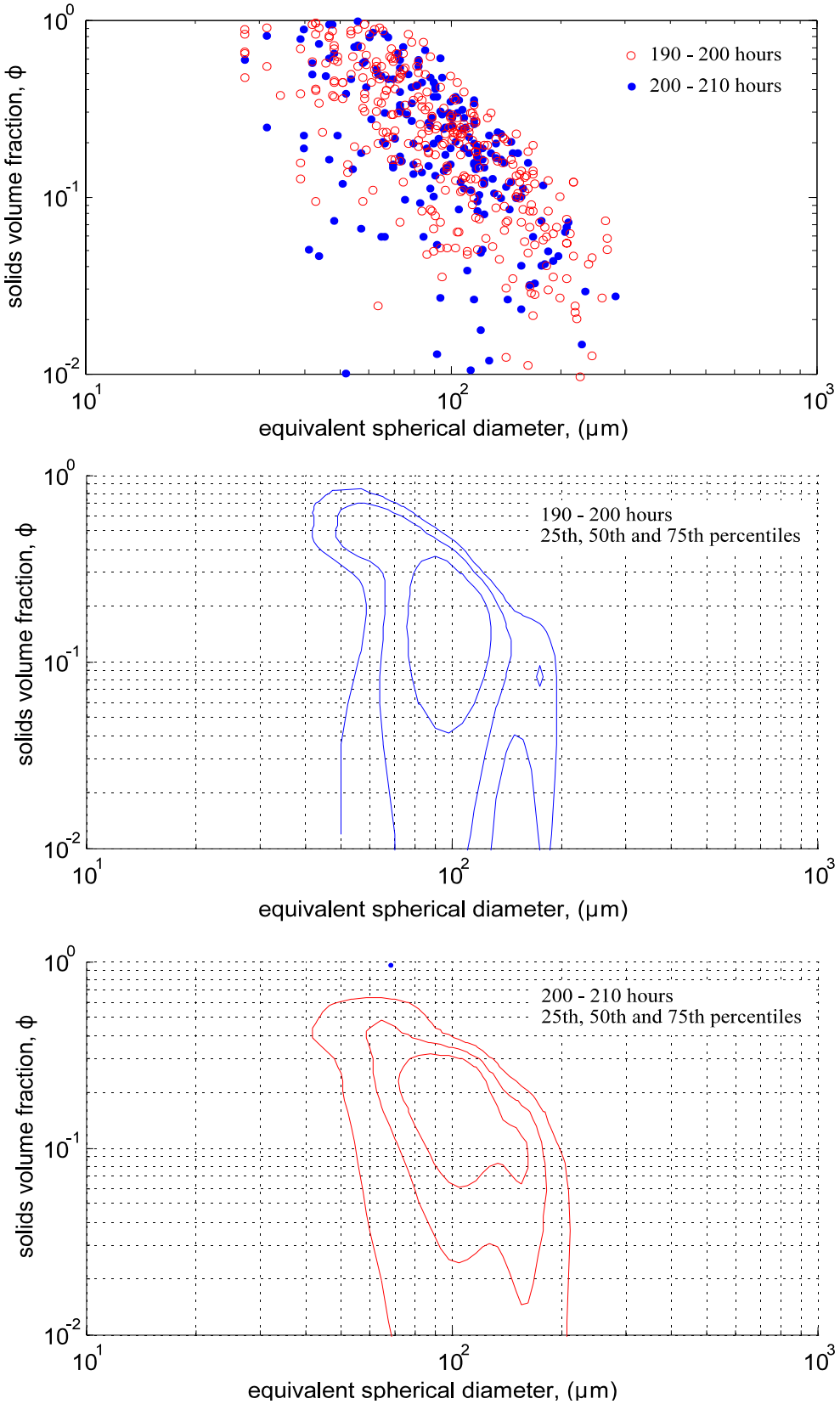

Figure 8.4 Volume fractions calculated from images at specified times. a. volume fraction versus ESD. b and c. Contours for the density probabilities at the different times.

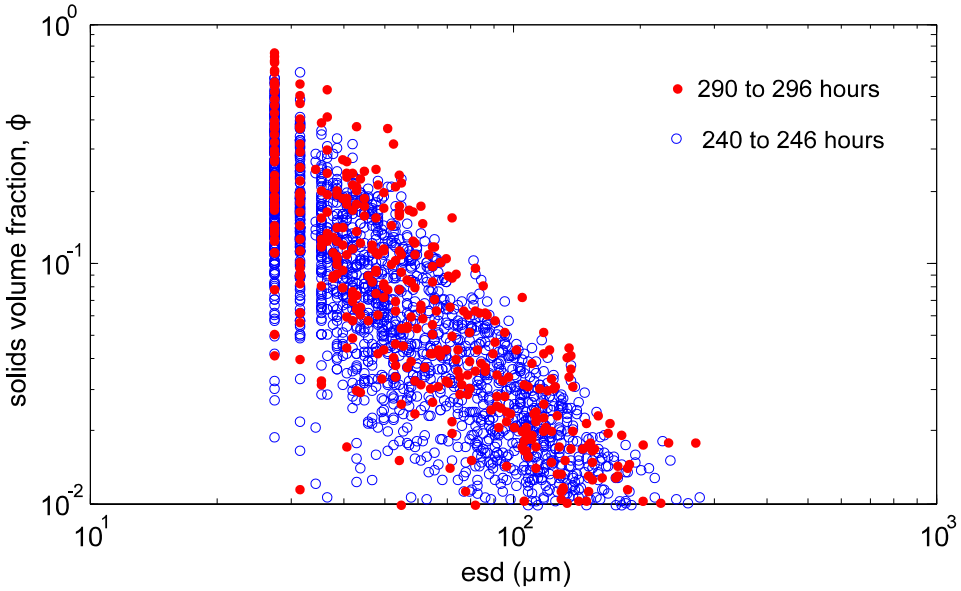

Figure 8.5 Volume fraction versus esd at different times for experiment cos17.

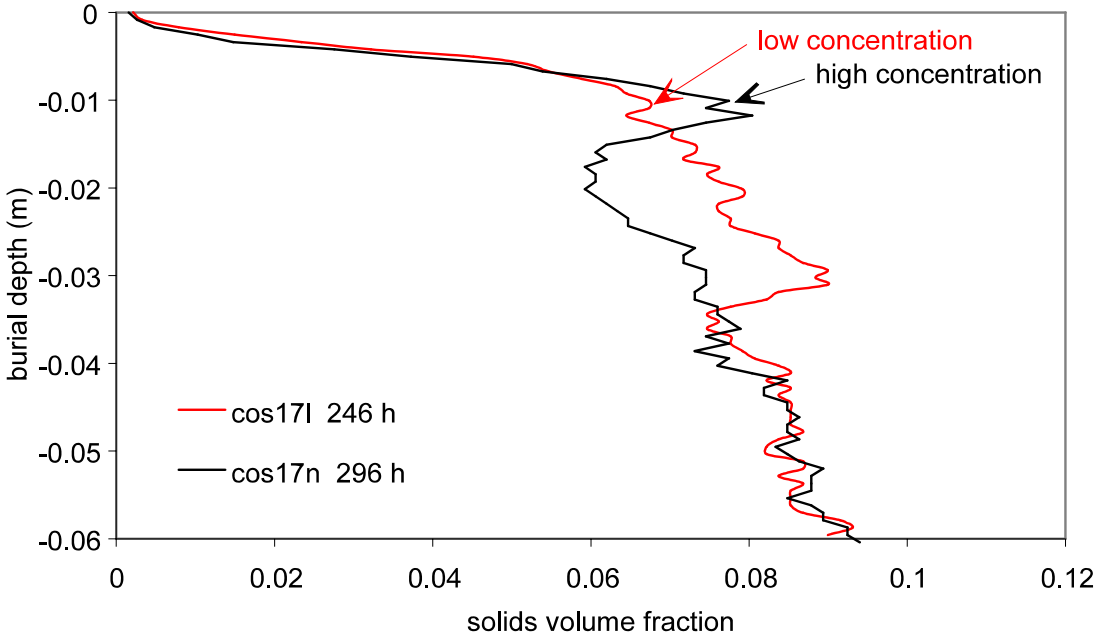

Figure 8.6 Solids volume fraction versus burial depths at different times for experiment cos17.

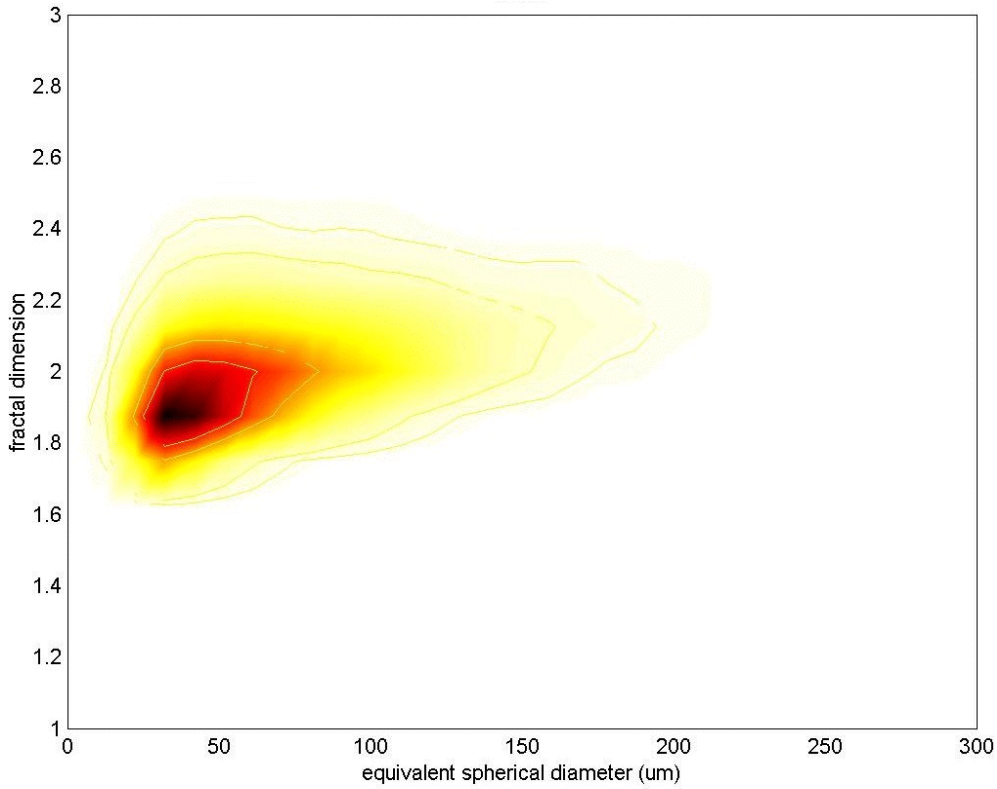

Figure 8.7 Density of the datapoints for the relationship between fractal dimension and equivalent spherical diameter for experiment dbd2.

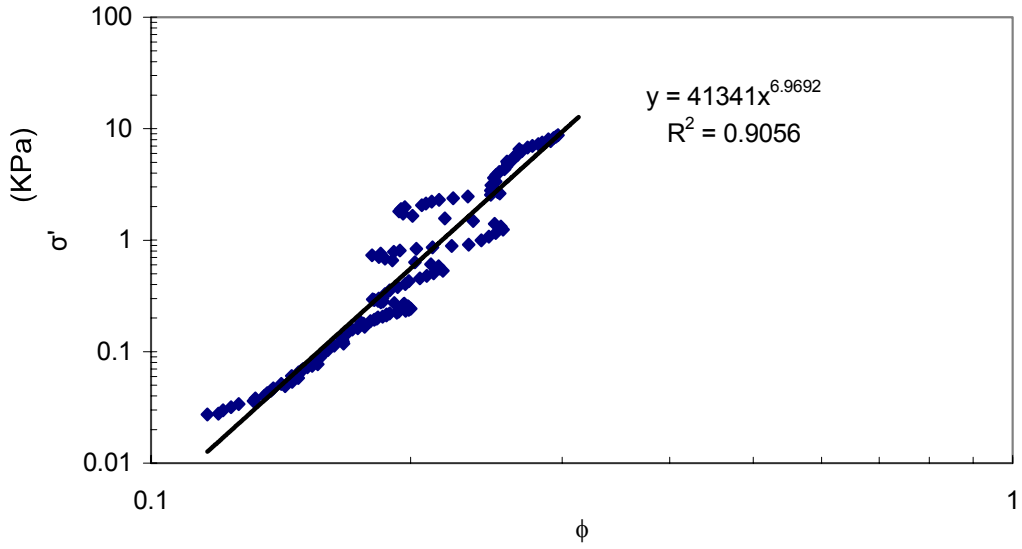

Figure 8.8 Effective stress versus solids volume fraction for the bed of experiment dbd2f.

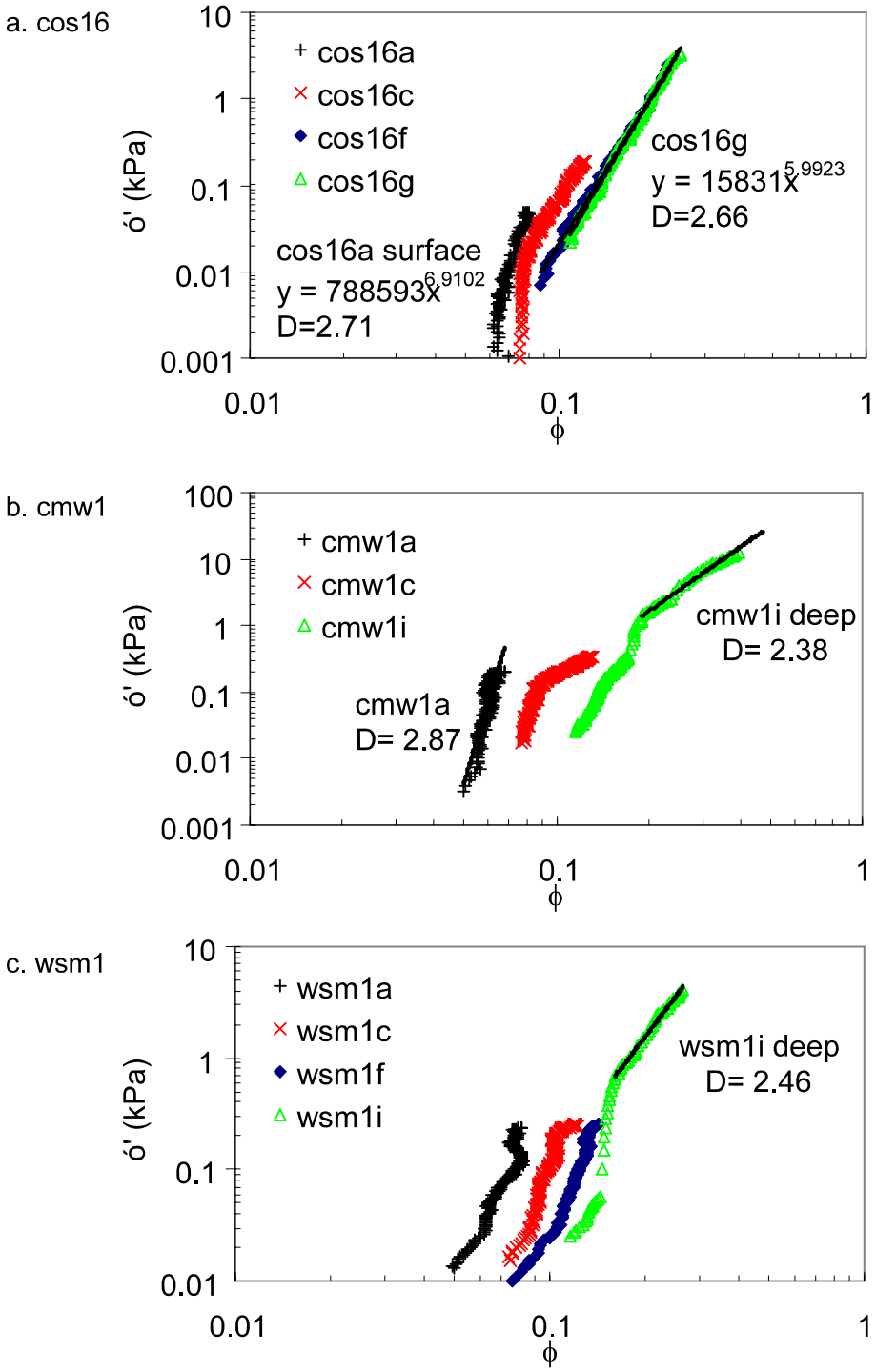

Figure 8.9 Solids volume fraction versus effective stress for experiments cos16, cmw1, and wsm1, as a means of finding the fractal dimension.

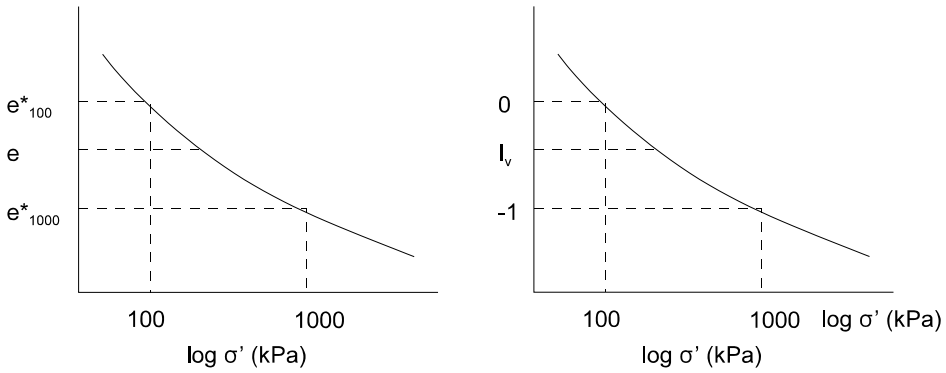

Figure 8.10 Converting the compression curve to the intrinsic compression line.

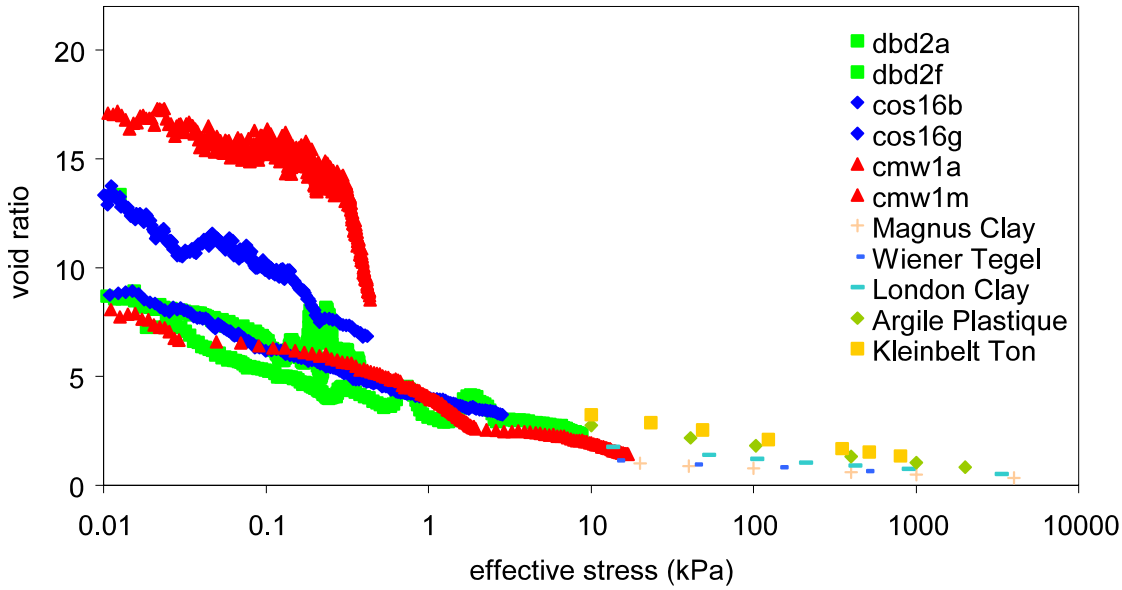

Figure 8.11 Upper and lower compression curves for experiments dbd2, cos16 and cmw1, taken from the first and last measurements of each experiment.

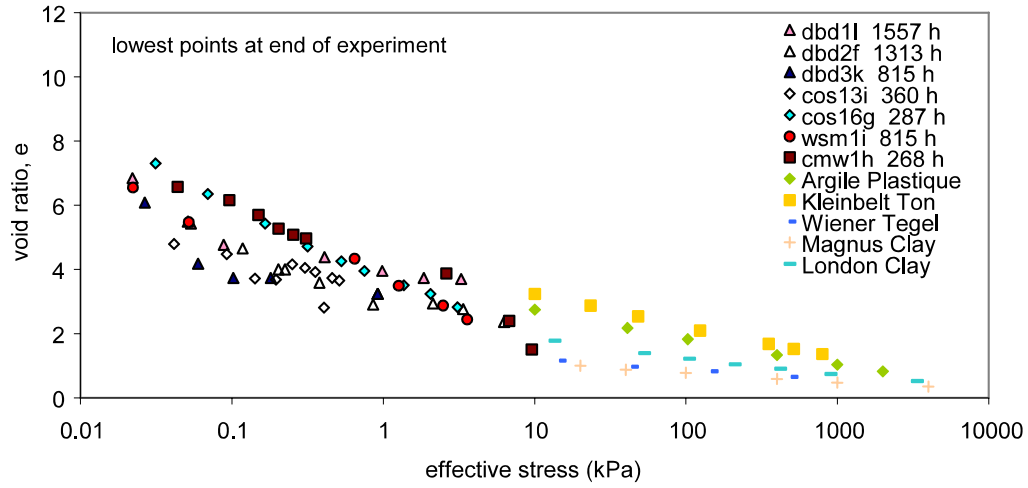

Figure 8.12 Void ratio effective stress relationship for the lowest points at the end of several experiments. Data also shown for experiments reported in Burland (1990).

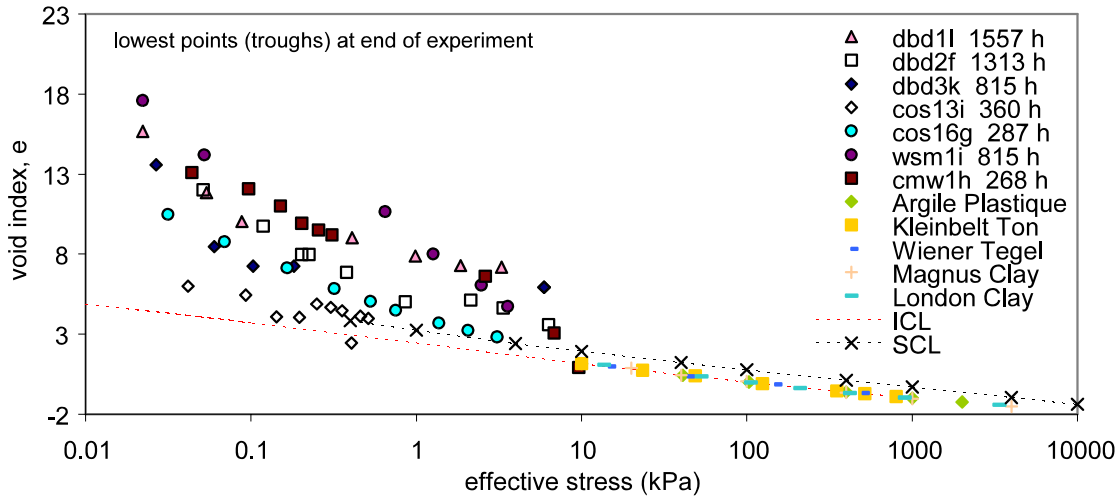

Figure 8.13 Void index versus effective stress for the lowest points at the end of several experiments. Data also shown for experiments reported in Burland (1990).

Chapter 9 Conclusions and Future Research

An investigation has been undertaken on the influence that flocs have on bed properties for natural cohesive sediment. Novel apparatus has been developed, and existing apparatus has been modified, to allow observations and measurements to be made on the entire sediment cycle, from sedimentation and flocculation, through consolidation and creep, to resuspension. This chapter summarises the equipment developments, along with the major findings, and concludes with suggestions for further research directions.

9.1 Floc Properties

Automated apparatus has been designed, developed, and improved to allow sediment to be steadily sedimented in laboratory columns, thereby closely representing natural sedimentation rates. Computerised video capture and image analysis techniques have been implemented, and have provided useful information about sedimentation and flocculation properties.

- Flocs in the lab closely resemble those seen *in situ*, in size, shape and settling velocity. The lab flocs are mainly elongated with the longer dimension oriented vertically. Some flocs appear as stringers.
- Flocculation efficiencies increase with increasing column concentration. This allows the flocs to become larger and initially to settle faster. The floc size distributions can be calculated for each of the different muds based only on column sediment concentration- this type of analysis could be useful for models of mass sediment transport in estuaries.
- Hindered settling is observed at a certain concentration. The mean settling velocities decrease, and the calculated slope of ESD vs. settling velocity decreases and eventually levels. That is, larger flocs and smaller flocs settle at similar rates.
- Effective density, porosity and fractal dimensions of the laboratory flocs match those of *in situ* flocs. Some theoretical equations specific to flocs (and not solid spheres) have been applied, although Stokes' law seems to give reasonable results which are comparable to other studies.

- Statistical techniques such as kernel density estimation allow important information to be extracted from large and highly variable floc data.

9.2 Influences of flocs on beds

An x-ray technique has been used to measure bed densities. Pore pressure profiles allow the calculation of effective stress. Bender elements (shear wave) instrumentation has been developed to indicate the stiffness, or the degree of consolidation in the beds. Shear vane apparatus is used for the same purpose. Image analysis techniques have also been applied to images of the beds.

Work has been conducted at Oxford University using H.R. Wallingford's Instrument for measuring Shear stress In Situ (isis). The experiments show that the equipment is working well in a column setup. Each bed tested is initially eroded by a distinct critical shear stress, or erosion threshold, which may depend on the properties of the mud and the length of consolidation time.

- The beds seem to erode in a laminar fashion, until at a very high shear rate a large (2 to 3 cm) liquified section of the surface gives way.
- Contrary to what might be expected, the beds become less resistant to erosion as they mature. This is likely due to the development of a biochemical surface layer, often containing gas. The feeding and soil reworking by marine worms contribute to this weakening over time.

Many interesting properties have been observed in slowly deposited and slurry deposited beds, and features of the beds can be related to flocculation conditions under which they have been formed.

- Photographs reveal that slowly sedimented beds have a much more aggregated structure than those deposited from a slurry
- The height of a consolidated bed, normalised by the mass of sediment, appears to be dependant on the rate of sedimentation. Beds deposited at a medium rate of sedimentation are the least dense. Beds deposited at very low sedimentation rates, and those deposited from slurries have higher densities.

- The aggregates at the surface of a freshly deposited bed break down over time, without any application of load.
- Variations in sedimentation rate, even if slight, lead to large variations in the structure of the beds as revealed by density profiles and void ratio values
- Variations in bed structures lead to variations in the strength of the bed
- The structure of the beds is not determined solely by the effective stress. Time dependent behaviour is apparent in all slowly deposited beds, particularly in the initial stages of consolidation
- Stiffness, measured with bender elements, may provide a means to monitor the development of bed structure
- Applying a hydraulic gradient to increase the total pressure on the bed indicates in all of the experiments that even at total pressures exceeding 15 kPa there are clear remnants of the flocculation conditions.
- Calculations of solids concentration and fractal dimension may provide a means to compare floc measurements with bed measurements.

9.3 Recommendations for future research

The purpose of conducting this research in a laboratory was to eliminate many of the variables which exist in an estuary. Even so, it is recognised that it is extremely difficult to couple the three processes of flocculation, sedimentation and consolidation. This is because of the many processes that oppose one another. For example, the formation of bed from a slurry bed is reasonably well understood and can be quite adequately predicted in terms of its bulk density, void ratio and effective stress over time. However the consolidation of a bed, which is simultaneously being built up by further sedimentation is a much more difficult problem, since now the drainage path lengths are increasing, while different parts of the bed are at different stages of consolidation. The time-dependent collapse of flocs, which is very poorly understood, is also at work at the surface. In the water column an increase in sediment concentration leads to larger flocs which leads to increased sedimentation rate. A further increase in concentration (or perhaps the increased settling velocity itself) leads to destructuring of the flocs, and therefore a decrease in the sedimentation rate. Smaller flocs at lower settling velocities lead to a very slow build up of

the beds, so that it takes a much longer period of sedimentation to obtain reliable bed measurements. During the timescale that is required for the bed to reach a suitable height to make measurements, bed processes are also taking place, which may overshadow effects of the flocs. To quantify links between the processes is still an enormous task. It is recommended that the equipment that has been designed for this research is used, without further modification, to examine the processes of flocculation, consolidation and erosion separately.

In that respect, examples of smaller research projects follow. The equipment would be useful in examining the possible modifications to Stokes' settling equation that are discussed in Chapter 4, and also in examining flocculation efficiencies under various conditions. An experimental program dedicated to observing the bed surface as the flocs are deposited would be valuable. An analysis combining floc volume fractions and bed packing theories should be possible with the existing equipment. The automated pore pressure measuring system should be used in all future flocculation experiments so that expulsion of pore water from the bed can be closely monitored as the bed is deposited.

The sedimentation system has proved useful and reliable, and is able to simulate the deposition rates in estuaries. By the later experiments the system was able to maintain a fairly constant rate of sedimentation. It would be an interesting study to program the sedimentation system to deposit mud over a cyclic pattern, such as a tidal cycle in an estuary. An even more ambitious improvement would be to replace the magnetic stirring system to one, such as an oscillating grid or a rotary viscometer, so that the shearing history on the flocs could be precisely controlled before they are deposited.

The video cameras and image analysis system have worked well for the present study. However, to improve the results, the experiments must be able to run in a laboratory where the lights are not constantly being switched on and off. A pilot study done during this research showed that, if the ambient lighting was kept constant, the image brightness could be used as a measure of sediment concentration. This would be extremely useful data to have through the length of an experiment.

The bender element apparatus was adequate for monitoring the development of a consolidating bed. It would be interesting to analyse the results of column experiments using the stiffness results instead of effective stress. This would require that bender elements are placed at frequent intervals on the column walls, and that shearwave measurements are made continually throughout th\e experiment.

The ISIS gave interesting results on the erodibility of the beds under biological influences. It would be interesting to remove the biological components to study independently the geotechnical properties of an eroding bed. Specifically, the development of pore pressures and density as the bed erodes is of interest to many researchers in the field of sediment resuspension. Conversely, experiments should be carefully designed to investigate further the influences of various types of organisms.

Advances towards several of these suggested research directions have already been made. For instance, sophisticated column apparatus has been built at the Technical University of Delft using an oscillating grid to control flocculation conditions. The researchers have expressed their interest in the Oxford apparatus, and future collaborations are likely. Proposals have been submitted, and well-received, to investigate further the effect of organisms on bed strength. A paper is in preparation which describes the geotechnical behaviour of beds under both ISIS erosion, and an oscillating grid erosion device subsequently developed at Oxford. Finally, the image analysis algorithms, and erosion combined with bender element methods are being used in an investigation of the storm-generated resuspension of material from the Continental Arctic Shelf in the International CASES project. The work that has been reported in this thesis has provided new insights into the effects of flocs on bed structures, and has raised many interesting questions to be answered by future research.

References

Al Ani, S., K.R. Dyer and D.A. Huntley (1991). "Measurement of the influence of salinity on floc density and strength." Geo-marine Letters **11**: 154-158.

Allain, C., M. Cloitre, et al. (1995). "Aggregation and sedimentation in Colloidal Suspensions." Physical Review Letters **74**(8): 1478-1481.

Alldredge, A. L. and C. Gotschalk (1988). "In situ settling behaviour of marine snow." Limnology and Oceanology **33**: 339.

Allersma, E., A. J. Hoekstra, et al. (1967). "Transport patterns in the Chao Phya Estuary."

Amos, C. L., T. Feeney, et al. (1997). "The stability of fine-grained sediments from the Fraser River Delta." Estuarine, Coastal and Shelf Science **45**: 507-524.

Bache, D. H., C. M. Johnson, J.F., et al. (1997). "A conceptual view of floc structure in the sweep floc domain." Water Science and Technology **36**(4): 49-56.

Been, K. (1980). Stress-strain behaviour of a cohesive soil deposited under water. Engineering Science. Oxford, Oxford University.

Been, K. (1981). "Non-destructive soil bulk density measurement using X-ray attenuation." Geotechnical Testing Journal **December 1981**: 69-176.

Been, K. and G. C. Sills (1981). "Self-weight consolidation of soft soils: an experimental and theoretical study." Geotechnique **31**: 519-535.

Bennett, R. H., W. R. Bryant, et al. (1991). Microstructure of Fine-Grained Sediments, From Mud to Shale. London, Springer-Verlag.

Bowden, R. K. (1988). Compression behaviour and shear strength characteristics of a natural silty clay sedimented in the laboratory. Engineering Science, Oxford University.

Bürger, R. and W. L. Wendland (2001). "Sedimentation and suspension flows: Historical perspective and some recent developments." Journal of Engineering Mathematics **41**: 101-116.

Burland, J. B. (1990). "The Rankine Lecture: On the compressibility and shear strength of natural clays." Geotechnique **40**(3): 329-378.

Burt, T. N. (1994). VII. Field settling velocities of estuary muds. Estuarine Cohesive Sediment Dynamics. Lecture notes on coastal and estuarine studies 14. Proceedings of a workshop in Tampa, Florida, November 12-14. A. J. Mehta, R. T. Barber, C. N. K. Mooers and M. J. Bowman, Springer-Verlag**:** 126-150.

Coe, H. S. and G. H. Clevenger (1916). "Methods for determining the capacity of slime settling tanks." Transactions of the American Institute of Mining, Metallurgical, and Petroleum Engineers **55**: 356-384.

Craig, R. F. (1974). Soil Mechanics. Wokingham, England, Van Nostrand Reinhold Company.

Drapeau, D. T., H. G. Dam, et al. (1994). "An improved flocculator design for use in particle aggregation experiments." Limnology and Oceanography 39 **3**: 723-729.

Droppo, I. G. (2001). "Rethinking what constitutes suspended sediment." Hydrological processes **15**: 1551-1564.

Dyer, K. R. (1985). Coastal and Estuarine Sediment Dynamics, John Wiley and Sons.

Dyer, K. R. and A. J. Manning (1999). "Observation of the size, settling velocity and effective density of flocs, and their fractal dimensions." Journal of Sea Research **41**: 87-95.

Edgerton, H. E. (1979). "Silhouette photography of small active subjects." Journal of

Microscopy **110**: 79-81.
Einstein, H. A. and R. B. Krone (1962). "Experiments to determine modes of cohesive sediment transport in salt water." Journal of Geophysical Research **67**(4): 1451-1464.
Eisma, D. (1986). "Flocculation and deflocculation of suspended matter in estuaries." Netherlands Journal of Sea Research **20**: 183-199.
Eisma, D. (1991). "Particle size of suspended matter in estuaries." Geo-Marine Letters **11**(3-4): 147-153.
Eisma, D., P. Bernard, et al. (1991). "Suspended matter particle size in some West European estuaries. 1. Particle size distribution." Netherlands Journal of Sea Research **28**(3): 193-214.
Elder, D. M. and G. C. Sills (1985). Thickening and consolidation of sediment due to self weight. Engineering Foundation Conference, Cloister, Sea Island, Georgia, USA.
Faas, R. W. (1984). "Time and density dependent properties of fluid mud suspensions, NE Brazilian Continental Shelf." Geo-Marine Letters **4**: 147-152.
Feates, N., J R Hill, et al. (1999). COSINUS Field Experiment Tamar Estuary: Measurement of properties of suspended sediment flocs and bed properties.
Firth, B. A. and R. J. Hunter (1976). "Flow properties of coagulated colloidal suspensions." Journal of Colloid and Interface Science **57**: 248-275.
Fuerstenau, M. C. (1960). Department of Metallurgy, MIT. Unpublished Data.
Gibbs, R. J. (1983). "Effect of natural organic coatings on the coagulation of particles." Environmental Science Technology **17**: 237-240.
Gibbs, R. J. (1985a). "Estuarine flocs: Their size, settling velocity and density." Journal of Geophysical Research **90**(c2): 3249-3251.
Gibbs, R. J. (1985b). "Settling velocity, diameter and density for flocs of illite, kaolinite and montomorillinite." Journal of Sedimentary Petrology **55**: 65.
Gonzales, R. and G. C. Sills (1997). "The influence of sedimentation history on the behaviour of residimented Bothkennar clay. Final report (part 1) for Grant EU Capital and Mobility Coastal Environments (E Atlantic) Physical Process."
Goodman, C. (1995). Investigation and interpretation of shear wave velocities in soil. Department of Civil Engineering. Nottingham, University of Nottingham**:** 69 pages.
Gregory, J. (1997). "The density of particle aggregates." Water Science and Technology **36**(4): 1-13.
Gregory, J. and H. Chung (1995). "Continuous monitoring of floc properties in stirred suspensions." Journal of Water SRT-Aqua **44**: 125-131.
Head, K. H. (1992). Manual of Soil Laboratory Testing. London, Pentech Press.
Holdich, R. G. and G. Butt (1996). "Compression and channelling in gravity sedimenting systems." Minerals Engineering **9**(1): 115-131.
Holland, A. F., R. G. Zingmark, et al. (1974). "Quantitative evidence concerning the stabilisation of sediments by marine benthic diatoms." Marine Biology **27**: 191-196.
Huang, H. (1993). "Porosity size relationships of drilling mud flocs: fractal structure." Clays and Clay Minerals **41**: 373.
Huang, H. (1994). "Fractal properties of flocs formed by fluid shear and differential settling." Physics of Fluids **6**(10): 3229-3234.
Hunter, K. A. (1980). "Microelectrophoretic properties of natural surface-active organic matter in coastal seawater." Limnology and oceanography **25**(5): 807-822.
Imai, G. (1981). "Experimental studies on sedimentation mechanism and sediment

formation of clay minerals." Soils and Foundations **21**(1): 7-20.
Johnson, B. D. and P. J. Wankersky (1985). "A recording backward scattering meter and camera system for examination of the distribution and morphology of macroaggregates." Deep Sea Research **32**: 1143-1150.
Kranenburg, C. (1994). "The fractal structure of cohesive sediment aggregates." Estuarine, Coastal and Shelf Science **39**: 451-460.
Kretzschmar, R., W. P. Robarge, et al. (1993). "Flocculation of kaolinitic soil clays - effects of humic substances and iron oxides." Soil Science Society of America Journal **57**(5): 1277-1283.
Krone, R. B. (1962). "Flume studies of the transport of sediment in estuarine shoaling processes. Final Report prepared for San Francisco District Corps of Engineers, U.S. Army Contract No. DA-04-203 CIVENG-59-2. Prepared by Hydraulic Engineering Laboratory and Sanitary Engineering Research Laboratory, University of California, Berkely. 110 pgs."
Krone, R. B. (1978). Aggregation of suspended particles in estuaries. Kjerfve.
Krone, R. B. (1986). The significance of aggregate properties to transport processes. Lecture Notes on Coastal and Estuarine Studies. Berlin Heidelberg New York, Springer-Verlag. **14:** 66-84.
Krone, R. B. (1999). "Effects of Bed Structure on Erosion of Cohesive Sediments." Journal of Hydraulic Engineering: 1297-1301.
Kuenen, P. H. (1965). Experiments in connection with turbidity currents. Submarine Geology and Geophysics. W. F. Whittard and R. Bradshaw. London, Butterworths**:** 54-71.
Kusuda, T., K. Koga, et al. (1981). "Density and settling velocity of flocs." Memoirs of the Faculty of Engineering, Kyushu University **41**: 269-280.
Kynch, G. J. (1952). "A theory of sedimentation." Transactions of the Faraday Society **48**: 166-176.
Lagvankar, A. L. and R. S. Gemmell (1968). "A size-density relationship for flocs." Journal of the American Water Works Association **60**: 1040-1046.
Law, D. J., A. J. Bale, et al. (1997). "Adaptation of focussed beam reflectance measurement to in-situ particle sizing in estuaries and coastal waters." Marine Geology **140**: 47-59.
Lee, D. J., G. W. Chen, et al. (1996). "On the free-settling test for estimating activated sludge floc density." Water Research **30**(3): 541-550.
Leroueil, S., M. Kabbaj, et al. (1985). "Stress-strain rate relation for the compressibility of sensitive natural clays." Geotechnique **35**: 159-180.
Lewis, J. A. (2000). "Colloidal processing of ceramics." Journal of the American Ceramics Society **83**(10): 2341-2359.
Li, D. and J. Ganczarczyk (1989). "Fractal geometry of particle aggregates generated in water and wastewater treatment processes." Environmental Science Technology **23**: 1385.
Lintern, D. G. (2000). The transition from flocculated suspension to consolidated bed for a fine-grained cohesive sediment. Internal report. Oxford.
Lintern, D. G. a. G. C. S. (2000). "Description and discussion on flocculation and consolidation properties of Tamar Estuary sediment." EU MAST III COSINUS Project.
Loeb, G. I. and R. A. Neihof (1977). "Adsorption of an organic film at the platinum-

seawater interface." Journal of Marine Research **35**(2): 283-291.
Luckenbach, M. W. (1986). "Sediment stability around animal tubes. The roles of hydrodynamic processes and biotic activity." Limnology and Oceanology Acta **31**: 779-787.
Magara, Y., S. Nambu, et al. (1976). "Biochemical and physical properties of an activated sludge on settling characteristics." Water Research **10**: 71.
Manning, A. J. (2001). A study of the effect of turbulence on the properties of flocculated mud. Institute of Marine Studies. Plymouth, University of Plymouth**:** 282 pages.
McCave, I. N. (1975). "Vertical flux of particles in the ocean." Deep-Sea Research **22**: 491-502.
McDermott, I. R. (1992). "Seismo-acoustic investigations of consolidation phenomena." PhD Thesis, University of Wales.
Meadows, P. and J. Tait (1989). "Modification of sediment permeability and shear strength by two burrowing invertebrates." Marine Biology **101**: 75-82.
Meaken, P. (1988). "Fractal aggregates." Advances in Colloid Interface Science **28**: 249.
Mehta, A. J. (1991). "Review notes on cohesive sediment erosion." Coastal Sediments **91**(1): 40-53.
Merckelbach, L. M. (2000). Consolidation and strength evolution of soft mud layers. Civil Engineering. Delft, Technical University of Delft**:** 151.
Michaels, A. S. and J. C. Bolger (1962). "Settling rates and sediment volumes of flocculated kaoline suspensions." Industrial and Engineering Chemistry Fundamentals **1**: 24-33.
Migniot, C. (1968). "A study of the physical properties of various forms of very fine sediments and their behaviour under hydrodynamic actions." La Houille Blanche **7**: 591 - 620.
Migniot, C. (1987). "Synthese des connaissances sur le tassement et la rheologie des vases." Laboratoire Central d'Hydraulique de France **Sept. 1987, rap. 54238**: 89 pages.
Milligan, T. G. and P. S. Hill (1998). "A laboratory assessment of the relative importance of turbulence, particle composition and concentration in limiting maximal floc size and settling behaviour." Journal of Sea Research **39**: 227-241.
Munachen, S. E. (in prep). Cyclic behaviour of gassy soil. Department of Engineering Science. Oxford, Oxford University.
Murphy, R. M. (2001). The effect of density and salinity on sedimentation behaviour. Department of Engineering. Oxford, Oxford University**:** 33 Pages.
Neale, G., N. Epstein, et al. (1973). "Creeping flow relative to permeable spheres." Chemical Engineering Science **28**: 1865-1874.
Nichols, M. M. and R. B. Biggs (1985). Estuaries. Coastal Sedimentary Environments. R. A. Davis. New York, Springer-Verlag**:** 77-186.
Ortner, P. B., S. R. Cummings, et al. (1979). "Silhouette photography of oceanic zooplankton." Nature **277**: 50-51.
Owen, M. W. (1970). A detailed study of the settling velocities of an estuary mud. Wallingford, H.R. Wallingford.
Parker, D. S., W. J. Kaufman, et al. (1972). "Floc break-up in turbulent flocculation process." Journal of the sanitary engineers division. Proceedings of the American Society of Civil Engineers **98**: 79-99.
Partheniades, E. (1965). "Erosion and deposition of cohesive soils." Jounal of the

Hydraulics Division. American Society of Civil Engineers **91**(HY1): 105-139.
Paterson, D. M. and K. S. Black (1999). "Water flow, sediment dynamics and benthic biology." Advances in Ecological Research **29**: 155-193.
Roberts, J., R. Jepsen, et al. (1998). "Effects of particle size and bulk density on erosion of quartz particles." Journal of Hydraulic Engineering: 1261-1267.
Schramm, L. L. (1996). Suspensions: Basic Principles. Suspensions: Fundamentals and Applications in the Petroleum Industry. L. L. Schramm. Danvers, MA, American Chemical Society**:** 794.
Schultheiss, P. J. (1983). "The influence of packing structures on seismic wave velocities in sediments." Marine Geological Report N0. 83/1, University of Wales.
Shirley, D. J. and D. W. Bell (1978). "Acoustics of in situ laboratory sediment." Applied Research Laboratory, Austin, Texas. Report ARL-TR-78-36.
Shirley, D. J. and L. D. Hampton (1978). "Shear-wave measurements in laboratory sediments." J. Acoust. Am. **63**(2): 607-613.
Sills, G. C. (1995). Time dependent processes in soil consolidation. Proceedings of the International Symposium on Compression and Consolidation of Clayey Soils, Hiroshima, Japan. H. Yoshikuni and O. Kusakabe. Rotterdam, A.A. Balkema. **2:** 875-890.
Sills, G. C. (1997). Chapter 7 Consolidation of cohesive sediments in settling columns. Cohesive Sediments. Fourth Nearshore and Estuarine Cohesive Sediment Transport Conference. INTERCOH 94. N. Burt, R. Parker and J. Watts. Wallingford, UK.
Sills, G. C. (1998). "Development of structure in sedimenting soils." Phil. Trans. R. Soc. Lond. A **356**: 2515-2534.
Sills, G. C. and G. Bartholomeeusen (2001). Consolidation properties of Dibden Bay mud. Report submitted to ESSO Petroleum. Oxford, Department of Engineering Science. Oxford University.
Sills, G. C. and D. M. Elder (1984). The transition from sediment suspension to settling bed. Proceeding of a Workshop on Estuarine Cohesive Sediment Dynamics. Extract from series "Lecture Notes on Coastal and Estuarine Studies". SM Report No. SM053/84, Tampa, Florida, Springer-Verlag.
Sills, G. C. and D. G. Lintern (2001). Flocculation properties of Dibden Bay Mud. Report submitted to ESSO Petroleum. Oxford, Department of Engineering Science. Oxford University.
Sills, G. C. and R. C. Thomas (1984). Settlement and consolidation in the laboratory of steadily deposited sediments. Sea Bed Mechanics. B. Dennes, Graham and Trotman Publishers**:** 41-49.
Stephens, J. A., R. J. Uncles, et al. (1992). "Bulk properties of intertidal sedimentes in a muddy, macrotidal estuary." Marine Geology **103**: 445-460.
Suzuki, N. and K. Kato (1953). "Studies on suspended materials- marine snow in sea. Part I. Sources of marine snow." Hokkaido University Faculty of Fisheries Bulletin **4**: 132-135.
Tambo, N. and Y. Watanabe (1979). "Physical characteristics of flocs - I. The floc density function and aluminium floc." Water Research **13**: 409-419.
Terzaghi, K. (1936). "The shearing resistance of saturated soils and the angles between the planes of shear." Proceedings of the 1st International Conference on Soil Mechanics. **1**: 54-56.
Torfs, H., H. Mitchener, et al. (1996). "Settling and consolidation of mud/sand mixtures."

Coastal Engineering **29**: 27-45.
Tsai, C. H., S. Iacobellis, et al. (1987). "Flocculation of fine-grained lake sediments due to uniform shear stress." Journal of Great Lakes Research **13**: 135-146.
van de Ven, T. G. and R. J. Hunter (1977). "The energy dissipation in sheared coagulated sols." Rheology Acta **16**: 534-543.
Van Goethem, J., J. Berlamont, et al. (1985). "Avoiding mud accumulation in harbours and their entrances." Interim Research Report to S.B.B.M- SixCo, Hydraulics Laboratory: 52 pages (in Dutch).
van Leussen, W. (1988). Aggregation of particles, settling velocity of mud flocs A Review. Physical Processes in Estuaries. Symposium Papers, sponsored by the Dutch Ministry of Transport and Public Works. J. Dronkers and W. Van Leussen. Berlin, Springer-Verlag**:** 427-445.
Verreet, G. and J. Berlamont (1987). "Rheology and non-Newtonian behaviour of sea and estuarine mud." Rheology of Non-Newtonian Flows. Encyclopedia of Fluid Mechanics **III**.
Whitehouse, U. G., L. M. Jeffrey, et al. (1960). "Differential settling tendancies of clay minerals in saline water." Proceedings of the 7th Conference on Clays and Clay Minerals: 1-79.
Widdows, J., M. Brinsley, et al. (1998). Use of an in situ flume to quantify particle flux (biodeposition rates and sediment erosion) for an intertidal mudflat in relation to current velocity and benthic macrofauna. Sedimentary Processes in the Intertidal Zone. K. S. Black, D. M. Paterson and A. Cramp. London, Geological Society Special Publication. **139:** 85-97.
Wilkenson, K. J., J. C. Negre, et al. (1997). "Coagulation of colloidal material in surface waters: The role of natural organic matter." Journal of Contaminant Hydrology **26**(1-4): 229-243.
Williams, D. (1986). Rheology of cohesive suspensions. Estuarine Cohesive Sediment Dynamics. Lecture Notes on Coastal and Estuarine Studies. A. J. Mehta. Berlin, Heidelberg, New York, Springer. **14:** 110-125.
Williamson, H. J. and M. C. Ockenden (1996). "ISIS: An instrument for measuring erosion shear stress in situ." Estuarine, Coastal and Shelf Science **42**: 1-18.
Winterwerp, J. C. (1999). On the dynamics of high-concentrated mud suspensions. Department of Civil Engineering and Geosciences. Delft, Delft University of Technology**:** 171 pages.
Winterwerp, J. C. and C. Kranenburg (2000). Fine Sediment Dynamics in the Marine Environment. Proceedings in Marine Science, Delft, The Netherlands.
Wu, C. C., C. Huang, et al. (1998). "Bound water content and water binding strength on sludge flocs." Water Research **32**(3): 900-904.
Wu, C. C. and D. J. Lee (1998). "Hydrodynamic drag force exerted on a moving floc and its implication to free-settling tests." Water Research **32**(3): 760-768.
Yariv, S. and H. Cross (1979). Geochemistry of Colloid Sytems. Berlin Heidelberg New York, Springer-Verlag.
Yen, P. S., L. C. Chen, et al. (2002). "Network strength and dewaterability of flocculated activated sludge." Water Research **36**: 539-550.
Zreik, D. A., B. G. Krishnappan, et al. (1998). "Erosional and mechanical strengths of deposited cohesive sediments." Journal of Hydraulic Engineering **November 1998.**: 1076-1085.